Visualization and functional characterization of the postinfarction arrhythmogenic substrate

Visualisatie en functionele karakterisering van het aritmogene substraat na het hartinfarct

(Met een samenvatting in het Nederlands)

Proefschrift ter verkrijging van de graad van doctor aan de Universiteit Utrecht op gezag van de Rector Magnificus, Prof. Dr. W. H. van Gispen, ingevolge het besluit van het College voor Promoties in het openbaar te verdedigen op 20 November 2001 des middags te 14.30 uur.

door
Pascalis Franciscus Hubertus Maria van Dessel

geboren op 29 April 1963, te Bergen op Zoom

Promotores:

Prof dr N.M. van Hemel	Universitair Medisch Centrum Utrecht
Prof dr ir J.M.T. de Bakker	Universitair Medisch Centrum Utrecht Academisch Medisch Centrum Amsterdam

Copromotor:

dr A.C. Linnenbank	Universitair Medisch Centrum Utrecht Academisch Medisch Centrum Amsterdam

Financial support by the Netherlands Heart Foundation and the Sichting SORBO Hart Fonds, Duiven, The Netherlands, for the publication of this thesis is gratefully acknowledged. Part of the study described in this thesis was supported by a grant 94.147 of the Netherlands Heart Foundation.

Additional financial support, provided by ELA Medical Nederland and Medtronic B.V. is much appreciated.

Visualization and functional characterization of the postinfarction arrhythmogenic substrate

Voor mijn ouders

ISBN: 90-393-2852-8

Printed by: Budde Elinkwijk, Nieuwegein
Cover design: A.C. Linnenbank.
Lay-out: M. Potse, A.C. Linnenbank

Contents

List of abbreviations

ARI:	Activation recovery interval
ARTG:	Activation recovery time gradient
BSM:	Body surface mapping
CASM:	Catheter activation sequence mapping
ECG:	Electrocardiogram
IMEM:	Intraoperative multielectrode mapping
JL:	Josephson location
LAO:	Left anterior oblique
LADP:	Low amplitude discrete potential
LP:	Late potential
LPMAP:	Late potential integral map
RAO:	Right anterior oblique
SABSM:	Signal averaged body surface mapping
SAECG:	Signal averaged electrocardiograms
QRSTi:	QRST integral maps
QTd:	QT dispersion
VT:	Ventricular tachycardia

1 Introduction

P.F.H.M. van Dessel

Heart Lung Center Utrecht, Department of Cardiology,
St Antonius Hospital, Nieuwegein, The Netherlands

It is well established that ventricular arrhythmia is the primary mechanism of sudden death in patients who survive the acute phase of myocardial infarction [1–3].

For secondary prevention of sudden arrhythmic death, a wide range of therapies has become available. Treatment strategies for malignant postinfarction ventricular tachycardia can be subdivided into three categories: 1) those that prevent recurrences of ventricular arrhythmia by modulating the properties of the arrhythmogenic substrate; 2) those that prevent the fatal outcome of recurrences of ventricular arrhythmias and 3) those that can be considered curative, since they are capable of eliminating the arrhythmogenic substrate.

A wide variety of antiarrhythmic drugs has been developed to influence the electrophysiologic properties of the arrhythmogenic substrate, thereby preventing recurrences of arrhythmias. Antiarrhythmic drugs can be divided into subclasses that describe their electrophysiologic mode of action [4, 5]. Unfortunately, by the current standards, their efficacy in preventing sudden death appears to be low [6–10]. In addition, it has been reported that antiarrhythmic drugs may increase the risk for malignant arrhythmias in selected patients [11].

The concept of an implantable cardioverter (ICD) was developed to lower the risk of fatal outcome caused by recurrent ventricular arrhythmias [12–14]. ICDs are capable of detecting malignant ventricular tachyarrhythmias and can subsequently terminate the arrhythmia by antitachycardia pacing or internal defibrillation. ICD therapy has been shown to be both superior to antiarrhythmic drugs as well as cost-effective in secondary prevention of sudden cardiac death [6–10, 15]. More recently, ICD therapy proved to be effective in preventing sudden cardiac death in patients with coronary artery disease and asymptomatic, non-sustained ventricular arrhythmias [16]. ICD therapy does not prevent life-threatening rhythm disorders, but merely the utmost consequences of ventricular arrhythmias for the patient. Major disadvantage of ICD therapy appears therefore to be its effect on the quality of life of patients, caused by inappropriate shocks or the prevailing possibility of experiencing cardioversion shocks while still conscious [17].

The most definite solution for saving patients from postinfarction ventricular arrhythmias is the elimination of the substrate itself. In the late 1970's, antiarrhythmic surgery was introduced for this purpose [18–21]. Antiarrhythmic surgery can be guided by intraoperative mapping and results in removal of the arrhythmogenic substrate. It has proven its efficacy in the past, but major disadvantage of antiarrhythmic surgery remains that surgical ablation can only be performed during open-heart surgery [22]. In the early 1990's, first attempts to cure patients from ventricular arrhythmias by means of percutaneous radiofrequency catheter ablation were reported [23, 24]. Efficacy of radiofrequency ablation of postinfarction VT depends on the stability of the VT, the number of VT morphologies in one patient, hemodynamic tolerance and intramural depth of the radiofrequency target site [25, 26].

From the abovementioned considerations, it appears that identification of patients at risk for life threatening postinfarction ventricular arrhythmias is essential.

Furthermore, to tailor treatment strategy of postinfarction ventricular arrhythmias to individual patients, extensive knowledge on electrophysiologic mechanisms and anatomic localization of the arrhythmogenic substrate in individual patients is required.

1.1 Mechanisms of cardiac arrhythmias

At present, several mechanisms that underlie cardiac arrhythmias are recognized. The most important among these mechanisms are: triggered activity, enhanced abnormal automaticity, anatomically defined reentry and functional ('leading circle') reentry. Postinfarction ventricular arrhythmias are considered to be caused mainly by the latter two mechanisms.

1.1.1 Anatomic reentry

The first model of reentry in cardiac tissue was described by Mines in 1913 [27]. In an anatomically defined circuit he recognized that the duration of the refractory period and conduction velocity within the circuit determined whether or not reentry could occur. This resulted in the definition of conditions that are obligatory for the initiation of a circus movement tachycardia: (1) the existence of an arc of unidirectional block, (2) conduction around this arc of block and (3) re-excitation of tissue proximal to the site of conduction block [27, 28]. Several properties of anatomic reentry can be inferred from the intrinsic properties of the reentry circuit. In anatomically delineated reentry circuits the localization and length of the pathway are fixed and defined by the perimeter of the anatomic structure, which forms the unexcitable center of the circuit. The conduction velocity of the wave front and the length of the circuit determine the cycle length of the arrhythmias. The wavelength of the cardiac impulse is defined as the distance traveled by the depolarization wave in a time interval equal to the refractory period [29]. In anatomic reentry, the length of the circuitous pathway can be significantly longer than the wavelength of the impulse, leaving a segment of the reentrant circuit fully or partially excitable. This is called an 'excitable gap'. Because of such an excitable gap, the revolution time of the impulse in the circuit is determined primarily by its conduction velocity and will not be significantly influenced by moderate changes in the refractory period. Furthermore, rightly timed impulses originating from outside the circuit may enter it and either reset, entrain or terminate the rhythm.

1.1.2 Functional reentry

Anatomically bounded tracts or obstacles are not a prerequisite for the occurrence of reentry in the heart. Garrey was the first to observe this as he wrote in an article published in 1914: 'natural rings are not essential for the maintenance of circus contractions' [30]. Studies conducted by Allessie et al. have demonstrated the properties of reentry without an anatomical obstacle, e.g. the 'leading circle' concept [31–33]. In the absence of a fixed barrier, both localization and size of

the reentry circuit may vary, causing the 'leading circle' to drift through the myocardium. The central area of the circuit is kept refractory by centripetal wavelets and serves as an obstacle. The length of a functional reentrant circuit is therefore not fixed, but determined by the local electrophysiologic properties of the tissue, e.g. conduction speed and refractory period. The wavelength of the circulating impulse equals the dimensions of the circuit. This implies, that the depolarization wave circulates in the smallest possible pathway in which the electromotive force of the wave front is just strong enough to excite the tissue ahead, which is still in its relative refractory period. In other words, the head of the circulating wave front follows its own tail of refractoriness. The absence of an excitable gap implies that changes in the refractory period will influence the revolution time of the circuit. Thus, shortening of the refractory period will enable the impulse to circulate in a smaller circuit with a shorter revolution time thereby accelerating the circus movement rhythm. On the other hand, prolongation of the refractory period will result in a larger circular pathway and slowing of the rhythm or, if such a pathway is not available, in blocking of reentry and termination of the tachycardia.

The prevalence of unidirectional (functional) block remains mandatory for reentry to occur. Factors which may lead to transient functional conduction block are: 1) anisotropy of conduction in myocardial tissue [34–36]; 2) differences in membrane responsiveness of cardiac cells; 3) spatial dispersion in recovery from electrical activation. From the study of Allessie et al. in isolated rabbit left atrium, it emerged that a minimum difference of 11–16 ms in refractory period between adjacent areas, induced by a premature beat, may be sufficient to cause local conduction block [32].

In the absence of an anatomic obstacle, the dimensions of the arc of functional block is of great importance. This will determine, together with conduction speed and refractory period, whether or not reentry of the functional type will occur.

1.2 Localization of the arrhythmogenic substrate

Wellens et al. demonstrated that the predominant mechanism in postinfarction VT is indeed reentry and that VT can be reproducibly induced by using an extrastimulus technique [37–39]. The arrhythmogenic substrate is often anatomically localized in the subendocardium [38, 40]. De Bakker et al. proved that the extent of the slow conduction pathway can cover a substantial part of the left ventricle perimeter, confirming that VT in the postinfarction heart usually is caused by 'macro-reentry' [41–43].

When considering curative ablation of postinfarction ventricular tachycardia (VT), i.e. definite interruption of the anatomic reentry circuit, by means of either radiofrequency catheter ablation or antiarrhythmic surgery, several approaches are available for identification of ablation target sites. The anatomical localization of characteristic landmarks of the circuit can be derived from the electrophysiological properties of the reentrant circuit as described above. In general, two types of target sites can be selected: the VT exit site and the pathway of slow conduction.

1.2.1 Electrocardiographic localization of the exit site of VT

The terminal part of the tract of slow conduction, which inserts into the non-infarcted myocardium, is commonly called the exit site of VT. This VT exit site possesses distinguishable electrocardiographic features. Centrifugal spread of activation in non-infarcted myocardium that follows completion of conduction through the tract of slow conduction, results in a QS complex in the local unipolar electrogram. This implies that mapping of the left ventricular endocardium or epicardium can be performed to locate areas where QS complexes in the unipolar electrogram are found, displaying local activation that is early relative to the body surface QRS complex [44]. This concept should, however, be treated with caution since anisotropy of conduction due to the arrangement of fibers may also result in electrograms with QS complexes at sites where the wave front merely passes instead of originates [42]. At the body surface, intracardiac centrifugal spread of activation from the exit site will result in QS complexes in unipolar ECG leads, which are in close proximity to the VT exit site and observe a departing wave front. This principle has been used to localize the site of origin of VT by means of the 12-lead surface ECG [45, 46]. Both methods, endocardial catheter activation sequence mapping and 12-lead surface electrocardiographic mapping, have their own merits and drawbacks. For endocardial mapping, inducibility of VT, hemodynamical tolerance of the arrhythmia and paucity of VT morphologies are a prerequisite. Localization of the VT exit site by means of the 12-lead ECG is mostly hampered by the limited amount of spatial information that can be derived from a restricted set of predominantly precordial surface ECG leads. To circumvent the limitations associated with endocardial catheter activation sequence mapping and 12-lead ECG localization of VTs, body surface mapping (BSM) was introduced by SippensGroenewegen et al [47, 48]. In summary, this technique consists of obtaining spatially dense electrocardiographic data at the body surface. First, body surface QRS integral maps are constructed [49]. These dipolar QRS isointegral maps are characteristic for specific endocardial sites of origin of activation and subsequent spread of activation. By comparing these QRS isointegral maps to a database containing mean paced QRS isointegral maps from known endocardial sites, predictions about the presumed endocardial site of origin can be made on a beat-to-beat basis.

1.2.2 Localization of areas of slow conduction

Localization of the isthmus of slow conduction during ventricular tachycardia.

Whereas localization of exit sites of VT is considered to be adequate for surgical ablation of postinfarction VT, success rates of VT exit site directed radiofrequency catheter ablation appear to be lower [50–52]. This is presumably due the relative confined thermal lesion inflicted by radiofrequency catheter ablation in relation to the often large endocardial exit site area. This finding has encouraged other investigators to search for methods that allow for ablation of the tract of slow conduction.

Josephson et al. were the first to report that sites, where continuous electrical activity can be recorded during the diastole of VT, represent tracts of preserved conduction in the infarction scar [53]. De Bakker et al. later demonstrated that conceptualizing the reentrant circuit as a structure consisting of relatively few, anatomically bounded, tracts of slow conduction within the infarction scar is a histological and electrophysiological simplification [54]. In fact, the chronic postinfarction scar often consists of an intricate network of interconnecting, surviving fibers, some of which appear to be a critical part of the reentrant circuit, whereas others merely play a role as bystander [55]. Therefore, when aiming at interruption of the reentrant circuit, anatomical localization of tracts of slow conduction does not suffice: also the functional significance of pathways of slow conduction within the circuit will have to be clarified.

Functional characterization of tracts of slow conduction can be done by pace mapping of the infarction scar during VT [56]. Stevenson et al. introduced a structured approach for determination of the significance of tracts of slow conduction [55]. If concealed entrainment is obtained and specific stimulus-to-electrogram interval criteria are met, it is not only possible to identify a surviving bundle within the infarction scar, but it is also possible to identify whether that specific site is critical to the reentrant circuit [57]. At these sites radiofrequency energy can then be delivered. Still, for this method inducibility and sustenance of VT as well as hemodynamical tolerance of the arrhythmia are a prerequisite.

Instead of ablation during VT, attempts can be made to reconstruct the entire left ventricular area containing tracts of slow conduction during VT and subsequently perform the ablation during sinus rhythm. This can be done, if accurate information on the 3D position of the ablation catheter in the left ventricle can be combined with local activation times derived from that site. Several catheter position monitoring methodologies are currently available for this purpose [58, 59]. More recently, non-contact mapping techniques have been developed that give information on activation sequences in the heart on a beat-to-beat basis [60]. Some authors have reported on this approach of reconstructing the isthmus of slow conduction during VT with the aid of these 3D endocardial mapping techniques and subsequent creation of linear radiofrequency ablation lesions across this isthmus during sinus rhythm [61].

Localization of the substrate during sinus rhythm

Ideally, the critical part of the arrhythmogenic substrate should be localized during sinus rhythm. This would preclude the problems of multiple VT morphologies and non-inducibility or non-sustenance of VT. Furthermore, it would save patients from having to endure prolonged periods of VT during the ablation session [62].

Several methods to localize the area of functional or anatomical block during sinus rhythm have been proposed. Localization of the tract of slow conduction can be done by ventricular pacing of the postinfarction scar while measuring the delay between stimulus and QRS complex or comparing the derived paced QRS complexes with the VT QRS morphology [63–66]. This can be combined with the

timing of diastolic potentials relative to the QRS complex during sinus rhythm, but overall results appear to be disappointing [67]. More recently, elaborate techniques to locate the isthmus of VT by adaptive template matching or difference maps obtained by pacing in the setting of sinus rhythm at multiple sites have been proposed, but their clinical value remains to be proven [68, 69].

1.3 Identifying patients at risk for sudden cardiac death

1.3.1 Non-invasive identification of patients with areas of slow conduction

Berbari et al. were the first to describe the recording of arrhythmogenic signals at the end of the QRS complex in the late 1970's [70]. Later the concept of these late potentials was elaborated by Simson [71]. Late potentials are considered the body surface correlate of conduction in the intracardiac pathways of slow conduction and therefore signify the patient's predisposition for life threatening arrhythmias. Over the years, a large body of evidence has been gathered that links the presence of late potentials — in conjunction with other clinical variables — to an increased risk of sudden cardiac death [16,72–77]. Sensitivity of late potentials for predicting arrhythmic events appears to be limited [78].

1.3.2 Non-invasive identification of patients with disparity in repolarization

Disparity in repolarization is an important etiologic factor in postinfarction ventricular arrhythmias that have functional reentry as an underlying mechanism, e.g. ventricular fibrillation [79]. Several techniques have been developed to non-invasively identify patients subject to increased arrhythmia vulnerability because of their increased dispersion in repolarization. Among these techniques are QT dispersion, non-dipolar content of body surface mapped QRST integrals, and T-wave alternans [80–91].

1.4 Aim of this thesis

Much knowledge concerning the mechanisms and nature of the postinfarction arrhythmogenic substrate has been gathered in the past decades. The ever-expanding therapeutic options require more insight in the selection of postinfarction patients at risk for developing life-threatening arrhythmias as well as a better understanding of which therapy should be selected for an individual patient. Ideally, methods should be developed that 1) are non-invasive in nature 2) allow mapping during sinus rhythm 3) allow ablation during sinus rhythm.

Aim of this thesis was to gain more knowledge on the genesis of postinfarction arrhythmias by utilizing combined electrophysiologic and computational techniques that allow visualization and functional characterization of the mechanisms

underlying postinfarction ventricular arrhythmias. In **chapter 2** the clinical value of body surface mapping to guide antiarrhythmic surgery is investigated. In **chapter 3** the electrophysiological basis for failure of body surface mapping to identify the correct site of origin of postinfarction VT was analyzed by means of simultaneous multi-lead endocardial and body surface mapping of VT. In **chapter 4** new ways are explored that allow mapping of the postinfarction arrhythmogenic substrate during sinus rhythm. In **chapter 5** the use of signal averaged electrocardiography for detection of late potentials is extended to electrocardiographic monitoring of the entire body surface area. The purpose was twofold: 1) to investigate whether the sensitivity of signal averaged electrocardiography for detection of patients at risk can be increased and 2) to analyze the potential of spatially distributed late potentials at the body surface to anatomically delineate areas of slow conduction within the left ventricle. In **chapter 6** disparity in repolarization is investigated. Invasively obtained, spatially dense endocardial electrophysiologic repolarization measurements are compared with non-invasive ECG and body surface map parameters that are believed to estimate disparity in repolarization. In **chapter 7** the physical principles that form the basis of the computational techniques used for analysis of the postinfarction arrhythmogenic substrate in this thesis are explained. Finally, in **chapter 8** clinical implications of the currently presented work are discussed and future directives for arrhythmia research are suggested.

References

1] A. J. Moss and The Multicenter Postinfarction Research Group. Risk stratification and survival after myocardial infarction. *New England Journal of Medicine*, 309:331–336, 1983.

2] J. T. Bigger, J. L. Fleiss, R. Kleiger, J. P. Miller, L. M. Rolnitzky, and The Multicenter Postinfarction Research Group. The relationships among ventricular arrhythmias, left ventricular dysfunction, and mortality in the 2 years after myocardial infarction. *Circulation*, 69:250–258, 1984.

3] A. R. Willems, J. G. P. Tijssen, F. J. van Capelle, J. H. Kingma, R. N. Hauer, F. E. Vermeulen, P. Brugada, D. C. A. van Hoogenhuyze, and M. J. Janse. Determinants of prognosis in symptomatic ventricular tachycardia or ventricular fibrillation late after myocardial infarction. *Journal of the American College of Cardiology*, 16:521–530, 1990.

4] E. M. Vaughan Williams. A classification of antiarrhythmic actions reassessed after a decade of new drugs. *Journal of Clinical Pharmacology*, 17:129–147, 1984.

5] Task Force of the Working Group on Arrhythmias of the European Society of Cardiology. The sicilian gambit. A new approach to the classification of antiarrhythmic drugs based on their actions on arrhythmogenic mechanisms. *Circulation*, 84:1831–1851, 1991.

6] E. F. Wever, R. N. Hauer, F. J. van Capelle, J. G. Tijssen, H. J. Crijns, A. Algra, A. C. Wiesfeld, P. F. Bakker, and E. O. Robles de Medina. Randomized study of implantable defibrillator as first-choice therapy versus conventional strategy in postinfarct sudden death survivors. *Circulation*, 91:2195–2203, 1995.

7] E. F. Wever, R. N. Hauer, G. Schrijvers, F. J. van Capelle, J. G. Tijssen, H. J. Crijns, A. Algra, H. Ramanna, P. F. Bakker, and E. O. Robles de Medina. Cost-effectiveness of implantable defibrillator as first-choice therapy versus electrophysiologically guided, tiered strategy in postinfarct sudden death survivors. A randomized study. *Circulation*, 93:489–496, 1996.

8] The Antiarrhythmics versus Implantable Defibrillators (AVID) Investigators. A comparison of antiarrhythmic-drug therapy with implantable defibrillators in patients resuscitated from near-fatal ventricular arrhythmias. *New England Journal of Medicine*, 337:1576–1583, 1997.

9] S. J. Connolly, M. Gent, R. S. Roberts, P. Dorian, D. Roy, R. S. Sheldon, L. B. Mitchell, M. S. Green, G. J. Klein, and B. O'Brien. Canadian implantable defibrillator study (CIDS) : a randomized trial of the implantable cardioverter defibrillator against amiodarone. *Circulation*, 101:1297–1302, 2000.

10] K. H. Kuck, R. Cappato, J. Siebels, and R. Ruppel. Randomized comparison of antiarrhythmic drug therapy with implantable defibrillators in patients resuscitated from cardiac arrest : the cardiac arrest study hamburg (CASH). *Circulation*, 102:748–754, 2000.

11] H. M. Greenberg, E. M. Dwyer Jr., J. S. Hochman, J. S. Steinberg, D. S. Echt, and R. W. Peters. Interaction of ischaemia and encainide/flecainide treatment: a proposed mechanism for the increased mortality in CAST I. *British Heart Journal*, 74:631–635, 1995.

12] A. Langer, M. S. Heilman, M. M. Mower, and M. Mirowski. Considerations in the development of the automatic implantable defibrillator. *Medical Instrumentation*, 10:163–167, 1976.

13] M. Mirowski and M. M. Mower. Transvenous automatic defibrillator as an approach to prevention of sudden death from ventricular fibrillation. *Heart & Lung*, 2:867–869, 1973.

14] M. Mirowski, M. M. Mower, and A. I. Mendeloff. Implanted standby defibrillators. *Circulation*, 47:1135–1136, 1973.

15] A. I. Mushlin, W. J. Hall, J. Zwanziger, E. Gajary, M. Andrews, R. Marron, K. H. Zou, and A. J. Moss. The cost- effectiveness of automatic implantable cardiac defibrillators: results from MADIT. Multicenter Automatic Defibrillator Implantation Trial. *Circulation*, 97:2129–2135, 1998.

16] A. E. Buxton, K. L. Lee, J. D. Fisher, M. E. Josephson, E. N. Prystowsky, and G. Hafley. A randomized study of the prevention of sudden death in patients with coronary artery disease. Multicenter Unsustained Tachycardia Trial Investigators. *New England Journal of Medicine*, 341:1882–1890, 1999.

17] M. Glikson and P. A. Friedman. The implantable cardioverter defibrillator. *Lancet*, 357:1107–1117, 2001.

18] N. M. van Hemel, J. H. Kingma, J. J. Defauw, F. E. Vermeulen, E. G. Mast, J. M. P. G. Ernst, and C. A. Ascoop. Left ventricular segmental wall motion score as a criterion for selecting patients for direct surgery in the treatment of postinfarction ventricular tachycardia. *European Heart Journal*, 10:304–315, 1989.

19] N. M. van Hemel, J. H. Kingma, J. J. Defauw, E. Hoogteijling-van Dusseldorp, J. C. Kelder, W. P. Beukema, and F. E. Vermeulen. Continuation of antiarrhythmic drugs, or arrhythmia surgery after multiple drug failures. A randomized trial in the treatment of postinfarction ventricular tachycardia. *European Heart Journal*, 17:564–573, 1996.

20] M. E. Josephson, A. H. Harken, and L. N. Horowitz. Endocardial excision: a new surgical technique for the treatment of recurrent ventricular tachycardia. *Circulation*, 60:1430–1439, 1979.

21] L. N. Horowitz, A. H. Harken, J. A. Kastor, and M. E. Josephson. Ventricular resection guided by epicardial and endocardial mapping for treatment of recurrent ventricular tachycardia. *New England Journal of Medicine*, 302:589–593, 1980.

22] M. E. Josephson, L. N. Horowitz, S. R. Spielman, A. M. Greenspan, C. VandePol, and A. H. Harken. Comparison of endocardial catheter mapping with intraoperative mapping of ventricular tachycardia. *Circulation*, 61:395–404, 1980.

23] F. Morady, M. Harvey, S. J. Kalbfleisch, R. el Atassi, H. Calkins, and J. J. Langberg. Radiofrequency catheter ablation of ventricular tachycardia in patients with coronary artery disease. *Circulation*, 87:363–372, 1993.

24] Y. H. Kim, G. Sosa-Suarez, T. G. Trouton, S. S. O'Nunain, S. Osswald, B. A. McGovern, J. N. Ruskin, and H. Garan. Treatment of ventricular tachycardia by transcatheter radiofrequency ablation in patients with ischemic heart disease. *Circulation*, 89:1094–1102, 1994.

25] H. Kasanuki, S. Ohnishi, T. Nirei, M. Shoda, and S. Hosoda. Evaluation of proarrhythmic effect of antiarrhythmic drugs on ventricular tachycardia associated with congestive heart failure. *Japanese Circulation Journal*, 56:69–76, 1992.

26] T. A. Simmers, F. H. Wittkampf, R. N. Hauer, and E. O. Robles de Medina. In vivo ventricular lesion growth in radiofrequency catheter ablation. *Pacing & Clinical Electrophysiology*, 17:523–531, 1994.

27] G. R. Mines. On dynamic equilibrium in the heart. *The Journal of Physiology*, 46:349–382, 1913.

28] G. R. Mines. On circulating excitations in the heart muscles and their possible relation to tachycardia and fibrillation. *Transactions of the Royal Society of Canada*, pages 43–52, 1914.

29] N. Wiener and A. Rosenbluth. The mathematical formulation of the problem of conduction of impulses in a network of connected elements, specifically in cardiac muscle. *Archivas de Instituta Cardiologica Mexicana*, 16:205–265, 1946.

30] W. E. Garrey. The nature of fibrillatory contraction of the heart. Its relation to tissue mass and form. *American Journal of Physiology*, 33:414, 1914.

31] M. A. Allessie, F. I. Bonke, and F. J. Schopman. Circus movement in rabbit atrial muscle as a mechanism of tachycardia. *Circulation Research*, 33:54–62, 1973.

32] M. A. Allessie, F. I. Bonke, and F. J. Schopman. Circus movement in rabbit atrial muscle as a mechanism of tachycardia. II. The role of nonuniform recovery of excitability in the occurrence of unidirectional block, as studied with multiple microelectrodes. *Circulation Research*, 39:168–177, 1976.

33] M. A. Allessie, F. I. Bonke, and F. J. G. Schopman. Circus movement in rabbit atrial muscle as a mechanism of tachycardia. III. The "leading circle"concept: a new model of circus movemnet in cardiac tissue without the involvement of an anatomical obstacle. *Circulation Research*, 41:9–18, 1977.

34] M. S. Spach, W. T. Miller III, D. B. Geselowitz, R. C. Barr, J. M. Kootsey, and E. A. Johnson. The discontinuous nature of propagation in normal canine cardiac muscle. Evidence for recurrent discontinuities of intracellular resistance that affect the membrane currents. *Circulation Research*, 48:39–54, 1981.

35] M. S. Spach, W. T. Miller III, P. C. Dolber, J. M. Kootsey, J. R. Sommer, and Jr. Mosher Jr., C. E. The functional role of structural complexities in the propagation of depolarization in the atrium of the dog. Cardiac conduction disturbances due to discontinuities of effective axial resistivity. *Circulation Research*, 50:175–191, 1982.

36] M. S. Spach and P. C. Dolber. Relating extracellular potentials and their derivatives to anisotropic propagation at a microscopic level in human cardiac muscle. Evidence for electrical uncoupling of side-to-side fiber connections with increasing age. *Circulation Research*, 58:356–371, 1986.

37] H. J. Wellens, K. I. Lie, and D. Durrer. Further observations on ventricular tachycardia as studied by electrical stimulation of the heart. chronic recurrent ventricular tachycardia and ventricular tachycardia during acute myocardial infarction. *Circulation*, 49:647–653, 1974.

38] H. J. Wellens, D. Durrer, and K. I. Lie. Observations on mechanisms of ventricular tachycardia in man. *Circulation*, 54:237–244, 1976.

39] H. J. Wellens, R. M. Schuilenberg, and D. Durrer. Electrical stimulation of the heart in patients with ventricular tachycardia. *Circulation*, 46:216–226, 1972.

40] M. E. Josephson, L. N. Horowitz, A. Farshidi, and J. A. Kastor. Recurrent sustained ventricular tachycardia. I. mechanisms. *Circulation*, 57:431–440, 1978.

41] J. M. de Bakker, F. J. van Capelle, M. J. Janse, A. A. Wilde, R. Coronel, A. E. Becker, K. P. Dingemans, N. M. van Hemel, and R. N. Hauer. Reentry as a cause of ventricular tachycardia in patients with chronic ischemic heart disease: electrophysiologic and anatomic correlation. *Circulation*, 77:589–606, 1988.

42] J. M. de Bakker, R. Coronel, S. Tasseron, A. A. Wilde, T. Opthof, M. J. Janse, F. J. van Capelle, A. E. Becker, and G. Jambroes. Ventricular tachycardia in the infarcted, Langendorff-perfused human heart: role of the arrangement of surviving cardiac fibers. *Journal of the American College of Cardiology*, 15:1594–1607, 1990.

43] J. M. de Bakker, F. J. van Capelle, M. J. Janse, N. M. van Hemel, R. N. Hauer, J. J. Defauw, F. E. Vermeulen, and P. F. Bakker-de Wekker. Macroreentry in the infarcted human heart: the mechanism of ventricular tachycardias with a "focal" activation pattern. *Journal of the American College of Cardiology*, 18:1005–1014, 1991.

44] M. E. Josephson, L. N. Horowitz, A. Farshidi, J. F. Spear, J. A. Kastor, and E. N. Moore. Recurrent sustained ventricular tachycardia. 2. Endocardial mapping. *Circulation*, 57:440–447, 1978.

45] M. E. Josephson, L. N. Horowitz, H. L. Waxman, M. E. Chain, S. R. Spielman, A. M. Greenspan, F. E. Marchlinski, and M. D. Ezri. Sustained ventricular tachycardia: role of the 12-lead electrocardiogram in localizing site of origin. *Circulation*, 64:257–272, 1981.

46] D. L. Kuchar, J. N. Ruskin, and H. Garan. Electrocardiographic localization of the site of origin of ventricular tachycardia in patients with prior myocardial infarction. *Journal of the American College of Cardiology*, 13:893–903, 1989.

47] A. SippensGroenewegen, H. Spekhorst, N. M. van Hemel, J. H. Kingma, R. N. Hauer, J. M. de Bakker, M. J. Janse, and A. J. Dunning. The value of body surface mapping in localization of the site of origin of ventricular tachycardia:

catheter pacemapping compared with intraoperative activation mapping. *Circulation*, 82:237, 1990.

48] A. SippensGroenewegen, H. Spekhorst, N. M. van Hemel, J. H. Kingma, R. N. Hauer, J. M. de Bakker, C. A. Grimbergen, M. J. Janse, and A. J. Dunning. Localization of the site of origin of postinfarction ventricular tachycardia by endocardial pace mapping. Body surface mapping compared with the 12-lead electrocardiogram. *Circulation*, 88:2290–2306, 1993.

49] A. SippensGroenewegen, H. Spekhorst, N. M. van Hemel, J. H. Kingma, R. N. Hauer, M. J. Janse, and A. J. Dunning. Body surface mapping of ectopic left and right ventricular activation. QRS spectrum in patients without structural heart disease. *Circulation*, 82:879–896, 1990.

50] R. N. Hauer, M. T. de Zwart, J. M. de Bakker, J. F. Hitchcock, O. C. Penn, M. Nijsen-Karelse, and E. O. Robles de Medina. Endocardial catheter mapping: wire skeleton technique for representation of computed arrhythmogenic sites compared with intraoperative mapping. *Circulation*, 74:1346–1354, 1986.

51] R. N. Hauer, R. M. Heethaar, M. T. de Zwart, R. N. van Dijk, I. van der Tweel, C. Borst, and E. O. Robles de Medina. Endocardial catheter mapping: validation of a cineradiographic method for accurate localization of left ventricular sites. *Circulation*, 74:862–868, 1986.

52] S. M. Blanchard, G. P. Wallcott, J. M. Wharton, and R. E. Ideker. Why is catheter ablation less successful than surgery for treating ventricular tachycardia that results from coronary artery disease? *Pacing & Clinical Electrophysiology*, 17:2315–2335, 1994.

53] M. E. Josephson, L. N. Horowitz, and A. Farshidi. Continuous local electrical activity. A mechanism of recurrent ventricular tachycardia. *Circulation*, 57:659–665, 1978.

54] J. M. de Bakker, F. J. van Capelle, M. J. Janse, S. Tasseron, J. T. Vermeulen, N. de Jonge, and J. R. Lahpor. Slow conduction in the infarcted human heart. 'Zigzag' course of activation. *Circulation*, 88:915–926, 1993.

55] W. G. Stevenson, H. Khan, P. Sager, L. A. Saxon, H. R. Middlekauff, P. D. Natterson, and I. Wiener. Identification of reentry circuit sites during catheter mapping and radiofrequency ablation of ventricular tachycardia late after myocardial infarction. *Circulation*, 88:1647–1670, 1993.

56] F. Morady, A. Kadish, S. Rosenheck, H. Calkins, W. H. Kou, M. De Buitleir, and J. Sousa. Concealed entrainment as a guide for catheter ablation of ventricular tachycardia in patients with prior myocardial infarction. *Journal of the American College of Cardiology*, 17:678–689, 1991.

57] F. Bogun, M. Bahu, B. P. Knight, R. Weiss, W. Paladino, M. Harvey, R. Goyal, E. Daoud, K. C. Man, S. A. Strickberger, and F. Morady. Comparison of effective and ineffective target sites that demonstrate concealed entrainment in patients with coronary artery disease undergoing radiofrequency ablation of ventricular tachycardia. *Circulation*, 95:183–190, 1997.

58] W. G. Stevenson, E. Delacretaz, P. L. Friedman, and K. E. Ellison. Identification and ablation of macroreentrant ventricular tachycardia with the carto electroanatomical mapping system. *Pacing & Clinical Electrophysiology*, 21:1448–1456, 1998.

59] F. H. Wittkampf, E. F. Wever, R. Derksen, H. Ramanna, R. N. Hauer, and E. O. Robles de Medina. Accuracy of the Localisasystem in catheter ablation procedures. *Journal of Electrocardiology*, 32:7–12, 1999.

60] R. J. Schilling, N. S. Peters, and D. W. Davies. Mapping and ablation of ventricular tachycardia with the aid of a non-contact mapping system. *Heart*, 81:570–575, 1999.

61] F. E. Marchlinski, D. J. Callans, C. D. Gottlieb, and E. Zado. Linear ablation lesions for control of unmappable ventricular tachycardia in patients with ischemic and nonischemic cardiomyopathy. *Circulation*, 101:1288–1296, 2000.

62] K. Soejima, M. Suzuki, W. H. Maisel, C. B. Brunckhorst, E. Delacretaz, L. Blier, S. Tung, H. Khan, and W. G. Stevenson. Catheter ablation in patients with multiple and unstable ventricular tachycardias after myocardial infarction: short ablation lines guided by reentry circuit isthmuses and sinus rhythm mapping. *Circulation*, 104:664–669, 2001.

63] W. G. Stevenson, P. T. Sager, P. D. Natterson, L. A. Saxon, H. R. Middlekauff, and I. Wiener. Relation of pace mapping QRS configuration and conduction delay to ventricular tachycardia reentry circuits in human infarct scars. *Journal of the American College of Cardiology*, 26:481–488, 1995.

64] F. Bogun, M. Bahu, B. P. Knight, R. Weiss, R. Goyal, E. Daoud, K. C. Man, S. A. Strickberger, and F. Morady. Response to pacing at sites of isolated diastolic potentials during ventricular tachycardia in patients with previous myocardial infarction. *Journal of the American College of Cardiology*, 30:505–513, 1997.

65] T. Harada, W. G. Stevenson, D. Z. Kocovic, and P. L. Friedman. Catheter ablation of ventricular tachycardia after myocardial infarction: relation of endocardial sinus rhythm late potentials to the reentry circuit. *Journal of the American College of Cardiology*, 30:1015–1023, 1997.

66] K. E. Ellison, W. G. Stevenson, M. O. Sweeney, D. C. Lefroy, E. Delacretaz, and P. L. Friedman. Catheter ablation for hemodynamically unstable monomorphic ventricular tachycardia. *Journal of Cardiovascular Electrophysiology*, 11:41–44, 2000.

67] R. J. Schilling, D. W. Davies, and N. S. Peters. Characteristics of sinus rhythm electrograms at sites of ablation of ventricular tachycardia relative to all other sites: a noncontact mapping study of the entire left ventricle. *Journal of Cardiovascular Electrophysiology*, 9:921–933, 1998.

68] E. J. Ciaccio, M. M. Scheinman, and A. L. Wit. Relationship of specific electrogram characteristics during sinus rhythm and ventricular pacing determined by adaptive template matching to the location of functional reentrant circuits that cause ventricular tachycardia in the infarcted canine heart. *Journal of Cardiovascular Electrophysiology*, 11:446–457, 2000.

69] E. J. Ciaccio, A. C. Tosti, and M. M. Scheinman. Relationship between sinus rhythm activation and the reentrant ventricular tachycardia isthmus. *Circulation*, 104:613–619, 2001.

70] E. J. Berbari, B. J. Scherlag, R. R. Hope, and R. Lazzara. Recording from the body surface of arrhythmogenic ventricular activity during the S-T segment. *American Journal of Cardiology*, 41:697–702, 1978.

71] M. B. Simson. Use of signals in the terminal QRS complex to identify patients with ventricular tachycardia after myocardial infarction. *Circulation*, 64:235–242, 1981.

72] M. E. Josephson, M. B. Simson, A. H. Harken, L. N. Horowitz, and R. A. Falcone. The incidence and clinical significance of epicardial late potentials in patients with recurrent sustained ventricular tachycardia and coronary artery disease. *Circulation*, 66:1199–1204, 1982.

73] G. Breithardt, J. Schwarzmaier, M. Borggrefe, K. Haerten, and L. Seipel. Prognostic significance of late ventricular potentials after acute myocardial infarction. *European Heart Journal*, 4:487–495, 1983.

74] G. Breithardt, M. Borggrefe, B. Quantius, U. Karbenn, and L. Seipel. Ventricular vulnerability assessed by programmed ventricular stimulation in patients with and without late potentials. *Circulation*, 68:275–281, 1983.

75] D. L. Kuchar, C. W. Thorburn, and N. L. Sammel. Late potentials detected after myocardial infarction: natural history and prognostic significance. *Circulation*, 74:1280–1289, 1986.

76] J. A. Gomes, S. L. Winters, D. Stewart, S. Horowitz, M. Milner, and P. Barreca. A new noninvasive index to predict sustained ventricular tachycardia and sudden death in the first year after myocardial infarction: based on signal-averaged electrocardiogram, radionuclide ejection fraction and holter monitoring. *Journal of the American College of Cardiology*, 10:349–357, 1987.

77] D. L. Kuchar, C. W. Thorburn, and N. L. Sammel. Prediction of serious arrhythmic events after myocardial infarction: signal-averaged electrocardiogram, holter monitoring and radionuclide ventriculography. *Journal of the American College of Cardiology*, 9:531–538, 1987.

78] G. Breithardt, M. E. Cain, N. El-Sherif, N. C. Flowers, V. Hombach, M. Janse, M. B. Simson, and G. Steinbeck. Standards for analysis of ventricular late potentials using high-resolution or signal-averaged electrocardiography. A statement by a task force committee of the european society of cardiology, the american heart association, and the american college of cardiology. *Circulation*, 83:1481–1488, 1991.

79] C. J. Wiggers. The mechanism and nature of ventricular fibrillation. *American Heart Journal*, 20:399, 1940.

80] A. Ramdat Misier, T. Opthof, N. M. van Hemel, J. T. Vermeulen, J. M. de Bakker, J. J. Defauw, F. J. van Capelle, and M. J. Janse. Dispersion of 'refractoriness' in noninfarcted myocardium of patients with ventricular tachycardia or ventricular fibrillation after myocardial infarction. *Circulation*, 91:2566–2572, 1995.

81] C. P. Day, J. M. McComb, and R. W. Campbell. QT dispersion: an indication of arrhythmia risk in patients with long QT intervals. *British Heart Journal*, 63:342–344, 1990.

82] D. S. Rosenbaum, L. E. Jackson, J. M. Smith, H. Garan, J. N. Ruskin, and R. J. Cohen. Electrical alternans and vulnerability to ventricular arrhythmias. *New England Journal of Medicine*, 330:235–241, 1994.

83] C. S. Barr, A. Naas, M. Freeman, C. C. Lang, and A. D. Struthers. QT dispersion and sudden unexpected death in chronic heart failure. *Lancet*, 343:327–329, 1994.

84] R. L. Verrier and B. D. Nearing. Electrophysiologic basis for T wave alternans as an index of vulnerability to ventricular fibrillation. *Journal of Cardiovascular Electrophysiology*, 5:445–461, 1994.

85] D. S. Rosenbaum, P. Albrecht, and R. J. Cohen. Predicting sudden cardiac death from T wave alternans of the surface electrocardiogram: promise and pitfalls. *Journal of Cardiovascular Electrophysiology*, 7:1095–1111, 1996.

86] A. A. Armoundas, M. Osaka, T. Mela, D. S. Rosenbaum, J. N. Ruskin, H. Garan, and R. J. Cohen. T-wave alternans and dispersion of the QT interval as risk stratification markers in patients susceptible to sustained ventricular arrhythmias. *American Journal of Cardiology*, 82:1127–9, A9, 1998.

87] S. H. Hohnloser, T. Klingenheben, Y. G. Li, M. Zabel, J. Peetermans, and R. J. Cohen. T wave alternans as a predictor of recurrent ventricular tachyarrhythmias in ICD recipients: prospective comparison with conventional risk markers. *Journal of Cardiovascular Electrophysiology*, 9:1258–1268, 1998.

88] J. M. Pastore, S. D. Girouard, K. R. Laurita, F. G. Akar, and D. S. Rosenbaum. Mechanism linking T-wave alternans to the genesis of cardiac fibrillation. *Circulation*, 99:1385–1394, 1999.

89] S. H. Hohnloser. Macroscopic T wave alternans as a harbinger of sudden death. *Journal of Cardiovascular Electrophysiology*, 10:625, 1999.

90] T. Ikeda, T. Sakata, M. Takami, N. Kondo, N. Tezuka, T. Nakae, M. Noro, Y. Enjoji, R. Abe, K. Sugi, and T. Yamaguchi. Combined assessment of T-wave alternans and late potentials used to predict arrhythmic events after myocardial infarction. A prospective study. *Journal of the American College of Cardiology*, 35:722–730, 2000.

91] O. Costantini, C. Drabek, and D. S. Rosenbaum. Can sudden cardiac death be predicted from the T wave of the ECG? A critical examination of T wave alternans and QT interval dispersion. *Pacing & Clinical Electrophysiology*, 23:1407–1416, 2000.

2 Contribution of Body Surface Mapping to clinical outcome after surgical ablation of postinfarction ventricular tachycardia

P.F.H.M. van Dessel [1], N. M. van Hemel [1], A. SippensGroenewegen [5], J.M.T. de Bakker [3,4], A.C. Linnenbank [3,4], J.J.A.M.T. Defauw [2]

From the Heart Lung Center Utrecht, Department of Cardiology[1] and Cardio-Thoracic Surgery[2], St Antonius Hospital, Nieuwegein, and Department of Cardiology[3], University Medical Center, Utrecht, Experimental and Molecular Cardiology Group of the Cardiovascular Research Institute[4], Academic Medical Center, Amsterdam, The Netherlands, and the Section of Cardiac Electrophysiology, Department of Medicine and The Cardiovascular Research Institute[5], University of California, San Francisco, United States of America.

Submitted to the Journal of Electrocardiology

Part of this study was presented at the Annual Scientific Session of the American Heart Association, Dallas, 1994 and the Annual Scientific Sessions of the European Society of Cardiology, Amsterdam, 1995

2.1 Abstract

Objectives: To *investigate* the influence of body surface mapping on outcome of ventricular antiarrhythmic surgery.

Methods: Preoperative mapping is advocated to optimize map-guided antiarrhythmic surgery of postinfarction ventricular tachycardia. We sequentially analyzed the results of catheter activation sequence mapping, body surface mapping and intraoperative multielectrode mapping in 54 patients (Group A) and made a comparison with 30 control patients (group B) in whom catheter activation sequence mapping was omitted. Endpoints were actuarial survival, freedom of arrhythmia and comparability of the localization of sites of ventricular tachycardia origin.

Results: A total of 128 morphologically different monomorphic sustained ventricular tachycardias were mapped in group A. In group A, 87 ventricular tachycardias were mapped preoperatively with body surface mapping and 30 ventricular tachycardias with catheter activation sequence mapping. In 19 of 24 ventricular tachycardias (79%) that were localized with both mapping methods the ventricular tachycardia exit site was similar. In-hospital death was 1 of 85 (1.2 %). Actuarial freedom from ventricular arrhythmias at 4-year follow-up was 74.1±6.0% in group A vs. 90.0±5.5% in group B (p=0.10). In group A 14 of 54 patients died (29.6%), whereas 4 of 30 patients (13.3%) died in group B (p=0.09).

Conclusions: Arrhythmia freedom and survival is as good in patients mapped with body surface mapping only as in patients mapped with body surface mapping and catheter activation sequence mapping.

2.2 Introduction

Ventricular arrhythmias occurring late after myocardial infarction constitute an important etiologic factor in mortality from cardiac disease [1]. In contrast to symptomatic treatment strategies such as implantable cardioverter/defibrillators or antiarrhythmic drug therapy, percutaneous radiofrequency catheter ablation and map-guided surgical ablation of the arrhythmogenic substrate are considered to be curative approaches for treatment of these life-threatening postinfarction ventricular arrhythmias [2–4]. Detailed delineation of the site of the arrhythmogenic substrate is an essential prerequisite for both surgical and radiofrequency ablation [5].

Several authors have reported that extensive pre- and intraoperative mapping may improve surgical outcome [6–9]. Preoperative mapping remains an important method in surgical work-up since due to general anesthesia, ventriculotomy or removal of mural thrombi ventricular tachycardia (VT) may not be inducible during surgery. Historically, mapping efforts have been directed at detecting the site of VT origin — i.e. the exit from the zone of slow conduction into the non-infarcted myocardium — since this site offers the best discernible local electrographic features [10, 11]. Several non-invasive techniques, like the 12-lead electrocardiogram (ECG) and body surface mapping (BSM) and invasive techniques,

such as percutaneous endocardial catheter activation sequence mapping (CASM) and intraoperative endocardial and epicardial multielectrode mapping (IMEM), are presently available for electrophysiologic delineation of the site of VT origin [11–13]. Josephson et al. have shown that there is an adequate correlation between preoperative mapping data acquired with CASM and intraoperative mapping results obtained with IMEM [14]. Therefore CASM is generally accepted as the current method of choice for preoperative mapping of the site of origin of postinfarction VT.

SippensGroenewegen et al. reported on the use of non-invasive BSM as a means of detecting the site of origin of postinfarction VT [12]. Due to its non-invasive nature and its capability of determining the site of origin on the basis of one single heartbeat, BSM is not limited by the many disadvantages associated with CASM. At present, detailed information about the feasibility, applicability, and reproducibility of BSM, as well as the correlation in outcome between BSM and the other aforementioned mapping techniques is lacking. Furthermore, the issue whether BSM can replace CASM, which is often patient burdening and time consuming, remains unresolved. Therefore, we performed a prospective sequential group analysis study to analyze surgical outcome, survival and therapeutic efficacy data in a group of consecutive patients with postinfarction VT who underwent map-guided surgery after mapping with BSM, CASM and IMEM. These data were compared with another group patients undergoing postinfarction VT surgery after application of only BSM and IMEM.

2.3 Methods

Study patients and preoperative examination

All patients admitted to our hospital for arrhythmia surgery between July 1990 and July 1995 with a history of coronary artery disease, documented recurrent ventricular arrhythmias with or without aborted sudden cardiac death, as well as inducible monomorphic VT during preoperative programmed electrical stimulation, were included in the study. Patients were considered eligible for map-guided arrhythmia surgery if at least 3 of 9 segments of the left ventricle showed a normal contraction pattern according to a previously described angiographic wall motion score [15]. Ventricular arrhythmia surgery was considered indicated if the patient was refractory to antiarrhythmic drug treatment or as additional procedure in patients with postinfarction VT who underwent cardiovascular surgery for other reasons. Preoperative analysis was performed according to a routine preoperative protocol that included left and right sided heart catherization, coronary angiography, nuclear left ventricular ejection fraction determination, exercise stress testing, Holter monitoring, two-dimensional and Doppler echocardiography and programmed electrical stimulation. Patients, who underwent antiarrhythmic surgery between July 1990 and July 1993, constituted Group A and patients operated between July 1993 and July 1995 formed Group B. Group A intentionally underwent BSM, CASM and IMEM, whereas Group B was mapped with BSM and IMEM

only.

Preoperative electrophysiologic studies and body surface mapping

Conventional 12-lead ECG recordings and 64-lead BSM of spontaneously occurring clinical VTs were obtained. A VT was considered sustained, if it lasted for more than 30 seconds or if electrical cardioversion was required for termination due to hemodynamical deterioration. A particular VT morphology was considered documented if at least standard ECG leads I, II, III and V1 were available. All patients underwent an electrophysiologic study in the postabsorptive state at least five half-lives after discontinuation of antiarrhythmic medications. Induction of VT was carried out using a routine stimulation protocol including delivery of up to 3 extrastimuli with increasing prematurity following a train of 8 driven beats with three different cycle lengths (600, 500 and 430 ms). Stimulation impulses (width 2 ms, strength twice the diastolic threshold) were delivered by a 6 Fr quadripolar catheter positioned in the right ventricular apex or right ventricular outflow tract. If necessary, isoproterenol infusion was used to facilitate VT induction. Catheter mapping was performed by sequentially obtaining unipolar and bipolar local electrograms from multiple endocardial sites of the left ventricle with an exploring 7 Fr quadripolar catheter. A VT was defined mappable by catheter if it proved to be sustained and if mapping data from at least 15 different endocardial sites could be obtained. If a VT appeared to be non-mappable by catheter, because of hemodynamical deterioration, attempts were made to increase the VT cycle length with intravenous delivery of low dose procainamide. If multiple VT morphologies were induced, mapping was executed for these subsequent morphologies as well. The site of VT origin was defined as the mapping site at which the earliest local endocardial activation, i.e. the steepest descending slope (dV/dt_{min}) in the unipolar signal of the exploring ventricular catheter, was recorded with respect to the onset of the QRS complex on the simultaneously recorded surface ECG [10].

Body surface mapping data were recorded using a 64-channel ECG recording system and a radiotransparent carbon unipolar electrode grid that does not interfere with fluoroscopic imaging during catherization (figure 2.1). The electrodes were positioned in 14 flexible vertical straps and applied on the anterior and posterior thoracic surface as described elsewhere [16]. Analogue to digital conversion occurred at a sampling frequency of 1 kHz, and 14-bits resolution. Wilson's central terminal was used as the reference [17, 18]. The amplifier system had a bandpass characteristic using a frequency range of 0.16 – 120 Hz (3 dB frequencies). Data were transmitted using a fiberoptic transmission unit and stored in a 486 PC microcomputer. For on-line data processing and analysis a second computer system was available (Commodore Amiga 2000, Commodore ltd.) which was connected to the data acquisition personal computer by a parallel connection.

To correct for any contribution of baseline drift to the QRS integral, baseline correction was performed. Two markers were placed in isoelectrical intervals before and after the QRS complex under study. If the cycle length of VT was short,

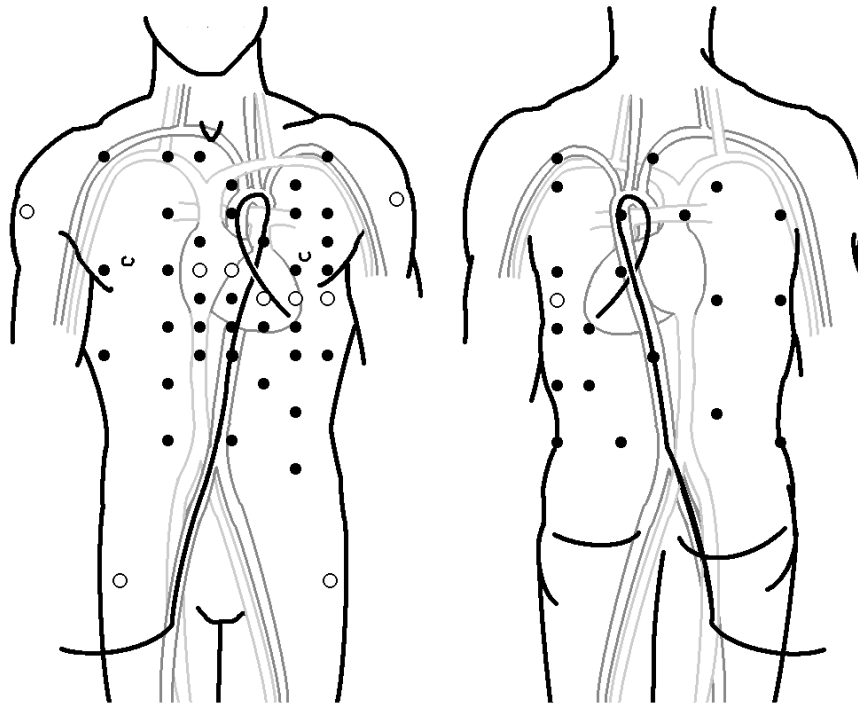

Figure 2.1: *Orientation of the body surface mapping electrode array relative to the heart. Open dots represent electrodes also utilized in standard 12-lead electrocardiography. Solid dots represent the additional electrodes in the array.*

baseline markers were placed at the putative onset of the QRS complex of the next and preceding complex of the QRS complex under study. Linear interpolation was performed between the baseline markers and each sample of the QRS complex was adjusted proportionally according to the newly derived baseline. After baseline adjustment, the QRS integral area was calculated. For each ECG tracing the QRS integral was obtained by integrating the area within an interval between onset and offset of the QRS complex. The onset and offset of the QRS complex are considered to be isoelectrical and therefore selection of onset and offset was such, that instantaneous voltages of less than 0.05 V in all ECG tracings were reached.

Body surface isointegral maps were calculated from the individual QRS integrals by spatial interpolation (figure 2.2) and were quantitatively correlated with two previously developed databases comprising mean paced QRS integral maps produced at 18 to 22 different specific endocardial segments. These twp databases included inferior myocardial infarction and anterior myocardial infarction to correct for geometrical deformations of the left ventricle due to earlier infarctions [19]. The computational derived VT origin was based on the location of the segment

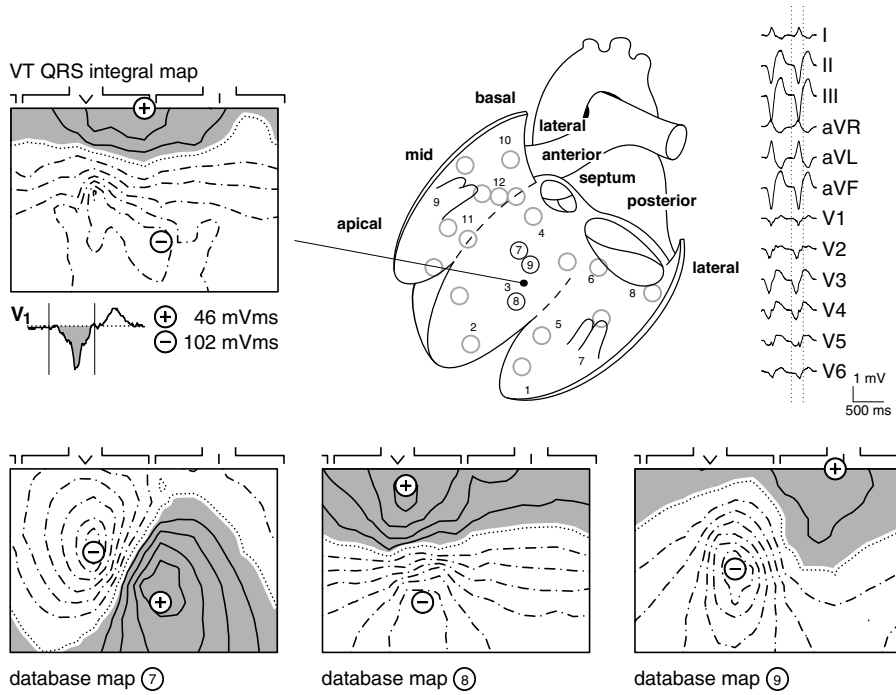

Figure 2.2: *Calculation of the site of origin with body surface mapping. The left upper map displays the body surface QRS integral map with corresponding ECG lead V1 of a ventricular tachycardia (VT) in a patient with anterior myocardial infarction. Three QRS integral maps from midseptal pacing segments of the anterior myocardial infarction pacing database (7, 8 and 9) are displayed in the bottom part. The locations of the endocardial segments at which the mean paced QRS integral patterns were previously generated as well as the Josephson localization scheme are represented in the left ventricular diagram. Best match in zero line configuration and mutual distance and orientation of the positive and negative extreme is obtained in database map 8, thereby indicating a midseptal site of origin of the VT under study.*

corresponding to the best matching QRS integral map from the database. Quantitative map comparison was checked by visual analysis of the VT QRS integral and individual mean paced QRS integral maps from the database and adapted when necessary if agreement was reached between 2 observers.

Intraoperative electrophysiologic study and surgical techniques

The same cardiovascular surgeon performed all operative procedures. Surgery took place in the drug free state whenever possible. All patients were anaesthetized using nitrous oxide, narcotics and muscle relaxants. Normothermic cardiopulmonary bypass was initiated with the perfusion temperature maintained at

37°C. Two needle electrodes were attached to the left and right shoulder to serve as far field reference electrodes for the unipolar balloon electrodes. Epicardial electrodes were placed on the right ventricular outflow tract and the right atrium. The left ventricular aneurysm or scar was incised and an inflatable balloon containing 64 unipolar electrodes was placed in the left ventricular cavity. Depending on the anterior or inferior location of the left ventricular aneurysm a choice was made between 2 differently shaped endocardial balloons [20]. Standard surface ECG leads I, II and III and V1 as precordial lead were simultaneously recorded during the operation. Recordings of sinus rhythm before and during surgery were compared to check for any possible electrical heart axis rotation caused by the opening of the thorax, the ventriculotomy and the positioning of the balloon. Programmed electrical stimulation using the right ventricular electrode and an induction protocol of up to 4 extrastimuli was carried out, if necessary with additional infusion of isoproterenol. After induction of every new sustained monomorphic VT endocardial maps were obtained using a computerized mapping system [20]. The site of origin was defined as the site at which the earliest local presystolic activation — characterized by the steepest descending slope (dV/dt_{min}) in the unipolar signal — was recorded with reference to the onset of the simultaneously recorded QRS complex on the surface ECG. Pre- and intraoperative VT morphologies were considered to be the same if surface ECG leads I, II, and III during sinus rhythm and during VT were identical. Information on the site of origin as obtained with BSM, IMEM and CASM was handed to the surgeon and presented in a schematic diagram of the left ventricular endocardium that was based on the Josephson 12-site left ventricular mapping scheme [10]. The surgical procedure consisted of subendocardial resection, endocardial cryoablation or a combination of these procedures [21]. After completion of the surgical arrhythmia ablation, the ventriculotomy was closed and if additional surgical procedures, such as ventricular aneurysm remodeling, valve replacement or myocardial revascularization, were mandatory, the patient was cooled, the aorta was cross-clamped, cold crystalloid cardioplegia was administered and the surgical procedure was completed by standard techniques.

Postoperative electrophysiologic study

In all patients, a postoperative electrophysiologic study using temporary epicardial right ventricular wires and a stimulation protocol up to 3 extrastimuli in accordance to the preoperatively applied methodology was performed 7 to 10 days after surgery. A sustained monomorphic VT induced using one extrastimulus, was considered clinically significant and in these cases antiarrhythmic drug therapy guided by sequential electrophysiologic drug testing was instituted. Induction of sustained monomorphic VT using two or more extrastimuli was not considered to be a surgical failure per se, but antiarrhythmic drug treatment was administered until follow-up programmed electrical stimulation in the drug free state was undertaken after 6 months to evaluate the indication for prolonged antiarrhythmic drug therapy. Induction of polymorphic VT or ventricular fibrillation was not considered a surgical failure and antiarrhythmic drugs were not given routinely.

Comparison of sites of origin

For each mapping method, sites of origin were assessed as described above. Ventricular tachycardias were considered morphologically identical if the ECG morphology — as determined from the ECG leads I, II and III and other ECG leads if available — were identical during sinus rhythm and during VT for each mapping procedure. If no match with any known VT morphology could be found then the VT morphology was classified as a new morphology.

Since each mapping technique used a different classification system to indicate a specific endocardial area of VT origin, all sites of origin were translated into the 12 "Josephson locations" for catheter mapping as a common denominator. Each Josephson location comprises an endocardial area of approximately 4 cm^2 [14]. Sites of VT origin identified by different mapping techniques were considered identical if they originated from the same or the bordering half of the adjacent Josephson location. Although translating mapping data to a Josephson location meant a loss of spatial resolution concerning the specific delineation of the site of VT origin as derived from BSM and IMEM mapping data, Josephson locations were considered to contain sufficient information for targeted guidance of surgical ablation.

Long-term follow-up

Long-term follow-up was obtained in all patients. Data concerning recurrence of VT and mortality were collected from out-patient clinic visits, letters from referring cardiologists or direct telephonic contacts with patients, relatives or local physicians. Surgical failure was classified as spontaneous recurrence of VT, inducible VT during programmed electrical stimulation requiring antiarrhythmic drug therapy or (aborted) sudden death.

Statistical analysis

All data were stored in a computerized patient record database. Data analysis was performed on a personal computer using the 'The SAS System for Windows 6.08 statistical software' (SAS Institute, Inc). Continuous data are presented as mean values $\pm$ SD unless stated otherwise. Subgroup comparisons were made using χ-square or Fisher's exact test, whenever appropriate. Analysis of therapeutic failure and survival was performed by the Kaplan-Meier method and compared in both groups by the log-rank test. Proportional hazard analysis was performed using the Cox regression model. Statistical significance was defined as a P value < 0.05.

2.4 Results

Study population

Fifty-seven consecutive patients who underwent ventricular arrhythmia surgery for recurrent VT between July 1990 and July 1993 were included in group A. One patient underwent emergency surgery without intraoperative mapping attempts and one patient turned out to be non-inducible during preoperative and intraoperative programmed electrical stimulation. In 1 patient mapping attempts were deliberately omitted because of the extent of the associated coronary artery disease. Therefore these 3 patients were excluded from the study. Group B consisted of 30 patients who were operated on between July 1993 and July 1995. Baseline clinical characteristics for both groups were comparable (Table 2.1). All patients underwent arrhythmia surgery more than 3 weeks after their most recent myocardial infarction to allow for adequate healing of the myocardial scar.

Comparison of sites of origin

Group A. In total, 160 distinct sustained monomorphic VT morphologies were recorded in 54 patients. Successful mapping with at least 1 mapping method was performed in 128 (80 %) of these 160 VTs. No mapping data were available in 32 documented VT morphologies (24 patients) because these VT morphologies were documented outside the electrophysiology laboratory, e.g. in referring hospitals without BSM facilities, or because the VT terminated before a mapping attempt was completed. The distribution of the mapping procedures is shown in figure 2.3. In only 12 VT morphologies (12 patients), localization data from all three mapping methods could be obtained. In 24 VT morphologies (22 patients) mapping data was acquired with BSM and CASM, in 16 VTs (16 patients) IMEM and CASM was performed and in 36 VTs (20 patients) the site of origin was derived using IMEM and BSM. In 10 patients, no intraoperative VT mapping could be performed due to non-inducibility of sustained monomorphic VT.

Results on concordance in mapping findings are shown in Table 2.2. For 19 of 24 VTs documented with BSM and CASM (79 %) a similar exit was found, whereas 21 of 36 VTs (58 %) localized with IMEM and BSM showed comparable exits. Mapping data obtained exclusively from IMEM and CASM were available from 16 VTs of which 9 VTs (56 %) were considered to have the same site of origin. If all 3 mapping methods could be applied 7 of 12 VTs (58 %) were found to have the same exit in all mapping procedures. Although BSM and CASM tended to correlate better than IMEM and BSM (difference 21 %, 95% CI -2 to 44 %) or CASM and IMEM (difference 23 %, 95% CI -6 to 52 %), no statistical significance was reached.

Group B. In 30 patients 58 VT morphologies were documented. Successful mapping with BSM, IMEM or both was achieved in 41 (70.7 %) of these 58 VTs. No successful mapping could be performed in 17 VTs (12 patients). Distribution of the mapping procedures is shown in figure 2.3. Comparable exit sites were found in 3 (50 %) of 6 VTs mapped with both IMEM and BSM, which is not significantly different from Group A.

	Group A (N=54)	Group B (N=54)
Age (years)	64.1 ± 7.8	63.7 ± 8.8
Sex		
Male	47 (87 %)	27 (90 %)
Female	7 (13 %)	3 (10 %)
No. of VT morphologies per patient[&]	2.3 (1 – 7)	1.6 (1 – 7)
No. of AAD trials prior to surgery[&]	1.2 (1 – 5)	1.0 (1 – 5)
Baseline PES		
No. of VT morphologies[&]	1.9 (1 – 5)	1.2 (1 – 7)
VT cycle length (ms)	314.2 ± 60.7	313.4 ± 54.5
Scintigraphic LVEF (%)	28.3 ± 11.5	36.0 ± 12.6
WMS (max. 9 of 9 segments)[&]	3.6 (3-6)	3.3 (3-7)
Extent of coronary artery disease		
1 vessel	18 (33 %)	9 (30 %)
2 vessel	17 (32 %)	9 (30 %)
3 vessel	19 (35 %)	12 (40 %)
Location of myocardial infarction		
Anterior	31 (57 %)	16 (53 %)
Inferior	21 (39 %)	14 (47 %)
Anterior and Inferior	2 (4 %)	0 (0 %)
Concomitant surgery		
CABG	32 (59 %)	5 (9 %)
MVR/MVP	23 (77 %)	3 (10 %)
Cardiopulmonary bypass (min)	119.5 ± 39.9	133.7 ± 53.5
Intraoperative mapping (min)	22.4 ± 6.8	24.0 ± 6.8
Aortic cross clamping time (min)	56.8 ± 24.9	60.4 ± 33.1

Table 2.1: *Baseline characteristics (AAD = antiarrhythmic drugs; CABG = coronary artery bypass grafting; LVEF = left ventricular ejection fraction; MVR/MVP = mitral valve replacement or valvuloplasty; PES = programmed electrical stimulation; WMS = wall motion score; VT = ventricular tachycardia.* [&] *= Data shown as median (range)).*

Analysis of survival and freedom of arrhythmic events

Group A. One of 85 patients (1.2 %) died in-hospital due to a flucloxacillin resistant staphylococcal sepsis. The follow-up for the entire group A was 4.0 years. Actuarial survival at 4-year follow-up as estimated by the Kaplan-Meier product-limit method was 70.4 ± 6.2 % (mean ± standard error) (Figure 2.4). In total, 14 of 54 (25.9%) patients died. Causes of death are summarized in table 2.3. Spontaneous recurrence of VT was documented in 9 patients after 0.2 to 33.2 months following surgery. Cumulative freedom of recurrence of fatal or non-fatal ventricular

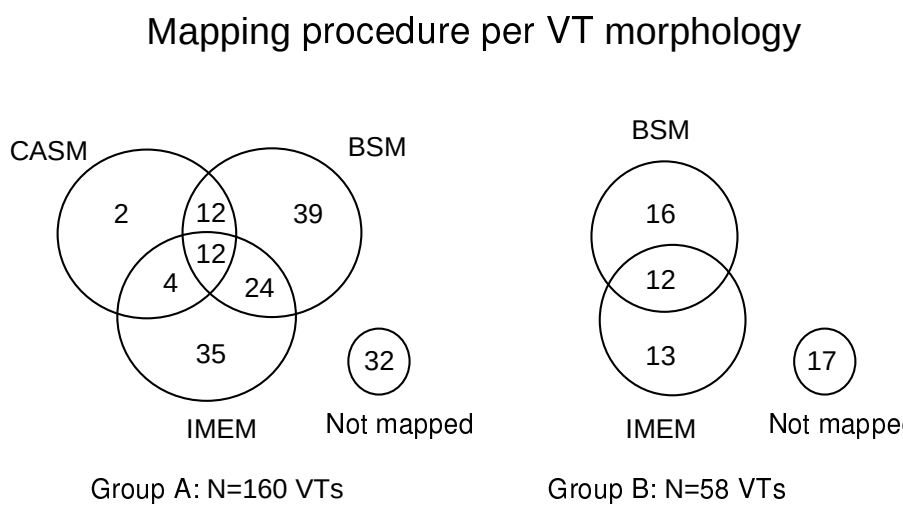

Figure 2.3: *Distribution of successful mapping attempts indicated by procedure, for a total of 160 ventricular tachycardia morphologies induced in group A and Group B. Group A includes patients who intentionally underwent body surface mapping, catheter activation sequence mapping and intraoperative multielectrode mapping to guide arrhythmia surgery, while Group B includes patients who intentionally underwent body surface mapping and intraoperative multielectrode mapping. (CASM = catheter activation sequence mapping, BSM = body surface mapping, IMEM = intraoperative multielectrode mapping).*

	Group B			
Mapping Methods	Number of VTs	Similar findings	Number of VTs	Similar findings
BSM vs. CASM	24 (18.8 %)	79 %	N/A	N/A
BSM vs. IMEM	36 (28.1 %)	58 %	6 (14.6 %)	50 %
IMEM vs. CASM	16 (12.5 %)	56 %	N/A	N/A
IMEM vs. CASM vs. BSM	12 (9.4 %)	58 %	N/A	N/A

Table 2.2: *Concordance of mapping results using Body Surface Mapping (BSM=Body Surface Mapping; CASM=Catheter Activation Mapping; IMEM=Intraoperative Multi-Electrode Mapping; VT=Ventricular Tachycardia)*

	Group A (N=54)	Group B (N=30)
Congestive heart failure	6	0
Sudden death	5	1
Non-cardiac mortality	3	2

Table 2.3: *All cause mortality.*

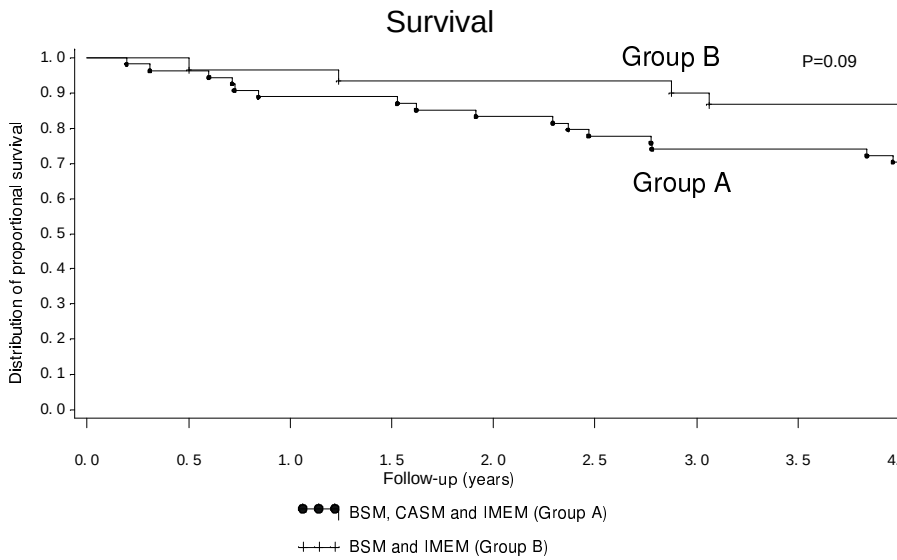

Figure 2.4: *Proportional survival from all causes of death during 4-year follow-up after map-guided postinfarction ventricular tachycardia surgery. Group A includes patients who intentionally underwent body surface mapping, catheter activation sequence mapping and intraoperative multielectrode mapping to guide arrhythmia surgery, while Group B includes patients who intentionally underwent body surface mapping and intraoperative multielectrode mapping.*

arrhythmia at 4-year follow-up was 74.1 $\pm$ 6.0 % (Fig. 4)

Group B. There were no in-hospital deaths. During follow-up of 48 to 72 months 3 patients died (Table 2.3). In 4 of 30 (13.3%) patients inducibility of VT during postoperative programmed electrical stimulation using 3 extrastimuli persisted and programmed electrical stimulation guided antiarrhythmic drug treatment was instituted and were scheduled to undergo programmed electrical stimulation after 6 months. One of these 4 patients had a spontaneous recurrence 2 weeks later and therefore this patient was considered a surgical failure. Cumulative survival at 4-year follow-up as estimated by the Kaplan-Meier product-limit method was 86.6 $\pm$ 6.2 % (Figure 2.4). Cumulative survival in group B did not differ significantly from group A (P = 0.09). In total, spontaneous recurrence of VT or persisting inducibility of VT requiring antiarrhythmic drugs was documented in 5 patients. Cumulative freedom of any recurrence of ventricular arrhythmia at 4-years of follow-up was 90.0 $\pm$ 5.5 % (Figure 2.5). Again, postoperative recurrence of ventricular arrhythmias was not significantly different in both groups (P = 0.10).

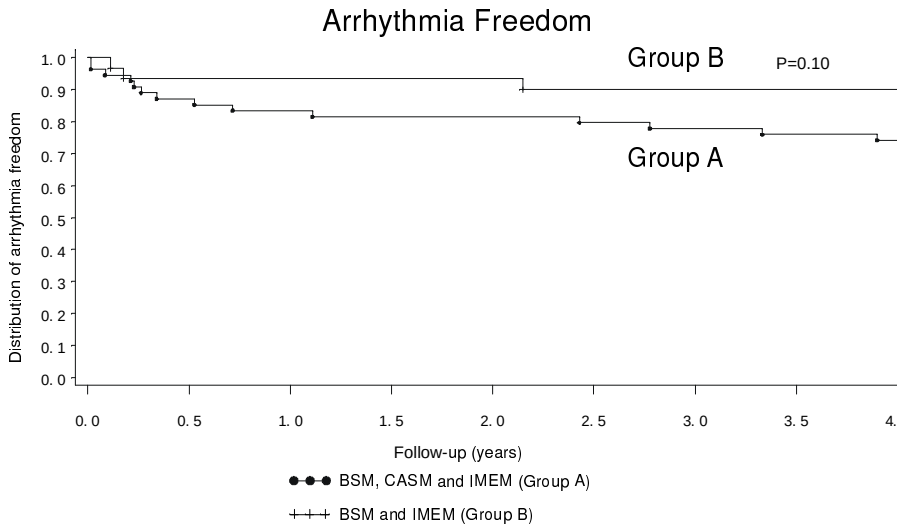

Figure 2.5: *Proportional freedom of recurrences of fatal or non-fatal ventricular arrhythmias or (aborted) sudden death during 4-year follow-up after map-guided postinfarction ventricular tachycardia surgery. Group A include patients who intentionally underwent body surface mapping, catheter activation sequence mapping and intraoperative multielectrode mapping to guide arrhythmia surgery, while Group B includes patients who intentionally underwent body surface mapping and intraoperative multielectrode mapping.*

Proportional hazard analysis

To identify factors predisposing for recurrence of fatal or non-fatal ventricular arrhythmias or death, a proportional hazard analysis according to the Cox regression model was performed. Clinically relevant variables at baseline such as age, gender, pre- and intraoperative mapping strategy, concomitant myocardial revascularization, the period in which the operation occurred, number of preoperative VT morphologies, average VT cycle length, preoperative angiographic wall motion score and extent of coronary artery disease were included in a forward selection model. The P value for entry into the model was set at 0.10. Two models were constructed. In model A, the recurrence of ventricular arrhythmias was analyzed. None of the aforementioned clinical variables appeared to contribute to the model, with the entry level of significance set at 0.10. In model B the occurrence of death from all causes and recurrence of fatal or non-fatal ventricular arrhythmias was reviewed. The resulting model B (Table 2.4) consisted of a single variable, namely the period in which the patient underwent surgery, as the only significantly contributing variable (P=0.04).

	Relative Risk (95% CI)	P-value
Operated between 01.07.90 and 01.07.93	2.4 (1.0 - 6.0)	0.04
Age		0.36
Concomitant coronary revascularization		0.36
Average VT cycle length		0.39
Catheter activation sequence mapping		0.43
Intraoperative mapping		0.47
Number of VT morphologies		0.82
Female gender		0.85
Body surface mapping		0.91

Table 2.4: *Proportional hazard analysis of occurrence of death from all causes or recurrence of fatal or non-fatal ventricular arrhythmias using the Cox regression model (VT=ventricular tachycardia)*

2.5 Discussion

Although there has been a decline in the number of centers performing surgical ablations for postinfarction ventricular arrhythmias, antiarrhythmic surgery can still be considered an efficacious treatment of postinfarction VT in patients requiring open heart surgery for additional indications such as myocardial revascularization or aneurysmectomy. At present, 15 patients on average undergo antiarrhythmic surgery each year in our hospital (1998: 12 patients; 1999: 17 patients; 2000: 18 patients). Preoperative mapping remains mandatory since during surgery it may be impossible to localize the sites of origin of VT due to noninducibility.

The site of origin of postinfarction VT is electrocardiographically well defined in terms of earliest presystolic local endocardial activation and its detection can reliably be done by invasive measures such as CASM and IMEM. From our study, BSM and CASM appeared to correlate well (79 %). Comparability between CASM and IMEM on the one hand and BSM and IMEM on the other tended to be less, although the lack of data on the precordial ECG morphology during surgery seems to hamper correct identification of VT morphologies.

Major advantages of BSM are its convenience of use, its low cost and the possibility of mapping otherwise unmappable VTs, such as spontaneously occurring VTs, hemodynamically unstable tachycardias and non-sustained VTs. These advantages clearly increase the preoperative yield of BSM as compared to CASM. In group A 87 of 128 VTs (67.9 %) were localized with BSM whereas only 30 of 128 VTs (23.4 %) could be localized with CASM ($P<0.0001$).

The influence of mapping data on technical decisions of the surgeon during the operative procedure is difficult to measure. The surgeon's view on the arrhythmogenic substrate is undoubtedly influenced by the electrophysiological data ac-

quired with the pre- and intraoperative mapping procedures as well as by local anatomical data as obtained by direct visual inspection of the endocardial scar. Therefore, the question whether BSM can replace CASM as preoperative mapping procedure for arrhythmia surgery of postinfarction VT can best be answered in terms of clinical outcome. As compared to results reported by other authors, overall satisfying follow-up data were achieved [22]. Using the Kaplan-Meier estimate of event freedom, no significant difference could be found in survival analysis from all causes of mortality or freedom of recurrence of ventricular arrhythmias in patients intentionally mapped with CASM, BSM and IMEM as compared to patients in whom CASM was abandoned.

A proportional hazard analysis using a Cox regression model analysis was performed to investigate whether specific clinical variables predisposed for surgical failure. The preoperative mapping strategy appeared to have no independent influence on surgical outcome. Only the period, in which the patient underwent arrhythmia surgery, turned out to be an independent risk factor (relative risk = 2.4, 95%, confidence interval 1.0 – 6.0) for occurrence of major clinical events, not influenced by the pre- and intraoperative mapping strategy or other clinical variables. This information suggests that the indication for ventricular arrhythmia surgery may have changed over the years. It is our belief, that the advent of implantable cardioverter/defibrillator therapy allows for more stringent patient selection and that improved therapeutic strategies of patients with congestive heart failure, such as ACE inhibition and β-blockade, offer better postoperative management of these patients who often have a moderate to severe left ventricular dysfunction [23, 24]. We were not able to demonstrate any influence of the performance of CASM on the occurrence of fatal or non-fatal clinical events (Table 2.4). From this and other studies BSM appears to be a valid tool for delineating site of origin of postinfarction VT for map-guided surgical ablation [12, 19, 25]. Therefore, we conclude that catheter mapping, which is time consuming, potentially hazardous and patient burdening, can be safely omitted in the preoperative management of patients undergoing ventricular arrhythmia surgery and substituted by BSM.

Limitations

In order to compare mapping data obtained with BSM, CASM and IMEM, data on the site of origin had to be translated to Josephson locations as a common denominator. Although BSM and particularly IMEM are capable of providing high-resolution delineation of the endocardial site of origin, this resolution was decreased in the translation process. However, the objective of the mapping procedures was to provide the surgeon with data for surgical ablation of the arrhythmogenic substrate. The above-mentioned translation was considered to contain sufficient information for these purposes.

2.6 Conclusions

Ventricular arrhythmia surgery remains an efficacious treatment of late ventricular arrhythmias following myocardial infarction in selected patients. Detailed pre- and intraoperative mapping allows for selective elimination of the arrhythmogenic substrate. BSM appears to be an easy-to-use alternative method for localizing the site of origin of postinfarction VT and allows analysis of otherwise unmappable arrhythmias such as spontaneous VTs and hemodynamically not well-tolerated ventricular arrhythmias. As compared to the currently applied method for mapping of VTs in the electrophysiology laboratory BSM seems to offer comparable results in localizing the site of origin of postinfarction VTs. CASM can be safely omitted as a preoperative mapping method, since therapeutic efficacy and postoperative mortality are not influenced. Detailed VT exit site mapping for all spontaneous and induced VT morphologies increases the extent of the identified arrhythmogenic region. BSM can be expected to play an important role in these methodologies by determining the exit sites of the re-entry circuit and thereby delineating the area where crucial components can be found.

Acknowledgements

The authors wish to express their gratitude to Mrs. Elly Hoogteijling-van Dusseldorp for collecting patient data and Johannes C. Kelder, M.D., for statistical assistance.

References

1] A. R. Willems, J. G. P. Tijssen, F. J. van Capelle, J. H. Kingma, R. N. Hauer, F. E. Vermeulen, P. Brugada, D. C. A. van Hoogenhuyze, and M. J. Janse. Determinants of prognosis in symptomatic ventricular tachycardia or ventricular fibrillation late after myocardial infarction. *Journal of the American College of Cardiology*, 16:521–530, 1990.

2] Y. H. Kim, G. Sosa-Suarez, T. G. Trouton, S. S. O'Nunain, S. Osswald, B. A. McGovern, J. N. Ruskin, and H. Garan. Treatment of ventricular tachycardia by transcatheter radiofrequency ablation in patients with ischemic heart disease. *Circulation*, 89:1094–1102, 1994.

3] F. Morady, M. Harvey, S. J. Kalbfleisch, R. el Atassi, H. Calkins, and J. J. Langberg. Radiofrequency catheter ablation of ventricular tachycardia in patients with coronary artery disease. *Circulation*, 87:363–372, 1993.

4] J. P. Bourke, R. W. Campbell, J. M. McComb, S. S. Furniss, J. C. Doig, and C. J. Hilton. Surgery for postinfarction ventricular tachycardia in the preimplantable cardioverter defibrillator era: early and long term outcomes in 100 consecutive patients. *Heart*, 82:156–162, 1999.

5] J. M. Miller, C. D. Gottlieb, F. E. Marchlinski, W. C. Hargrove, and M. E. Josephson. Does ventricular tachycardia mapping influence the success of antiarhhythmic surgery? *Journal of the American College of Cardiology*, 11:112, 1988.

6] J. Krafchek, G. M. Lawrie, R. Roberts, S. A. Magro, and C. R. Wyndham. Surgical ablation of ventricular tachycardia: improved results with a map-directed regional approach. *Circulation*, 73:1239–1247, 1986.

7] A. S. Manolis, H. Rastegar, D. Payne, R. Cleveland, and N. A. Estes III. Surgical therapy for drug-refractory ventricular tachycardia: results with mapping-guided subendocardial resection. *Journal of the American College of Cardiology*, 14:199–208, 1989.

8] C. D. Swerdlow, J. W. Mason, E. B. Stinson, P. E. Oyer, R. A. Winkle, and G. C. Derby. Results of operations for ventricular tachycardia in 105 patients. *Journal of Thoracic & Cardiovascular Surgery*, 92:105–113, 1986.

9] D. M. Fitzgerald, K. J. Friday, J. A. Yeung Lai Wah, R. Lazarra, and W. M. Jackman. Electrogram patterns predicting successful catheter ablation of ventricular tachycardia. *Circulation*, 77:806–814, 1988.

10] M. E. Josephson, L. N. Horowitz, A. Farshidi, J. F. Spear, J. A. Kastor, and E. N. Moore. Recurrent sustained ventricular tachycardia. 2. Endocardial mapping. *Circulation*, 57:440–447, 1978.

11] M. E. Josephson, L. N. Horowitz, H. L. Waxman, M. E. Chain, S. R. Spielman, A. M. Greenspan, F. E. Marchlinski, and M. D. Ezri. Sustained ventricular tachycardia: role of the 12-lead electrocardiogram in localizing site of origin. *Circulation*, 64:257–272, 1981.

12] A. SippensGroenewegen, H. Spekhorst, N. M. van Hemel, J. H. Kingma, R. N. Hauer, J. M. de Bakker, M. J. Janse, and A. J. Dunning. The value of body surface mapping in localization of the site of origin of ventricular tachycardia: catheter pacemapping compared with intraoperative activation mapping. *Circulation*, 82:237, 1990.

13] D. L. Kuchar, J. N. Ruskin, and H. Garan. Electrocardiographic localization of the site of origin of ventricular tachycardia in patients with prior myocardial infarction. *Journal of the American College of Cardiology*, 13:893–903, 1989.

14] M. E. Josephson, L. N. Horowitz, S. R. Spielman, A. M. Greenspan, C. VandePol, and A. H. Harken. Comparison of endocardial catheter mapping with intraoperative mapping of ventricular tachycardia. *Circulation*, 61:395–404, 1980.

15] N. M. van Hemel, J. H. Kingma, J. J. Defauw, F. E. Vermeulen, E. G. Mast, J. M. P. G. Ernst, and C. A. Ascoop. Left ventricular segmental wall motion

score as a criterion for selecting patients for direct surgery in the treatment of postinfarction ventricular tachycardia. *European Heart Journal*, 10:304–315, 1989.

16] A. SippensGroenewegen, H. Spekhorst, R. N. Hauer, N. M. van Hemel, P. Broekhuijsen, and A. J. Dunning. A radiotransparent carbon electrode array for body surface mapping during cardiac catherization. *Proceedings of the IEEE Medical Biological Society*, pages 178–181, 1987.

17] C. A. Grimbergen, A. C. Metting van Rijn, A. P. Kuiper, A. C. Linnenbank, and A. Peper. Instrumentation for the recording and digital processing of multichannel ECG data. *Proceedings of the IEEE Medical Biological Society*, 40:726–727, 1992.

18] A. C. Metting van Rijn, A. P. Kuiper, A. C. Linnenbank, and C. A. Grimbergen. Patient isolation in multichannel bioelectric recordings by digital transmission through a single optical fiber. *IEEE Transactions on Biomedical Engineering*, 40:302–308, 1993.

19] A. SippensGroenewegen, H. Spekhorst, N. M. van Hemel, J. H. Kingma, R. N. Hauer, J. M. de Bakker, C. A. Grimbergen, M. J. Janse, and A. J. Dunning. Localization of the site of origin of postinfarction ventricular tachycardia by endocardial pace mapping. Body surface mapping compared with the 12-lead electrocardiogram. *Circulation*, 88:2290–2306, 1993.

20] J. M. de Bakker, M. J. Janse, F. J. van Capelle, and D. Durrer. An interactive computersystem for guiding the treatment of life threatening ventricular tachycardias. *IEEE Transactions on Biomedical Engineering*, 31:362–368, 1984.

21] M. E. Josephson, A. H. Harken, and L. N. Horowitz. Endocardial excision: a new surgical technique for the treatment of recurrent ventricular tachycardia. *Circulation*, 60:1430–1439, 1979.

22] S. M. Blanchard, G. P. Wallcott, J. M. Wharton, and R. E. Ideker. Why is catheter ablation less successful than surgery for treating ventricular tachycardia that results from coronary artery disease? *Pacing & Clinical Electrophysiology*, 17:2315–2335, 1994.

23] M. A. Konstam, M. F. Rousseau, M. W. Kronenberg, J. E. Udelson, J. Melin, D. Stewart, N. Dolan, T. R. Edens, S. Ahn, and D. Kinan. Effects of the angiotensin converting enzyme inhibitor enalapril on the long-term progression of left ventricular dysfunction in patients with heart failure. SOLVD investigators. *Circulation*, 86:431–438, 1992.

24] M. Packer. The effect of carvedilol on cardiovascular hospitalisations in patients with chronic heart failure. *New England Journal of Medicine*, 334:1349–1355, 1996.

25] A. SippensGroenewegen, H. Spekhorst, N. M. van Hemel, J. H. Kingma, R. N. Hauer, J. M. de Bakker, C. A. Grimbergen, M. J. Janse, and A. J. Dunning. Value of body surface mapping in localizing the site of origin of ventricular tachycardia in patients with previous myocardial infarction. *Journal of the American College of Cardiology*, 24:1708–1724, 1994.

3 Relation between body surface mapping and the endocardial spread of ventricular activation in the postinfarction heart

P.F.H.M. van Dessel[1], N.M. van Hemel[1], J.M.T. de Bakker[2,3], A.C. Linnenbank[2,3], M. Potse[4], E.R. Jessurun[1], A. SippensGroenewegen[5], E.F.D. Wever[1]

From the Heart Lung Center Utrecht, Department of Cardiology[1], St Antonius Hospital, Nieuwegein, and Department of Cardiology[2], University Medical Center, Utrecht, Experimental and Molecular Cardiology Group of the Cardiovascular Research Institute[3], and Department of Medical Physics[4], Academic Medical Center, Amsterdam, The Netherlands, and the Section of Cardiac Electrophysiology, Department of Medicine and The Cardiovascular Research Institute[5], University of California, San Francisco, United States of America.

To be published in the Journal of Cardiovascular Electrophysiology, November 2001

Part of this study was presented at the Annual Scientific Session of the American Heart Association, Dallas, 1999

3.1 Abstract

Background. Body surface mapping (BSM) can be used to identify the site of earliest endocardial activation of ventricular tachycardias (VTs). The multielectrode QRS morphology during VT is, however, determined not only by the site of earliest ventricular activation but also by the subsequent spread of electrical activation through the ventricles. This study investigated the relationship between the site of earliest endocardial activation, endocardial spread of activation and the morphology of the multielectrode surface map in patients with remote myocardial infarction.

Methods and Results. In 14 patients with VT late (8.2 $\pm$ 5.2 yrs) after myocardial infarction BSM and simultaneous left ventricular 64-site basket endocardial mapping was performed during a total of 17 monomorphic VTs. In addition, multisite pacing by sequential use of the 64 basket electrodes was performed in 9 patients. BSM and basket mapping revealed the same endocardial breakthrough sites in of 8 of 17 VTs (47 %) and 189 of 322 pacing sites (59 %); adjacent sites were found in 2 of 17 VTs (12 %) and 36 of 322 pacing sites (11 %). Large zones of conduction block explained the mismatch in localization in 2 of 17 VTs (12 %) and 52 of 322 pacing sites (16 %). Regional differences in endocardial electrogram amplitudes were found as a cause for dissimilarity in 3 of 17 VTs (18 %) and 73 of 322 pacing sites (23 %). Multiple endocardial breakthrough sites were found 1 of 17 VTs (6 %) and 8 of 322 pacing sites (2 %). Finally, an epicardial exit site was suggested in 3 of 17 VTs (18 %) as an explanation for mismatch since no early endocardial activity could be recorded.

Conclusion. Zones of conduction block, regional differences in signal amplitude and multiple endocardial breakthrough sites are frequent causes for mismatch between BSM and basket catheter activation mapping.

3.2 Introduction

Body surface mapping (BSM) can be used as a non-invasive tool to determine the site of earliest endocardial activation of postinfarction ventricular tachycardia (VT). For this purpose, integral maps of the total QRS complex acquired with multiple body surface leads are compared with a reference database of QRS integral maps previously obtained during endocardial pace mapping [1].

It is well known that the mechanism underlying postinfarction VT late after myocardial infarction can be attributed to reentry and that the arrhythmogenic substrate is often situated in the subendocardium [2–4]. The endocardial exit site, i.e. the site where surviving strands of myocardial fibers are connected to the non-infarcted myocardium, can be considered as an electrophysiologically well-defined anatomical landmark of the arrhythmogenic substrate. This landmark can be used as a starting point to identify other parts of the reentrant circuit, such as the central common pathway, which is often used as a direct target for radiofrequency or surgical ablation [5].

Because of its greater spatial resolution BSM has been shown to be superior to the conventional 12-lead electrocardiogram (ECG) for assessment of the VT exit site [6,7]. However, the potential at every point on the body surface is determined by summation of the electric activity in the entire heart. This implies that not only the site of earliest endocardial and epicardial activation, but also the global spread of activation will contribute to the genesis of the QRS complex on the surface ECG. In the structurally normal left ventricle, BSM is capable of providing a high spatial VT localization resolution [5]. In patients with prior myocardial infarction, the spread of activation during VT may be profoundly affected due to structural and functional changes, which may cause a spatial mismatch between the endocardial and epicardial breakthrough site [8,9]. This may partly explain why BSM is able to assess the exact endocardial exit site of postinfarction VT in only 60–70 % of cases while it offers an approximation of the origin in an additional 25 % of cases [1].

To date, there have been no clinical studies reported in which the total body surface QRS morphology was simultaneously compared with endocardial spread of left ventricular activation. It was the purpose of this study to identify mechanisms that may cause BSM to fail in assessing the correct site of earliest endocardial activation in patients with prior myocardial infarction. To reach this goal, we simultaneously recorded 62 body surface potentials and 64 endocardial unipolar left ventricular electrograms using a basket catheter in patients with VT remote after myocardial infarction. The endocardial breakthrough site and the BSM determined site of origin were compared during VT and endocardial pacing. These data were then evaluated with respect to the patterns of left ventricular activation.

3.3 Methods

3.3.1 Patient selection

All patients admitted to our hospital between November 1997 and February 1999 for antiarrhythmic surgery or radiofrequency catheter ablation of infarct related VT were considered for inclusion in this study. Specific eligibility criteria included: (1) documented recurrent ventricular arrhythmias with or without aborted sudden cardiac death; (2) inducible sustained monomorphic VT during programmed electrical stimulation. Transthoracic echocardiography was applied to assess the dimensions of the left ventricle and to exclude the presence of a mural left ventricular thrombus or significant aortic valve disease since these conditions can interfere with safe deployment of the basket catheter. All antiarrhythmic drugs were discontinued for at least 5 drug elimination halve times before the study. The research protocol was approved by the Ethical Committee of the St Antonius Hospital. Prior written informed consent was obtained.

3.3.2 Electrophysiologic study

Induction of VT was carried out using a routine stimulation protocol including delivery of up to 3 extrastimuli following a drive train of 8 stimuli (2 ms pulse

width at twice the diastolic threshold current) with three different cycle lengths (600, 500 and 430 ms). A 6 Fr quadripolar catheter was positioned in the right ventricular apex or right ventricular outflow tract for this purpose.

If VT proved to be inducible, a 64-electrode unipolar basket catheter (Constellation Catheter^{TM}, Boston Scientific, Inc.) was percutaneously inserted after termination of VT. In a subset of 9 patients pace mapping during sinus rhythm with the basket catheter was performed before renewed induction of VT was attempted. The threshold was determined separately for each electrode of the basket catheter and, if capture could be obtained, pacing just above the current threshold with a drive cycle of 500 ms was performed.

3.3.3 Data acquisition and mapping

Data from the endocardial basket catheter and BSM electrodes were recorded simultaneously on a battery-powered 128-channel digital acquisition device [10,11]. Analogue to digital conversion occurred at a sampling frequency of 2 kHz, 16-bits resolution and a bitstep of 2 μV/bit. Wilson's central terminal was used as reference for the unipolar surface ECGs. The amplifier system had a bandpass characteristic using a frequency range of 0.16 – 400 Hz (3 dB frequencies). Data were transmitted using a fiberoptic transmission unit and stored in a Pentium based PC.

3.3.4 Body surface mapping

Body surface ECGs were recorded using a radiotransparent carbon unipolar electrode grid that does not interfere with fluoroscopic imaging during catheterization. The 62 electrodes were positioned in 14 flexible vertical straps that were applied on the anterior and posterior thoracic surface as described elsewhere [12]. A mean of 2.0 $\pm$ 1.8 leads per map were rejected because of unsatisfactory signal quality and were replaced by a value computed from neighboring electrodes. Our methods of processing and analysis have been described previously [13]. In short, after performing a baseline correction to exclude any possible contribution of baseline drift or interelectrode offset difference, the beginning and end of the QRS complex were set at the time instant at which one of the extreme amplitudes reached $>$ 0.2 mV and at the J point, respectively. A QRS integral map was computed for each VT and for every paced ventricular complex. Each VT and paced QRS integral map pattern was correlated with an anterior or inferior myocardial infarction database comprising mean paced QRS integral maps produced previously at 18 and 22 different specific endocardial segments, respectively (Figure 3.1 and 3.2) [14]. Pattern matching of QRS integral maps was performed both visually and mathematically using correlation coefficients [14, 16]. Visual analysis involved comparison of the position and orientation of the extremes and the morphology of the zero line.

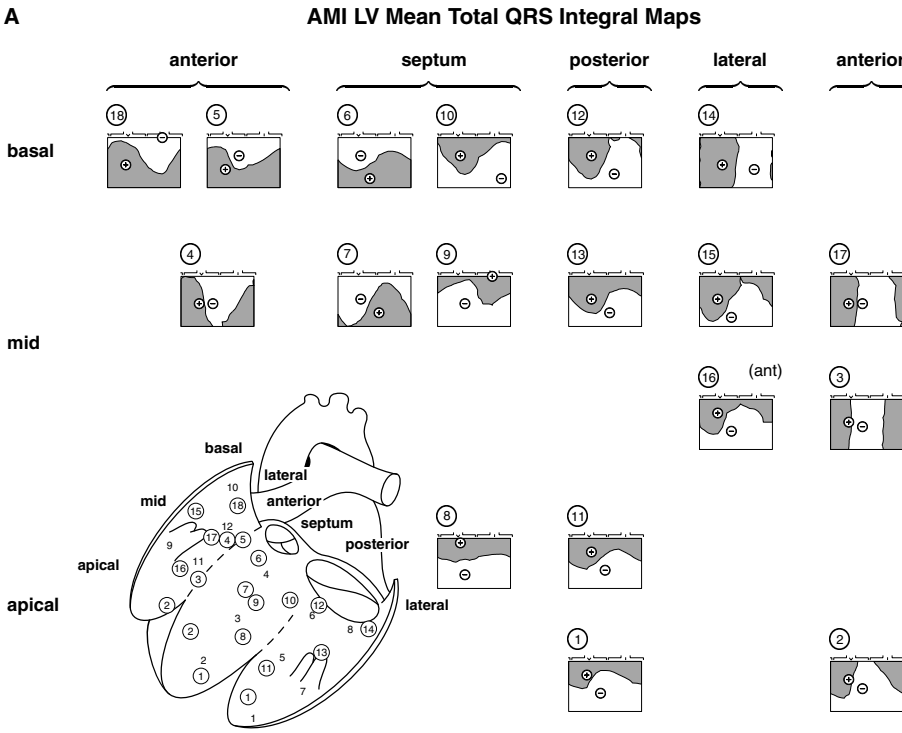

Figure 3.1: *This figure represents the database of mean paced QRS integral maps previously acquired in patients with prior anterior (AMI) myocardial infarction. Encircled numbers depict the location of pacing segments in a schematic overview of the endocardial surface of the left ventricle (LV) as defined in the previously developed AMI (18 segments) database. Mean paced QRS integral database maps are displayed and matched to the endocardial segment by the encircled number. Endocardial segments as defined by Josephson et al. are indicated by the regular numbers (12 segments) [15]. Reproduced with permission of the American Heart Association.*

3.3.5 Multielectrode endocardial mapping

Catheter placement

The basket catheter consists of 8 self-expanding nitinol splines mounted on a 110 cm long 8 Fr catheter shaft. Each spline has 8 symmetrically arranged electrodes. Selection of catheter size was based on the dimensions of the left ventricle as determined by 2D transthoracic echocardiography. In our series a basket catheter with a diameter of either 75 mm or 94 mm was chosen resulting in a vertical interelectrode spacing of 7 or 9 mm, respectively. Horizontal interelectrode distance varied with the positioning and deployment of the catheter. An 11 Fr introducer was inserted in the right femoral artery using the standard Judkins technique to advance

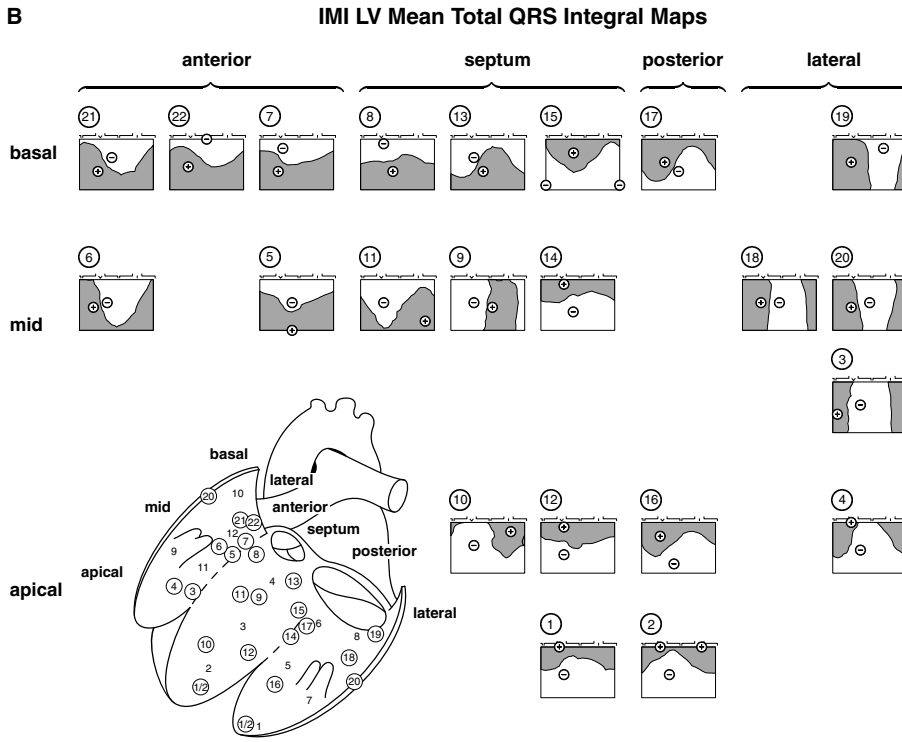

Figure 3.2: *The database representing mean paced QRS integral maps previously acquired in patients with prior inferior (IMI) myocardial infarction is shown. Encircled numbers depict the location of pacing segments in a schematic overview of the endocardial surface of the left ventricle (LV) as defined in the previously developed IMI (22 segments) database. Mean paced QRS integral database maps are displayed and matched to the endocardial segment by the encircled number. Endocardial segments as defined by Josephson et al. are indicated by the regular numbers (12 segments) [15]. Reproduced with permission of the American Heart Association.*

a 7 Fr pigtail catheter into the left ventricle. Then, a long 10 Fr guiding sheath was placed in the left ventricle across the aortic valve over the pigtail catheter and the collapsed basket catheter was advanced through the guiding sheath in the left ventricle after removal of the pigtail catheter. The guiding sheath was then pulled back allowing deployment of the basket catheter in the left ventricle. The activated clotting time was kept longer than 300 seconds by full heparinization to avoid thromboembolic complications. A 6 Fr quadripolar catheter was inserted percutaneously through the right femoral vein and positioned in the intra-abdominal part of the inferior caval vein to serve as a far field recording and pacing reference electrode for the unipolar basket catheter electrodes.

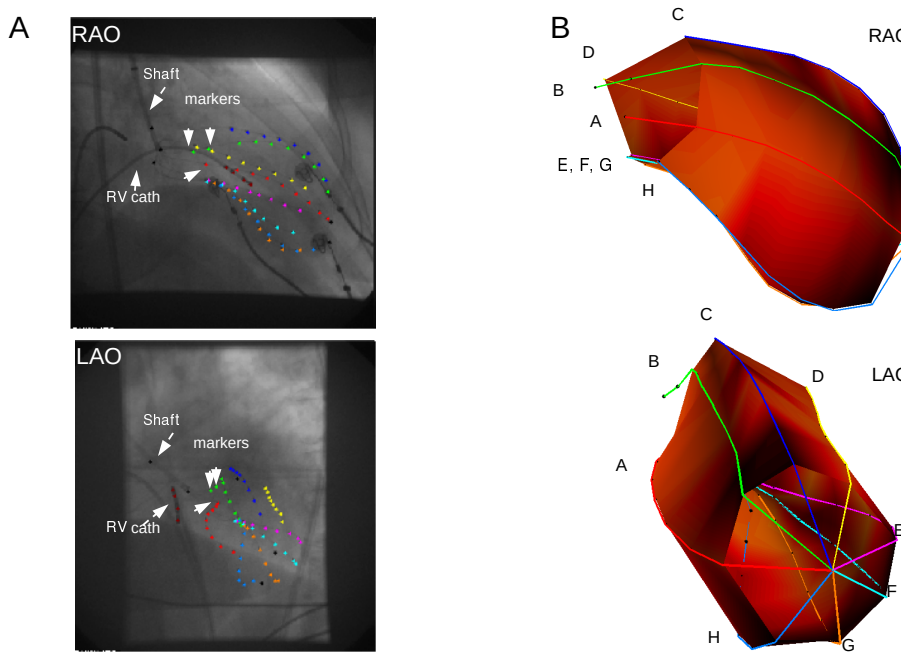

Figure 3.3: ***Panel A*** *shows right (RAO) and left (LAO) anterior oblique fluoroscopic projections of the deployed basket catheter in the left ventricle. Markers for the A- and B-spline are highlighted by small white arrows. The stimulation catheter (RV cath) is positioned in the right ventricle and marked with a dashed white arrow. The proximal part of the basket catheter (shaft) is located in the aorta and marked with a dashed white arrow. Recording electrodes are depicted with a dot of unique color for each spline.* ***Panel B*** *features the reconstruction of the 3D shape and positioning of the basket catheter in the left ventricle as viewed in the RAO and LAO projections. Letters A to H identify the 8 individual splines. Electrodes along splines are numbered 1 to 8 from apex to base of the heart.*

Fluoroscopic localization of the basket catheter

Since basket catheter positioning varies from patient to patient, the exact position of the individual basket electrodes was determined using biplane 45 ° right (RAO) and left 45 ° anterior oblique (LAO) digital cine fluoroscopy (Philips Medical Systems Integris). After selecting the same end-diastolic frames from both fluoroscopic projections, splines A and B, which carry one and two additional radiopaque markers, respectively, were identified (Figure 3.3A). After labeling electrodes of these two splines, the other splines could be identified by comparing their relative position with the known position of the first two splines. Each individual electrode and the central apical spline connector were then marked and given 2D coordinates in the RAO and LAO projections. A panel of three expe-

rienced interventional electrophysiologists verified correct identification of each electrode. Finally, by combining the data from the RAO and LAO projections, 3D coordinates for each electrode were calculated thereby allowing a realistic anatomical rendering of the position and shape of the basket catheter in the left ventricle for each individual patient (Figure 3.3B). The coloring of the basket in **panel B** does not have an electrophysiological meaning, but is merely used to enhance 3D visualization. To be able to compare basket catheter activation mapping and pace mapping data with electrocardiographic localization results, the location of each basket catheter electrode was mapped to an endocardial segment in one of the two databases of paced QRS integral maps.

Endocardial data processing

A software package was developed for on-line data processing based on MatLab 5.1 (The MathWorks, Inc.) [17]. The surface Laplacian has been proposed to optimize the detection of small deflections in the endocardial unipolar electrograms. These small sharp deflections are believed to result from local events as opposed to larger, more flaccid, deflections which are presumed to be caused by remote events [18–20]. The Laplacian suppresses remote deflections, but still has the characteristics of the unipolar electrogram. In contrast to bipolar electrograms, the Laplacian is direction independent. However, the surface Laplacian has only been validated for spatially dense electrode grids (interelectrode distances of 1 mm or less), and no data on its value for electrode systems with interelectrode systems of 5–10 mm are available at present. Therefore, in our study a co-axial electrogram was used. This co-axial electrogram was constructed by subtracting the mean electrogram from the 8 surrounding electrodes weighted for distance, from the unipolar signal recorded at the central electrode. This procedure is numerically equivalent to the surface Laplacian but differs from it by a factor that is determined by the electrode distances. Therefore, activation time parameters, such as zero line crossing, moment of $dVdt_{min}$and onset and offset of the electrogram are equal to those derived from a surface Laplacian. An example of activation sequences reconstructed with the aid of co-axial electrograms is shown in figure 3.4.

3.3.6 Definitions of parameters and related terminology

A VT was considered to be monomorphic and sustained if it lasted for at least 30 seconds without significant changes in the QRS morphology as monitored in the 12-lead ECG. The local endocardial activation time was determined by the steepest deflection (dV/dt_{min}) in the local electrogram. An endocardial breakthrough was defined as an endocardial site where an activation wave front emerged and from where it spread radially. The endocardial VT exit site was defined as the site where the earliest endocardial breakthrough occurred relative to the onset of the QRS complex on the simultaneously recorded surface ECG [15]. An epicardial breakthrough was defined as the absence of endocardial activity before or within

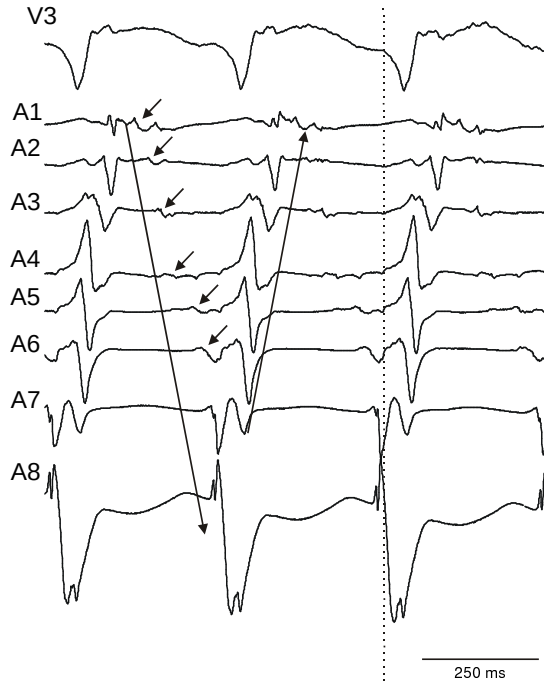

Figure 3.4: *An example of activation sequences reconstructed during VT. Standard precordial lead V3 and 8 endocardial electrograms (A1 to A8), obtained using co-axial electrogram reconstruction, are shown. The dotted line indicates the body surface QRS onset. The diastolic activation pattern is indicated by the large black arrow pointing downwards. Small black arrows indicate the presence of diastolic potentials. Diastolic activation leads to electrode A7, which precedes the QRS complex and is considered the exit site of VT. ¿From there, systolic activation (large upward pointing black arrow) can be traced back to the start of the diastolic wave front in electrode A1, completing the reentry circuit.*

10 ms after the onset of the body surface QRS complex. If activation times of signals recorded at contiguous sites (7–9 mm apart) differed by 50 ms, conduction block was considered present [21].

3.3.7 Statistical analysis

All data were stored in a computerized patient record database. Data analysis was performed on a personal computer using the "The SAS System for Windows 6.12" statistical software package (SAS Institute, Inc). Data are presented as mean values $\pm$ SD unless stated otherwise. Statistical significance was defined as a P value < 0.05.

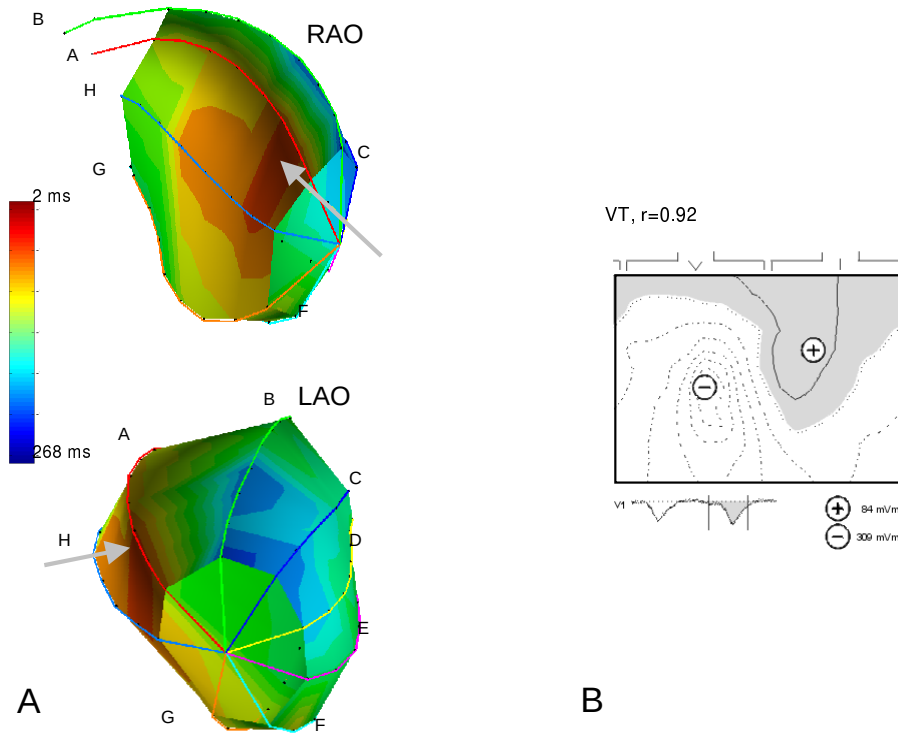

Figure 3.5: *Endocardial activation mapping and BSM during ventricular tachycardia (VT) in patient 6 (Table 2) who suffered from a previous anterior infarction.* ***Panel A*** *depicts the activation sequence of the left ventricle in right (RAO) and left (LAO) anterior oblique projections. Activation times in the isochrone maps are relative to the onset of the body surface QRS complex and range from 2 ms (red) to 268 ms (blue). The VT exit site is located midseptal at electrode A3 (origin of black arrows).* ***Panel B*** *depicts the VT QRS integral map, which is compatible with the mean paced QRS integral map belonging to segment AMI9 (correlation coefficient of 0.92) located in the midseptal wall, compatible with Josephson location 3.*

3.4 Results

3.4.1 Patient characteristics

Seventeen consecutive patients with documented infarct-related sustained ventricular arrhythmias were eligible for the study. In 2 of 17 patients (12 %), no adequate deployment of the basket catheter could be obtained, while in 1 of 17 patients (6 %), only non-sustained VTs could be induced. These three patients were excluded from further analysis. The characteristics of the remaining 14 patients are summarized in Table 3.1.

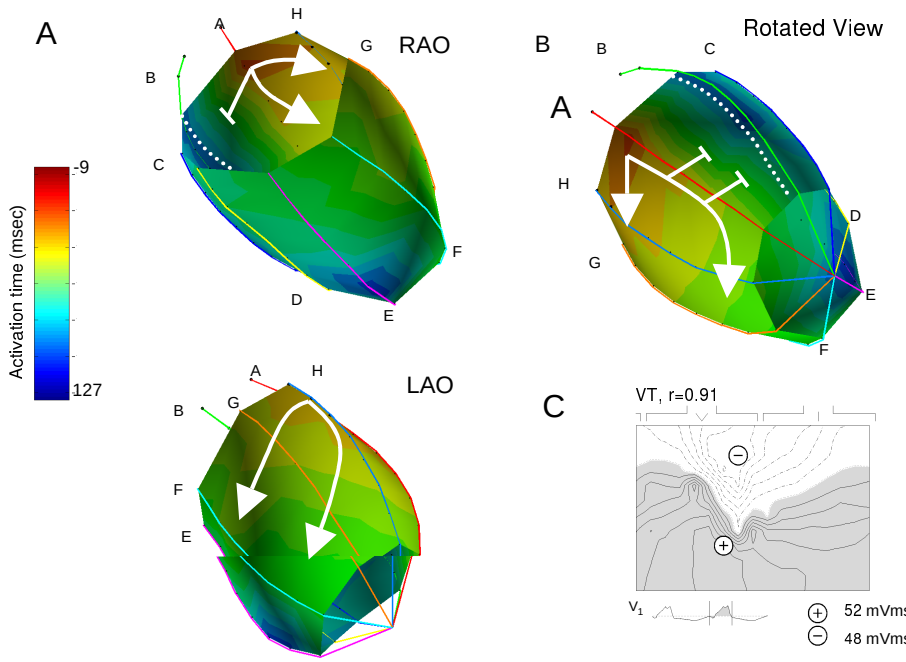

Figure 3.6: *Endocardial activation mapping and BSM during ventricular tachycardia (VT) in patient 2 (Table 2) who suffered from a previous posterolateral infarction.* ***Panel A*** *depicts the activation sequence of the left ventricle in right (RAO) and left (LAO) anterior oblique projections. Activation times in the isochrone maps are relative to the onset of the body surface QRS complex and range from -9 ms (red) to 127 ms (blue). The VT exit site is located basal and posterolateral at electrode A7 (origin of white arrows). A line of block extending from the basal posterolateral area to the apical posterolateral area (along spline B) can be noted (white dotted line). This line of block forces the activation front to propagate towards the anterolateral wall. In* ***panel B*** *the RAO basket projection has been rotated computationally in horizontal and vertical direction to provide a non-standard rear projection in order to demonstrate the area of interest, i.e. the line of block along the B-spline.* ***Panel C*** *depicts the VT QRS integral map, which is compatible with the mean paced QRS integral map belonging to segment IMI7 (correlation coefficient of 0.91) located at a remote segment in the basal anterior wall compatible with electrode 1 on spline G (Josephson location 12).*

Age (years)	70.1 ± 6.2
Sex	
Male	10
Female	4
No. of VT morphologies per patient*	1.3 (1– 4)
VT cycle length (ms)	318 ± 65
Scintigraphic LVEF (%)	27.8 ± 9.5
Echocardiographic dimensions	
LV end diastolic length (mm)	90.5 ± 9.6
LV end diastolic width (mm)	55.2 ± 6.8
WMS (max. 9 of 9 normal segments)*	3.2 (3 – 5)
Extent of CAD (> 70 % stenosis)	
1 vessel	5
2 vessel	4
3 vessel	5
Time since infarction (years)	8.2 ± 5.2
Site of myocardial infarction	
Anterior	9
Inferior	5

Table 3.1: *Baseline characteristics (N=14). (CAD = coronary artery disease; LV = left ventricle; LVEF = left ventricular ejection fraction; WMS = wall motion score; VT = ventricular tachycardia. * = median (range))*

3.4.2 Correlation of VT localization using body surface mapping and basket catheter activation mapping

A total of 17 sustained monomorphic VTs were localized using BSM and basket catheter activation mapping (Table 3.2).

In 8 of 17 VTs (47 %), the endocardial exit site was located in the endocardial segment predicted by BSM, whereas in 2 other VTs (12 %), the endocardial exit site was situated in a neighboring segment. Seven of 17 VTs (41 %), originated from a segment remote from the segment identified by BSM. Therefore, in 10 of 17 VTs (59 %), BSM appeared to correctly localize or regionalize the actual endocardial VT exit site. An example of a matching VT site of origin is shown in figure 3.5.

3.4.3 Body surface mapping during endocardial pace mapping

For a median of 30 of 64 electrodes (range 17 – 54) pacing capture could be obtained. This required a mean pacing current strength of 7.9 ± 6.4 mA. The mean interval between the pacing stimulus and the onset of the body surface QRS complex was 36 ± 20.4 ms. There was no significant difference in the mean stimulus-to-

	VT	VT morphology	Axis	Cycle Length (ms)	Segment of earliest endocardial activation (BSM) {JL}	Site of of earliest endocardial activation (Basket catheter){JL}	Distance between suggested endocardial segments
1	VT1	LBBB	Superior	340	IMI2 {1}	IMI2 {1}	Same
2	VT1	RBBB	Inferior	430	IMI7 {12}	IMI19 {10}	Remote
3	VT1	RBBB	Superior	200	IMI9 {3}	IMI20 {7}	Remote
	VT2	RBBB	Inferior	250	IMI6 {11−12}	IMI6 -12}	Same
4	VT1	RBBB	Superior	420	AMI17 {9-11}	AMI1 {1-7}	Remote
5	VT1	RBBB	Horizontal	380	AMI17 {9-11}	AMI3 {11}	Adjacent
6	VT1	LBBB	Superior	330	AMI9 {3}	AMI9 {3}	Same
7	VT1	RBBB	Superior	320	AMI8 {2-3}	AMI7+AMI13 {3}+{5-7}	Adjacent
8	VT1	RBBB	Inferior	230	AMI18 {10}	AMI18 {10}	Same
9	VT1	RBBB	Inferior	240	AMI18 {10}	AMI7 {3}	Remote
10	VT1	LBBB	Superior	260	AMI9 {3}	AMI15 {9-10}	Remote
11	VT1	RBBB	Superior	440	IMI16 {5}	IMI3 {11}	Remote
12	VT2	RBBB	Superior	320	AMI17 {9}	AMI17 {9}	Same
	VT3	LBBB	Superior	320	AMI9 {3}	AMI1 {1}	Remote
13	VT1	LBBB	Superior	320	IMI9 {3-4}	IMI9 {3-4}	Same
	VT2	RBBB	Superior	320	IMI13 {4}	IMI13 {4}	Same
14	VT1	LBBB	Superior	300	AMI9 {3}	AMI9 {3}	Same

Table 3.2: *Comparison of VT site of origin determined using body surface mapping and basket activation mapping. (AMI=Anterior myocardial infarction database segment; BSM=Body surface mapping; IMI=Inferior myocardial infarction database segment; JL=Josephson Location; LBBB=Left bundle branch block morphology; RBBB=Right bundle branch block morphology; VT=Ventricular tachycardia)*

QRS interval between matching and non-matching pace mappings (p=0.8). This implied that localization mismatch was not due to breakthroughs that were remote from the pacing site as can be seen when stimulation occurs within the zone of slow conduction. A total of 322 paced QRS maps (median 30, range 17 – 54 per patient) were obtained. The mathematical correlation between each paced QRS integral map and the best matching mean paced QRS integral map from the reference database was 0.87 ± 0.07 (range 0.48 – 0.98). For 189 of the 322 paced QRS integral maps (59 %), the fluoroscopic position of the pacing electrode was located in the same endocardial segment as the best matching mean paced QRS integral map from the database. An adjacent segment of the database was found in 36

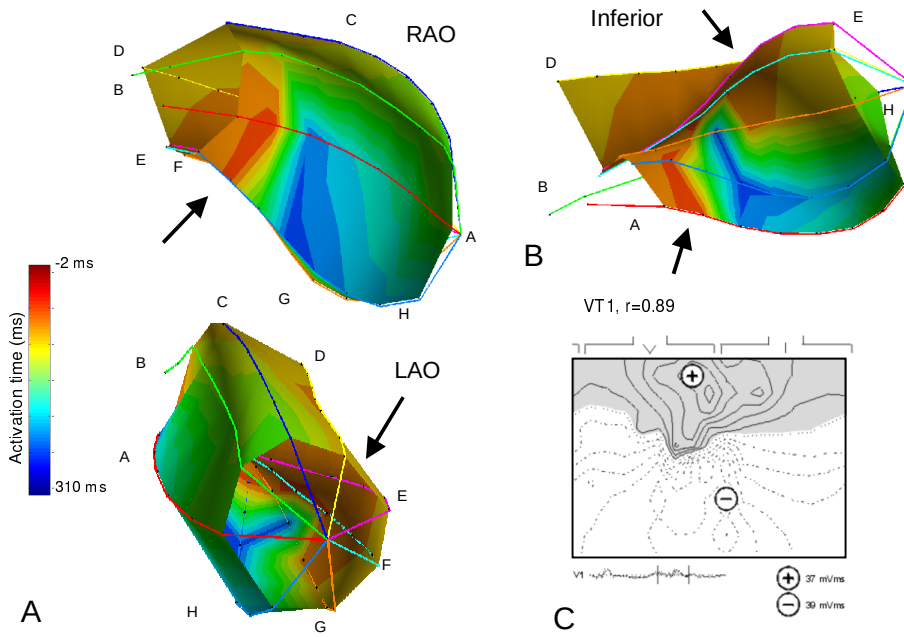

Figure 3.7: *Endocardial activation mapping and BSM during ventricular tachycardia (VT) in patient 7 (Table 2) who suffered from a previous anterior infarction.* ***Panel A*** *depicts the activation sequence of the left ventricle in right (RAO) and left (LAO) anterior oblique projections. Activation times in the isochrone maps are relative to the onset of the body surface QRS complex and range from -2 ms (red) to 310 ms (blue). The VT exit site is located anteroseptal and midposterior at electrode A7 and electrode F5 (origin of black arrows). In* ***panel B*** *the basket projection has been rotated computationally to provide a non-standard inferior view. Clearly, two distinct exit sites are visible.* ***Panel C*** *depicts the VT QRS integral map, which is compatible with the mean paced QRS integral map belonging to segment AMI8 (correlation coefficient of 0.89) located at an adjacent segment in the inferoseptal region, compatible with electrode 4 on spline H (Josephson location 3-5).*

of 322 pacing sites (11 %). The database segment was located remote from the endocardial pacing site in 97 of 322 paced QRS integral maps (30 %)

3.4.4 Electrophysiologic mechanisms responsible for mapping mismatches

Endocardial activation patterns and electrogram distributions acquired during VT and pacing with the basket catheter, were reviewed in detail to explain mismatches between sites of earliest endocardial activation identified with BSM and basket mapping. Three major mechanisms could be identified: extensive lines of conduction block, multiple endocardial exit sites, and regional differences in en-

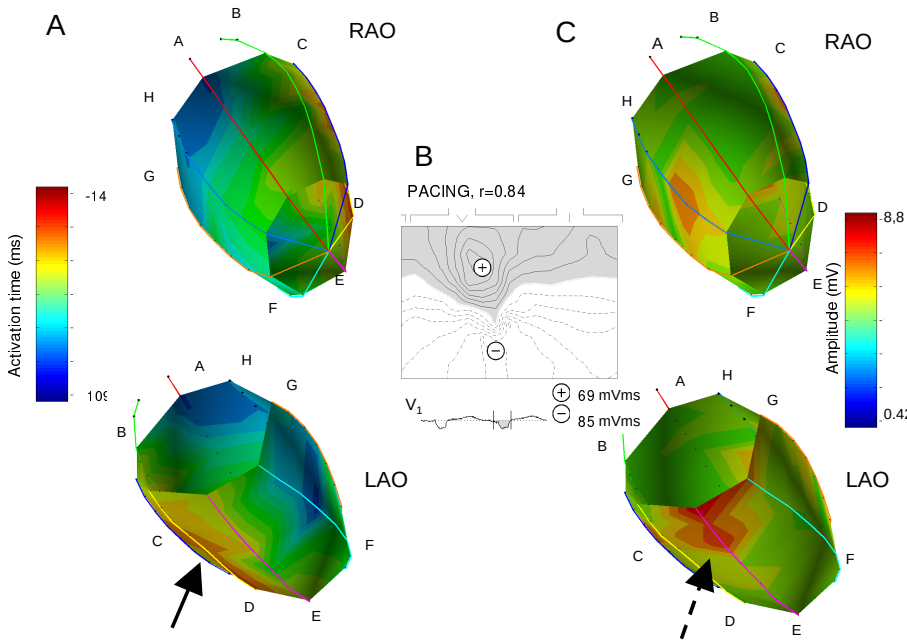

Figure 3.8: *Endocardial pace mapping data obtained in patient 2 with previous posterolateral myocardial infarction. The infarction scar is located basal posterolateral near splines A and B. Stimulation is performed at electrode C2, located midinferior (Josephson location 5).* ***Panel A*** *depicts the activation sequence of the left ventricle in right (RAO) and left (LAO) anterior oblique projections, ranging from -14 ms at electrode C2 (red) to 109 ms (dark blue). The solid black arrow indicates the site of stimulation.* ***Panel B*** *shows the paced QRS integral map that compares best (correlation coefficient of 0.84) with the mean paced QRS integral map of database segment IMI14 which is located basal inferoseptal (Josephson location 4-6).* ***Panel C*** *demonstrates RAO and LAO projections of the distribution of endocardial signal amplitude, ranging from 0.42 V (dark blue) to 8.8 V (red). The dashed black arrow indicates the position of database segment IMI14, which is situated adjacent to the stimulation site in an area where the signal amplitude is larger.*

docardial signal amplitude.

Conduction block

Substantial lines of conduction block were found in 2 of 17 VTs (12 %) that were both obtained in patients with inferior myocardial infarction preventing centrifugal spread of ventricular activation. In 52 of 322 paced activation sequences (16 %) lines of block prevented radial spread from the area of initial activation. This resulted in a mismatch between the segment of earliest activation determined with BSM and the actual location of the pacing electrode on the basket catheter. At 36 of

52 pacing sites (69 %) that were not correctly localized with BSM, the best matching database segment was situated remote from the pacing electrode, whereas in 16 of these 52 incorrectly identified pacing sites (31 %), the pacing location was localized to an adjacent database segment. An example of BSM mismatch as a result of conduction block is shown in figure 3.6.

Multiple endocardial breakthroughs

In 1 of 17 VTs (6 %) that was obtained in a patient with previous anterior myocardial infarction (Patient 7 in Table 2), two endocardial breakthroughs were found: one in the midanteroseptal area and the other near the posterior papillary muscle. Localization using the BSM database indicated a midinferoseptal segment of origin, which is located in between the two actual endocardial breakthrough sites. An example is shown in figure 3.7.

During pace mapping, multiple breakthrough sites (i.e. two distinct sites with radial spread of activation) were found in 8 of 322 maps (2 %). In these cases the site of stimulation appeared to be at a remote location remote with respect to the database segment identified with BSM.

Differences in signal amplitude

In 3 of 17 VTs (18 %) where the BSM database localized the site of origin to an adjacent endocardial segment, the electrogram amplitude at the endocardial segment of origin predicted by BSM was much larger than that measured at the true endocardial exit. At 73 of 322 pacing sites (23 %), differences in signal amplitude resulted in a mismatch between the two methods. The obtained database segment was remote in 52 of 73 incorrectly localized pacing sites (71 %). At 21 of 73 pacing sites (29 %), an adjacent database segment was predicted. An example of BSM mismatch caused by differences in magnitude of the endocardial potential, is shown in figure 3.8.

Epicardial breakthrough

In 3 of 17 VTs (18 %), no clear reason for mismatch could be found by examining the endocardial spread of activation. Two of these three VTs were documented in patients with previous anterior myocardial infarction, one VT was found in a patient with a prior inferior myocardial infarction. In these VTs, no early endocardial activity (i.e. within 10 ms after the onset of the body surface QRS) was noted. These findings were considered to be suggestive for an epicardial or intramural exit.

3.5 Discussion

The present study shows that BSM indicated the correct left ventricular segment of initial endocardial activation in 50 – 60% of VT episodes and endocardial pac-

ing sequences, whereas in an additional 10 – 20 % regional approximation was achieved. These localization results are comparable to previously reported retrospective data obtained in a similar patient cohort [1].

The earliest site of endocardial activation, the subsequent spread of ventricular activation and the site of epicardial breakthrough all contribute to the QRS morphology on the body surface ECG. In order to predict the earliest site of endocardial activation, one of the assumptions made in electrocardiography is that the activation front during VT spreads out centrifugal and travels predominantly in a perpendicular fashion from the presumed endocardial breakthrough site to the epicardial surface. However, in postinfarction VT the anatomical substrate is often extensively altered. Therefore, the spread of activation may deviate from its anticipated centrifugal pattern. This can give rise to alternative activation spread patterns after myocardial infarction [9]. It has also been shown that minor shifts in the endocardial exit site can lead to major differences in body surface ECG morphology if transmural spread of activation is not directly from endocardium to epicardium [22–25]. Although this problem is partially circumvented by using BSM databases that are specific for previous anterior or inferior myocardial infarction, it is conceivable that due to the complex anatomical nature of the postinfarction arrhythmogenic substrate, activation patterns may differ between individual patients. This may lead to incorrect BSM prediction of the presumed endocardial segment of origin of postinfarction VT. In our study, several patterns of activation were identified that can explain disparity in mapping outcome.

3.5.1 Electrophysiologic mechanisms causing disparity between body surface mapping and endocardial mapping

Non-homogeneous spread of endocardial activation due to large zones of conduction block caused dissimilarity in mapping findings in 2 of 17 VTs (12 %) and 52 of 322 paced activation sequences (16 %). Zones of conduction block prevented radial spread of activation from the site of endocardial breakthrough. This was also observed in a canine infarct model where the extent of the line block was one of the causes of different scalar ECG morphologies during sustained VT [26]. Osswald et al. have shown in a similar experimental model that minor changes in the site of endocardial breakthrough can lead to different activation spread patterns and subsequent body surface ECG morphology [25].

Two separate endocardial breakthrough sites were found in only a minority of cases during pacing and VT. Multiple breakthrough sites in the postinfarction heart, especially after anterior myocardial infarction, have been reported previously both during sinus rhythm [9] and VT [27]. Since database guided BSM of postinfarction VT is developed to localize a single segment of earliest activation, simultaneous occurrence of two or more distant breakthrough sites will by definition produce an incorrect localization result using the BSM approach. In our study, the segment of VT origin was, however, spatially localized by BSM between the two actual endocardial breakthrough sites.

In 15–20% of VT episodes or pacing sequences, the breakthrough site was situ-

ated in the infarct border generating small signal amplitudes, whereas signal amplitudes were larger in other non-infarcted endocardial areas. Since high-voltage areas will generate more electromotive force on the surface ECG, they may in fact partially suppress the low-voltage information resulting from the true endocardial site of VT origin. Mathematical correlation between measured VT QRS integral maps and reference database mean paced QRS integral maps is currently obtained by computing the normalized inner product of the vectorized measured map and all vectorized reference database maps and selecting the highest correlation coefficient [13]. This makes the computational result more susceptible to the number, location and magnitudes of the positive and negative extremes on the map. If the magnitude of the positive and negative extremes on the map differ considerably, the best mathematical match between the VT or paced QRS integral map and the reference database mean paced QRS integral map will be based primarily on the position of the larger extreme.

Although the reentrant circuit in postinfarction VT is believed to be located predominantly in the subendocardial layer, other mapping studies that combined endocardial and epicardial mapping have demonstrated that approximately 15 % of VTs have a partially subepicardial circuit and an earlier epicardial breakthrough of the activation wave front [28]. We did not find clear early endocardial activity within 10 milliseconds of the onset of the body surface QRS complex in 18 % of VTs. In these cases an earlier epicardial or intramural exit site was believed to be present although this could not be confirmed due to lack of epicardial activation data. The absence of early endocardial activation may also have been caused by insufficient endocardial basket coverage of the endocardial exit site. However, the incidence of our findings is similar to the incidence of early epicardial breakthrough of postinfarction VT reported in the literature [28].

3.5.2 Methodological considerations in QRS isointegral mapping

Apart from electrophysiologic considerations, methodological issues connected with reference database oriented QRS isointegral mapping should be taken into account as well. Correct identification of the baseline and onset QRS are crucial for accurate computation of QRS areas intended for QRS integral map localization of sites of VT origin. Two major problems concerning baseline correction and identification of the onset of the QRS complex are: superposition of the onset of the QRS complex on the T-wave of the preceding QRS-complex and non-simultaneous departure of the QRS complex in different leads. We think that two separate cases should be contemplated. The first case is when the VT under study does not have an extremely short cycle length**.** Then, usually an isoelectric interval between T-wave and QRS onset can be identified which can be utilized for baseline correction. The onset and offset QRS are subsequently chosen from an instantaneous isopotential map as the instant when the first electrode has reached a value of more than 0.2 mV (onset) and the instant when each lead has dropped below 0.2 mV (offset), respectively. In this case non-simultaneous departure of the QRS complex will not be of great influence since the integral of the QRS complex

is used: the contribution of the integral of a prolonged isoelectric interval before onset QRS in an individual lead with late QRS departure to the entire QRS integral will be approximately zero. It is possible that in leads with earliest QRS complex departure a small post J-point part of the ST-T segment is integrated, but since voltages in the early ST-T segment are usually low, the integral of these early ST-T segment parts over a small time interval will be neglectable as compared to the magnitude of the QRS integral.

The second case is when the VT under study has a short cycle length and there is no clear isoelectric interval between the T-wave end and onset QRS. VTs of this particular rapid rate usually will be sinusoid in shape with QRS complex and T-wave morphology that are approximately similar but opposite in sign. Baseline correction points are subsequently chosen at best clinical judgment. The possibility remains that — due to confluence of QRS complex and T-wave and non-simultaneous QRS complex departure — unequal parts of the T-wave are integrated with the QRS complex in different leads. However, in these leads with late QRS departure also unequal parts of the terminal QRS complex will not be included in the QRS integral. This will amount to approximately the same absolute value as the additional area of the T-wave end that was erroneously added in these leads since the T-wave has approximately the same shape as the QRS complex. We think that these errors of measurements will approximately annihilate each other, since QRS complex and T-wave are of opposite sign. This will still allow QRS integral map localization by reference database comparison.

3.5.3 Limitations of the study

The basket catheter used in this study is introduced in the left ventricle in a collapsed state. Before it is capable of providing high resolution mapping of endocardial activation it has to be fully deployed in the left ventricle. To reliably locate the exit site of VT adequate endocardial basket catheter coverage of the exit site area is mandatory. Since complete catheter deployment of the catheter is not always feasible endocardial VT breakthrough sites located in uncovered endocardial regions may have not been recorded. To prevent this, two patients with imperfect catheter deployment were omitted from further analysis. Additionally, localization differences were studied during basket pacing. When endocardial pacing is performed and capture is obtained, the exact site of earliest endocardial activation is the fluoroscopic location of the basket catheter electrode. Therefore endocardial basket coverage is less an issue during endocardial pacing.

No simultaneous epicardial mapping was performed and therefore VTs with an epicardial exit site may have been wrongly classified as VTs where the BSM localization and endocardial exit site did not match. In 3 of 17 VTs, in our series no early endocardial breakthrough could be detected and therefore an epicardial exit was believed to be present.

3.5.4 Clinical application of body surface mapping.

BSM has been used previously for guiding ventricular arrhythmia surgery. In our study, BSM has proven to identify or approximate the segment containing the VT exit site in 70–80 % of cases. Because the surgeon can ablate the reentrant circuit more substantially than the more circumscribed thermal lesion, produced during radiofrequency ablation, the resolution that BSM offers appears to be sufficient [29].

In a recent study BSM has proven to be of great clinical utility in guiding radiofrequency ablation of idiopathic VT [5]. The mapping results in their study are very well comparable to the localization results in our study. Reference database guided BSM was compared by Peeters et al. with endocardial pace mapping in the same patient. The same endocardial segment was found in 53 % of VTs and 47 % of VTs were mapped to an adjacent endocardial segment. It should be noted that the patients involved in this study did not have any structural heart disease. Therefore it can be expected that activation spread patterns were not influenced by altered anatomy of the left or right ventricle. Furthermore, when using pace mapping in combination with BSM and comparing the paced maps with the QRS integral map of VT induced in the same patient, as was done in the study of Peeters et al. [5], each patient is used as his own reference. Because all map comparisons are done in the same patient — i.e. the same electrophysiologic substrate — discrepancies due to differences in torso, heart geometry and individual activation spread patterns are no longer relevant.

Reference database guided BSM is a non-invasive tool that can greatly facilitate mapping of postinfarction VT including hemodynamic unstable and non-sustained VTs. In the normal left ventricle BSM offers a high spatial mapping resolution that is appropriate to directly guide radiofrequency ablation. However, changes in activation spread patterns in the structurally altered postinfarction heart cause BSM to provide inaccurate results in 20–30% of the localized VTs.

References

1] A. SippensGroenewegen, H. Spekhorst, N. M. van Hemel, J. H. Kingma, R. N. Hauer, J. M. de Bakker, C. A. Grimbergen, M. J. Janse, and A. J. Dunning. Value of body surface mapping in localizing the site of origin of ventricular tachycardia in patients with previous myocardial infarction. *Journal of the American College of Cardiology*, 24:1708–1724, 1994.

2] H. J. Wellens, D. Durrer, and K. I. Lie. Observations on mechanisms of ventricular tachycardia in man. *Circulation*, 54:237–244, 1976.

3] M. E. Josephson, L. N. Horowitz, A. Farshidi, and J. A. Kastor. Recurrent sustained ventricular tachycardia. I. mechanisms. *Circulation*, 57:431–440, 1978.

4] W. G. Stevenson, N. W. James, I. Wiener, and K. Nademanee. Slow conduction in the infarct scar: relevance to the occurrence, detection and ablation of ven-

tricular reentry circuits resulting from myocardial infarction. *American Heart Journal*, 117:452–467, 1989.

5] H. A. Peeters, A. SippensGroenewegen, E. F. Wever, H. Ramanna, A. C. Linnenbank, M. Potse, C. A. Grimbergen, N. M. van Hemel, R. N. Hauer, and E. O. Robles de Medina. Clinical application of an integrated 3-phase mapping technique for localization of the site of origin of idiopathic ventricular tachycardia. *Circulation*, 99:1300–1311, 1999.

6] A. SippensGroenewegen, H. Spekhorst, N. M. van Hemel, J. H. Kingma, R. N. Hauer, J. M. de Bakker, C. A. Grimbergen, M. J. Janse, and A. J. Dunning. Localization of the site of origin of postinfarction ventricular tachycardia by endocardial pace mapping. Body surface mapping compared with the 12-lead electrocardiogram. *Circulation*, 88:2290–2306, 1993.

7] D. L. Kuchar, J. N. Ruskin, and H. Garan. Electrocardiographic localization of the site of origin of ventricular tachycardia in patients with prior myocardial infarction. *Journal of the American College of Cardiology*, 13:893–903, 1989.

8] J. P. Boineau, S. D. Blumenschein, M. S. Spach, and D. C. Sabiston. Relationship between ventricular depolarization and electrocardiogram in myocardial infarction. *Journal of Electrocardiology*, 1:233–240, 1968.

9] R. Hatala, P. Savard, G. Tremblay, P. Page, R. Cardinal, F. Molin, T. Kus, and R. Nadeau. Three distinct patterns of ventricular activation in infarcted human hearts. an intraoperative cardiac mapping study during sinus rhythm. *Circulation*, 91:1480–1494, 1995.

10] C. A. Grimbergen, A. C. Metting van Rijn, A. P. Kuiper, A. C. Linnenbank, and A. Peper. Instrumentation for the recording and digital processing of multichannel ECG data. *Proceedings of the IEEE Medical Biological Society*, 40:726–727, 1992.

11] A. C. Metting van Rijn, A. P. Kuiper, A. C. Linnenbank, and C. A. Grimbergen. Patient isolation in multichannel bioelectric recordings by digital transmission through a single optical fiber. *IEEE Transactions on Biomedical Engineering*, 40:302–308, 1993.

12] A. SippensGroenewegen, H. Spekhorst, R. N. Hauer, N. M. van Hemel, P. Broekhuijsen, and A. J. Dunning. A radiotransparent carbon electrode array for body surface mapping during cardiac catherization. *Proceedings of the IEEE Medical Biological Society*, pages 178–181, 1987.

13] A. C. Linnenbank. *On-site recording, analysis, and presentation of multichannel ECG data*. PhD thesis, Univeristy of Amtserdam, Amsterdan, The Netherlands, 1996.

14] A. SippensGroenewegen, H. Spekhorst, N. M. van Hemel, J. H. Kingma, R. N. Hauer, M. J. Janse, and A. J. Dunning. Body surface mapping of ectopic left ventricular activation. QRS spectrum in patients with prior myocardial infarction. *Circulation Research*, 71:1361–1378, 1992.

15] M. E. Josephson, L. N. Horowitz, A. Farshidi, J. F. Spear, J. A. Kastor, and E. N. Moore. Recurrent sustained ventricular tachycardia. 2. Endocardial mapping. *Circulation*, 57:440–447, 1978.

16] A. SippensGroenewegen, H. Spekhorst, N. M. van Hemel, J. H. Kingma, R. N. Hauer, M. J. Janse, and A. J. Dunning. Body surface mapping of ectopic left and right ventricular activation. QRS spectrum in patients without structural heart disease. *Circulation*, 82:879–896, 1990.

17] M. Potse, A. C. Linnenbank, and C. A. Grimbergen. Software design for analysis of multichannel intracardiac and body surface electrocardiograms. *Computer Methods and Programs in Biomedicine*, In press, 2001.

18] G. Huiskamp. Difference formulas for the surface laplacian on a triangulated surface. *Journal of Computational Physics*, 95:477–496, 1991.

19] N. Maglaveras, J. M. de Bakker, F. J. van Capelle, C. Pappas, and M. J. Janse. Activation delay in healed myocardial infarction: a comparison between model and experiment. *American Journal of Physiology*, 269:H1441–9, 1995.

20] R. Coronel, F. J. Wilms-Schopman, J. R. de Groot, M. J. Janse, F. J. van Capelle, and J. M. de Bakker. Laplacian electrograms and the interpretation of complex ventricular activation patterns during ventricular fibrillation. *Journal of Cardiovascular Electrophysiology*, 11:1119–1128, 2000.

21] A. G. Kleber, M. J. Janse, F. J. Wilms-Schopman, A. A. Wilde, and R. Coronel. Changes in conduction velocity during acute ischemia in ventricular myocardium of the isolated porcine heart. *Circulation*, 73:189–198, 1986.

22] S. R. Spielman, E. L. Michelson, L. N. Horowitz, J. F. Spear, and E. N. Moore. The limitations of epicardial mapping as a guide to the surgical therapy of ventricular tachycardia. *Circulation*, 57:666–670, 1978.

23] J. F. Spear, E. L. Michelson, S. R. Spielman, and E. N. Moore. The origin of ventricular arrhythmias 24 hours following experimental anterior septal coronary artery occlusion. *Circulation*, 55:844–852, 1977.

24] S. Kimber, E. Downar, L. Harris, G. Langer, L. L. Mickleborough, S. Masse, E. Sevaptsidis, and T. C. Chen. Mechanisms of spontaneous shift of surface electrocardiographic configuration during ventricular tachycardia. *Journal of the American College of Cardiology*, 20:1397–1404, 1992.

25] S. Osswald, D. J. Wilber, J. L. Lin, D. Du, H. B. Holden, J. N. Ruskin, and H. Garan. Mechanisms underlying different surface ECG morphologies of recurrent monomorphic ventricular tachycardia and their modification by procainamide. *Journal of Cardiovascular Electrophysiology*, 8:11–23, 1997.

26] C. Costeas, N. S. Peters, B. Waldecker, E. J. Ciaccio, A. L. Wit, and J. Coromilas. Mechanisms causing sustained ventricular tachycardia with multiple QRS morphologies: results of mapping studies in the infarcted canine heart. *Circulation*, 96:3721–3731, 1997.

27] L. Harris, E. Downar, L. Mickleborough, N. Shaikh, and I. Parson. Activation sequence of ventricular tachycardia: endocardial and epicardial mapping studies in the human ventricle. *Journal of the American College of Cardiology*, 10:1040–1047, 1987.

28] W. Kaltenbrunner, R. Cardinal, M. Dubuc, M. Shenasa, R. Nadeau, Tremblay, G, M. Vermeulen, P. Savard, and P. L. Page. Epicardial and endocardial mapping of ventricular tachycardia in patients with myocardial infarction. Is the origin of the tachycardia always subendocardially localized? *Circulation*, 84:1058–1071, 1991.

29] S. M. Blanchard, G. P. Wallcott, J. M. Wharton, and R. E. Ideker. Why is catheter ablation less successful than surgery for treating ventricular tachycardia that results from coronary artery disease? *Pacing & Clinical Electrophysiology*, 17:2315–2335, 1994.

4 Pacemapping of the postinfarction scar to detect ventricular tachycardia exit sites and zones of slow conduction

P.F.H.M. van Dessel[1], J.M.T. de Bakker [3,4], N.M. van Hemel[1], A. C. Linnenbank[3,4], E.R. Jessurun[1], J.J.A.M.T. Defauw[2]

From the Heart Lung Center Utrecht, Department of Cardiology[1] and Cardio-Thoracic Surgery[2], St Antonius Hospital, and Department of Cardiology[3], University Medical Center, Utrecht, Experimental and Molecular Cardiology Group of the Cardiovascular Research Institute[4]

Published in the Journal of Cardiovascular Electrophysiology 2001;12:662-670

Part of this study was presented at the Annual Scientific Sessions of the North American Society for Pacing and Electrophysiology, New Orleans, 1997

This study was supported by grant 94.147 of the Dutch Heart Foundation.

4.1 Abstract

Introduction. The exit site and central common pathway of slow conduction are preferred sites to guide radiofrequency ablation of postinfarction ventricular tachycardia (VT). Both require inducibility of VT. In addition, their low amplitude hampers direct recording of potentials generated by activation in pathways of slow conduction. We hypothesized that pacemapping during sinus rhythm is able to detect the VT exit site and potentials generated by activation in pathways of slow activation.

Methods and Results: In 13 patients suffering from VT late after anterior (10 pts) or inferior (3 pts) myocardial infarction stimulation was performed in scarred endocardium at 23.5 (13–36) sites per patient during arrhythmia surgery. Multielectrode recordings (64 sites) during stimulation at fixed cycle length of 500 ms were obtained. Endocardial breakthrough sites distant (>2 cm) from the pacing site were found at 4.3 (3–19) pacing sites per patient. Low amplitude discrete potentials could be detected between the pacing site and the breakthrough site in 2.3 (0–13) of 4.3 stimulation sequences. In these patients 19 VTs were induced and the exit site determined. In 6 patients the distant pacing breakthrough site was identical to the VT exit site, whereas in 7 patients no similar exit sites were found. Low amplitude discrete potentials during VT were found at median 2.0 (0–14) sites per patient.

Conclusion: Pacemapping of the postinfarction endocardial scar during sinus revealed 46% of the endocardial exit sites of VT and the same number of low amplitude discrete potentials observed during VT.

4.2 Introduction

The mechanism underlying postinfarction ventricular tachycardia (VT) is reentry and the arrhythmogenic substrate is often anatomically localized in the subendocardium [1–3]. Surviving myocardial fibers, encased in a fibrous sheath, provide tracts of slow conduction that are essential for the emergence and perpetuation of VT [4]. Direct electrographic detection of these tracts of slow conduction is difficult due to short cycle length of VT and the limited size of these tracts resulting in relatively small electrographic deflections as compared to remote signals from surrounding viable myocardium [5]. Furthermore, the existence of presystolic potentials during VT does not necessarily imply a functional role of the corresponding tract in maintaining VT. Stevenson et al. reported on the contribution of concealed entrainment during VT in functionally localizing these tracts [6]. Concealed entrainment, however, can only be applied as localization method in patients with inducible VTs.

We hypothesized that pace mapping of the arrhythmogenic substrate during sinus rhythm may help to identify the VT exit site and surviving tracts of myocardium and clarify their anatomic relation to the site of origin of VT [7, 8]. We carried out multi site pace mapping and multi-electrode registration during sinus

rhythm to identify zones of slow conduction in the subendocardial scar that may be crucial pathways of the postinfarction VT substrate.

4.3 Methods

4.3.1 Study patients and preoperative examination

Patients admitted to our hospital for ventricular arrhythmia surgery between April 1995 and May 1998 with a history of coronary artery disease and documented recurrent ventricular arrhythmias with or without aborted sudden cardiac death were eligible for the study. Patients were considered eligible for map-guided arrhythmia surgery if at least 3 of 9 segments of the angiographically visualized left ventricle showed a normal contraction pattern according to a ventriculographic wall motion score [9]. Electrophysiologic recordings during pacing required less than 10 minutes of mapping time. Patients were informed about the arrhythmia mapping and surgical procedure according to our hospital policy. Informed consent was obtained from all patients.

4.3.2 Intraoperative electrophysiologic study and surgical techniques

Antiarrhythmic drugs were withdrawn for at least 5 half times before surgery in all patients. All patients were anaesthetized using nitrous oxide, narcotics and muscle relaxants. Normothermic cardiopulmonary bypass was initiated with the perfusion temperature maintained at 37 ^{o}C. A needle electrode impaled in non-excitable tissue served as far field reference electrodes for the unipolar balloon electrodes. Epicardial bipolar pacing electrodes were placed on the right ventricular outflow tract and the right atrium. A unipolar pacing far field reference electrode was positioned in the subcutis of the border of the sternotomy wound, which was considered remote electrically unexcitable tissue. The left ventricular aneurysm or scar was incised and a small opening was created to be able to insert a custom made inflatable balloon in collapsed state into left ventricular cavity (Figure 4.1). The balloon, which contained 64 unipolar terminals at an interelectrode distance of 1 to 1.5 cm, was then inflated to provide electrode endocardium contact. Depending on the anterior or inferior location of the left ventricular aneurysm or scar a choice was made between 2 differently shaped endocardial balloons [10]. Standard surface ECG leads I, II and III were simultaneously recorded during the mapping procedure.

Recordings of sinus rhythm were used to determine the extent of the postinfarction endocardial scar. An electrode was considered to be situated in scarred tissue if the derived endocardial unipolar signal was "fragmented" (Figure 4.2) and the putative moment of local activation displayed a dV/dt_{min} of less than 20% of the maximal negative dV/dt_{min} found in the endocardial recording area in the same patient [4].

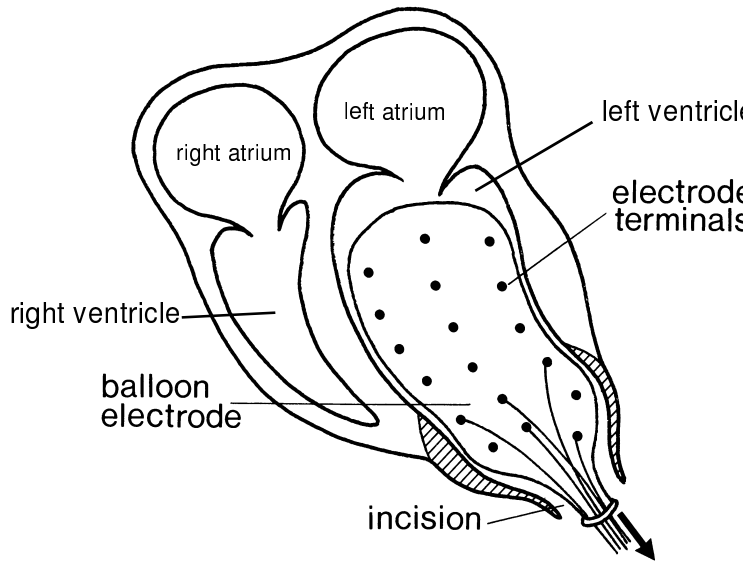

Figure 4.1: *The introduction of the balloon electrode designed for anterior myocardial infarction patients in the left ventricle is depicted. The apical aneurysm is opened just enough to allow insertion of the deflated balloon. Then, the ventriculotomy is partially closed and the balloon inflated to insure optimal electrode-endocardium contact.*

Prior to induction of VT unipolar pacing was performed on each balloon electrode, identified as situated in scarred endocardial tissue. Pacing was done with a fixed drive cycle of 500 ms, a pulse width of 2 ms and stimulus strength of just above the diastolic threshold. A standard external stimulation unit (Nihon Kohden VM186) was used for this purpose. Multi-electrode recordings were made for each pacing sequence with adequate capture using a computerized mapping system [10]. The mapping system consisted of a 256-channel analog-to-digital conversion amplifier with entrance characteristics of 2 μV/bit and 16-bit width.

Local main activation was defined as the steepest descending slope (dV/dt_{min}) in the unipolar electrogram (Figure 4.2). A breakthrough was defined as an endocardial site where an activation wave front emerged and from where it spread radially. The endocardial VT exit site was defined as the endocardial breakthrough that occurred earliest with respect to the onset of the QRS complex on the simultaneously recorded surface ECG [11]. The "breakthrough site" of pacing was defined as the site located near the infarction scar border where electrical activity entered viable myocardium.

To induce VT, programmed electrical stimulation with up to 4 extrastimuli was performed at a right ventricular electrode. After induction of VT, recordings were

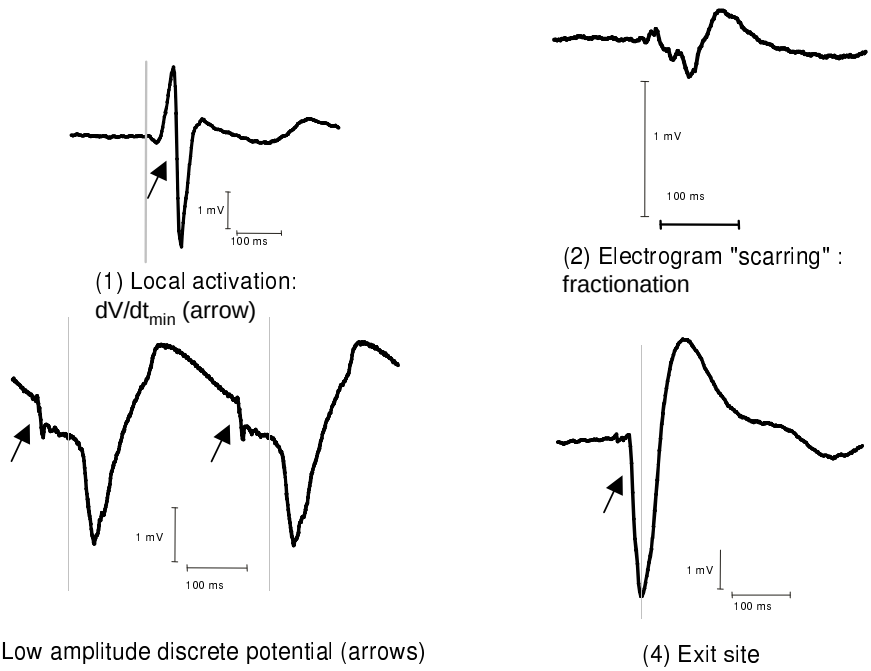

Figure 4.2: *Electrographic definitions. Local endocardial electrograms are shown which are considered: (1) normal. The black arrow indicates the moment of local activation; (2) fragmented as in scarred endocardium; (3) contain low amplitude discrete potentials (LADPs) (black arrows); (4) represent the exit site of VT. Note the Purkinje signal preceding the main electrographic deflection (black arrow). The vertical lines indicate the onset of the QRS complex on the surface ECG.*

made and endocardial activation maps determined. The endocardial site of origin was defined as that site at which the earliest local activation — characterized by the steepest descending slope (dV/dt_{min}) in the unipolar signal — was recorded with reference to the onset of the simultaneously recorded QRS complex on the body surface ECG. The surgical ablation procedure consisted of subendocardial resection, endocardial cryoablation or a combination of these procedures [12]. Surgical resection or cryoablation was performed as selectively and limited as possible. Selection of areas suitable for resection or cryoablation was guided by visual inspection of the endocardium by the surgeon and the endocardial maps obtained by mapping of the induced VTs.

After completion of the surgical arrhythmia ablation, the ventriculotomy was closed. If additional surgical procedures, such as ventricular aneurysm remodelling, valve replacement or myocardial revascularization, were mandatory, the patient was cooled, the aorta cross-clamped, cold crystalloid cardioplegia administered and the surgical procedure completed by standard techniques.

4.3.3 Signal processing

The electrographic deflections of interest often have low amplitude and may be masked by large remote deflections or stimulus artifacts during pacing. To enhance delectability of tiny electrograms the following signal processing techniques were applied.

Due to the exponential post pacing RC current decay, unipolar pacing tended to distort the initial 30 ms of post pacing interval of the electrograms recorded in neighboring electrodes. In order to improve the detection of early activations, an exponential decaying signal was subtracted from each channel starting from the end of the pacing spike. Fitting of the exponential decaying signal was performed by a least square fit of amplitude, time constant and offset to the interval 30 ms after the manually indicated end of pacing artifact. The exponential was subtracted in an interval of 50 ms if the timeconstant was in the expected range.

To further optimize the detection of small electrographic deflections indicating local events as opposed to large remote deflections a Laplacian transformation was used [13, 14]. The Laplacian is the second spatial derivative of the unipolar electrogram and a measure for the transmembrane current at the recording site. It therefore suppresses remote deflections, but still has the characteristics of the unipolar electrogram. Thus, in contrast to bipolar electrograms, the Laplacian is direction independent. In our study the Laplacian is determined by subtracting the mean of the signals of the 8 surrounding electrodes, weighed for interelectrode distance, from the signal recorded at the central recording electrode.

Finally, to improve signal to noise ratio and to emphasize the high frequency local deflections without a phase shift a Blackman filter with band pass characteristics of 40-200Hz was used.

4.3.4 Analysis of mapping data

All mapping data were reviewed in detail in a data committee consisting of 3 experienced electrophysiologists. Concomitant review of the original recording and filtered or otherwise processed signals was performed.

Breakthrough sites were considered distant relative to the pacing electrode if the breakthrough characteristics were found in other electrode recordings than those directly adjacent to the pacing electrode. In these cases, conduction was considered to follow strands of preserved myocardial fibers connecting the pacing site to non-infarcted myocardium. All other pacing electrodes were labeled as having non-distant breakthrough sites. Since electrode interspacing was 1.0 to 1.5 cm, distant breakthrough sites were more than 2 cm apart from the pacing electrode. Attempts were made to reconstruct the path of conduction from the pacing electrode to the breakthrough site by closely examining the interposed electrodes for low amplitude discrete potentials (LADPs).

The following definitions of LADPs were used. In sinus rhythm a LADP was defined as a small electrographic deflection, consistently present in all recorded QRS complexes, which was located *after* the offset of the body surface QRS com-

plex. During pacing and VT a LADP was defined as a small consistent electrographic deflection *preceding* activation recorded at the endocardial breakthrough or exit site respectively (Figure 4.2).

4.3.5 Statistical analysis

All data were stored in a computerized patient record database. Data analysis was performed on a personal computer using the "The SAS System for Windows 6.12 statistical software (SAS Institute, Inc)". Continuous data are presented as mean values $\pm$ SD unless stated otherwise. Subgroup comparisons were made using Chi-square or Fisher's exact test, whenever appropriate. Statistical significance was defined as a P value < 0.05.

4.4 Results

4.4.1 Study population

Thirteen patients who underwent arrhythmia surgery for recurrent postinfarction VT between April 1995 and May 1998 were included in the study. Baseline clinical characteristics are displayed in Table 4.1. All patients underwent arrhythmia surgery more than 6 months after their most recent myocardial infarction to allow for adequate healing of the myocardial scar. Most patients had multiple sustained VT morphologies during preoperative electrophysiologic testing (median 2.4 VT morphologies, range 1 – 5).

4.4.2 Clinical results

There was no in-hospital mortality. All patients underwent postoperative electrophysiologic testing 7 days after surgery. Two patients were inducible with an induction sequence including 2 extrastimuli. These patients were treated with sotalol and remained arrhythmia free during 2-year follow-up. In one patient one VT morphology remained inducible with a single extrastimulus, but the VT cycle length had increased from 240 ms to 420 ms. This patient underwent successful radiofrequency catheter ablation for this VT. Finally, one patient that was noninducible during postoperative electrophysiologic testing died suddenly 3 months later. An arrhythmic death was presumed in this case.

4.4.3 VT Morphologies

In total, 29 VT morphologies were induced during preoperative electrophysiologic testing. Fifteen of these 29 preoperative VT morphologies (52 %) were re-induced during ventricular antiarrhythmic surgery in these patients. Four of the 19 intraoperatively induced VT morphologies (21 %) were never documented before surgery. In 1 of 13 patients (8 %) no VTs could be induced during surgery. Only in

Age (years)	59.5 ± 8.2
Sex	
Male	11 (85 %)
Female	2 (15 %)
No. of VT morphologies per patient*	2.4 (1 – 5)
VT cycle length (ms)	295 ± 56
Scintigraphic LVEF (%)	30.1 ± 11.1
WMS (max. 9 of 9 normal segments)*	3.6 (3-6)
Extent of CAD (> 70 % stenosis)	
0 vessel	2 (15 %)
1 vessel	3 (24 %)
2 vessel	2 (15 %)
3 vessel	6 (46 %)
Time since infarction (years)	12.5 ± 7.8
Site of myocardial infarction	
Anterior	10 (77 %)
Inferior	3 (23 %)
Concomitant surgery	
CABG	7 (54 %)
MVR/MVP	1 (8 %)
Surgical procedure	
Cardiopulmonary bypass (min)	98.1 ± 36.8
Intraoperative mapping (min)	21.5 ± 3.1
Aortic cross clamping time (min)	42.5 ± 22.8

Table 4.1: *Baseline and surgical intervention characteristics (N=13). (CABG = coronary artery bypass grafting; CAD = coronary artery disease; LVEF = left ventricular ejection fraction; MVR/MVP = mitral valve replacement or valvuloplasty; WMS = wall motion score; VT = ventricular tachycardia. * = Median (range).)*

2 of 13 patients (15 %) all VT morphologies that were documented during preoperative electrophysiologic testing were re-induced intraoperatively.

4.4.4 Endocardial electrograms

Data on the endocardial electrograms are summarized in Table 4.2. The percentage of endocardium that was scarred was 36.7% (a median of 23.5 of 64 electrode terminals per patient). A significant correlation was found between the number of terminals situated in scarred endocardium and the mean dV/dt_{min} in sinus rhythm in all 64 electrodes (r=0.59, p=0.03). A schematic overview of the signal analysis flow sheet is presented in Figure 4.3.

Extent of endocardial scar (electrodes)*	23.5 (36.7 %) [13–36]
Adequate pacing capture (%)	59.0 ± 23.2
Non-distant breakthroughs per patient (electrodes)*	9.0 (14.1 %) [3–22]
Distant breakthroughs per patient (electrodes)*	4.3 (6.7 %) [3–19]
Distant breakthroughs per patient with bridging LADPs (electrodes)*	2.3 (3.6 %) [0–13]

Table 4.2: *Pacing intervention characteristics (* = Data shown as median (percentage)[range]).*

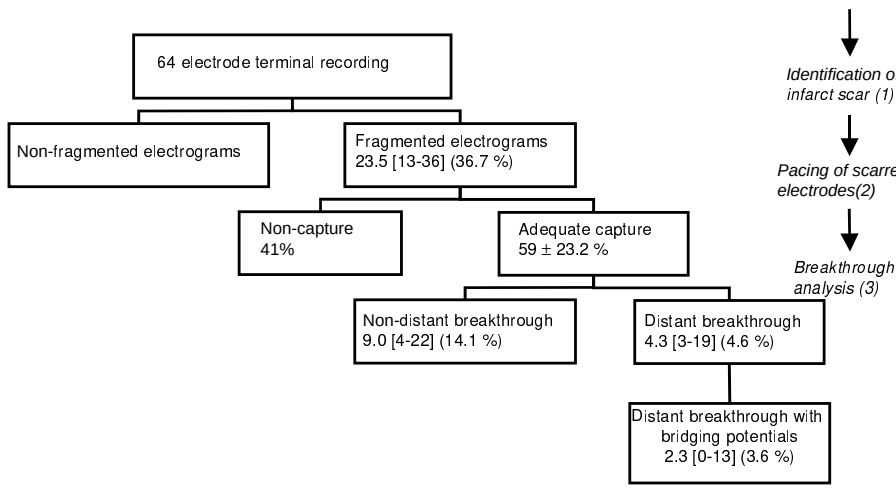

Figure 4.3: *Schematic overview of signal analysis. All electrograms are inspected for fragmentation to identify whether they are located in scar tissue (1). Electrode terminals situated in scarred endocardium are paced if capture can be obtained (2). If capture can be obtained activation maps are reviewed for distant breakthroughs and anatomical paths of conduction (3).*

4.4.5 Pacing in scar tissue and VT exit site

Adequate pacing capture could be obtained in 59.0 % of selected electrodes per patient using stimulus strengths up to 9.9 V at pulse width of 2.0 ms. Non distant breakthrough sites were found in median 9.0 (3-22) of these successful pacing attempts per patient, whereas distant breakthrough sites were found in median 4.3 (0-13) stimulation sequences per patient. In median 2.0 stimulation attempts per patient a distant breakthrough was found. Delay between the moment of stimulation and the emergence of electrical activity at the breakthrough site was significantly longer when the breakthrough was distant than in those stimulation attempts where the breakthrough was non-distant (44.8 ± 4.8 ms vs. 17.9 ± 2.1 ms, P=0.02).

Type of recording	*Number of electrode terminals displaying low amplitude discrete potentials*
Sinus rhythm	0.7 ± 1.3 (range 0–4) of 64 terminals
Ventricular tachycardia	2.0 ± 3.4 (range 0–14) of 64 terminals
Distant breakthrough	2.4 ± 3.7 (range 0–20) of 64 terminals
Non distant breakthrough	0.8 ± 1.5 (range 0–7) of 64 terminals

Table 4.3: *Low amplitude discrete potential characteristics.*

In 13 patients 19 intraoperative sustained monomorphic VTs with distinct VT morphology (median 1.1, range 1–3) were induced whereas in these patients in 54 distinct stimulation sites (median 2.3, range .0-13) a distant breakthrough was found during pacing. Thirty-seven of these 54 pacing sites with distant breakthroughs proved to be anatomically distinct (median per patient 2.3, range 0-6). The exit site of 7 of the 19 induced VTs (37 %) was identical with a distant breakthrough site during pacing. In 7 patients 1 VT exit site was identical to one of the distant breakthrough sites, whereas in 6 patients no intraoperative VT with similar pacing breakthrough site was found.

4.4.6 Isolated low amplitude discrete potentials

The distribution of the presence of LADPs is summarized in Table 4.3. More LADPs were identified during VT than during sinus rhythm. A distinction was made between LADPs recorded during VT in the border zone of the infarct (i.e. an electrode terminal located in scarred tissue bordering normal tissue) and LAPDs recorded in the inner scar. From a total of 75 recorded LADPs during VT, 34 LADPs were found in the infarct border, whereas 41 LADPs were found in the central scar.

When pacing was performed during sinus rhythm approximately the same number of electrode terminals was found displaying LADPs as during VT if a so-called distant breakthrough was present. However, in pacing interventions that showed a non-distant breakthrough the presence of isolated LADPs was equivalent to that during sinus rhythm. Significantly more LADPs were found when a distant breakthrough was present as compared to non-distant breakthroughs ($p=0.0001$). If LADPs could be identified in VT then in 70 % of cases (sites) LADPs were seen during pacing at these same anatomical sites. Only in 24 % of cases LADPs were seen during sinus rhythm at sites where LADPs had been noticed during VT.

4.4.7 Pathways during infarct pacing and VT

Isolated LADPs recorded during infarct pacing were found at more than 1 site in 33 cases (pacing interventions). In 35 of 37 cases with distinct distant exits we were

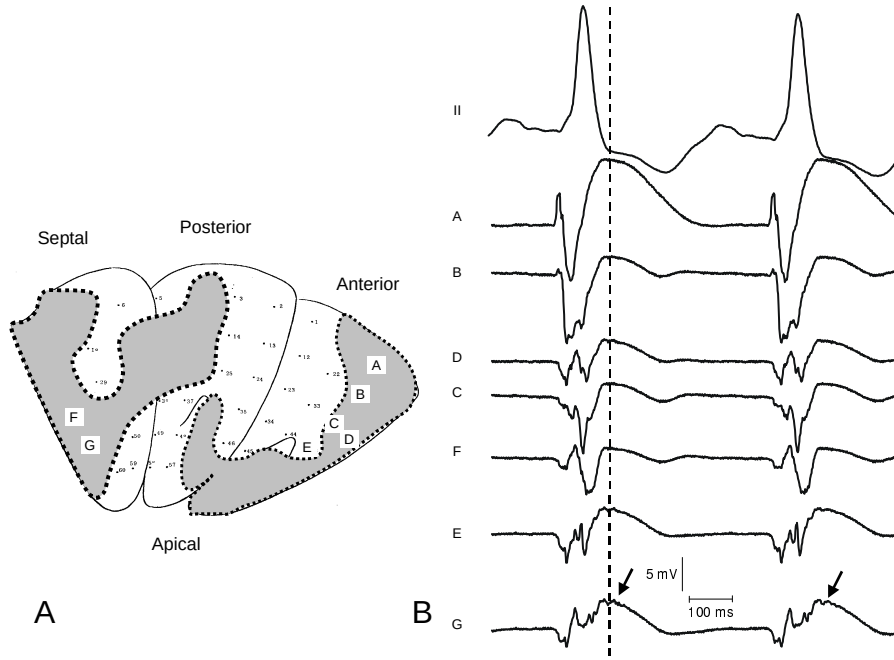

Figure 4.4: *Fractionated electrograms during sinus rhythm.* ***Panel A.*** *Schematic representation of the endocardial surface of the left ventricle. The outlined grayed septal and anterolateral area depicts the endocardial scar.* ***Panel B.*** *Electrographic tracings (A-G) obtained during sinus rhythm from electrode terminals located along the putative diastolic path of VT as indicated in Figure 4.5. The dotted line indicates the offset of the body surface QRS complex in lead II. Clear fragmentation is present in electrodes B, C, D, F and G. Only at site G a low amplitude deflection occurs after the offset of the surface QRS complex (arrow).*

able to reconstruct the tract from pacing site to breakthrough site and to correlate it with recordings during VT. An example is illustrated in the figures 4.4 to 4.8. A same schematic drawing of the left ventricular endocardium with the location of scar tissue indicated is shown in panel A. The myocardial wall is incised along the left anterior descending artery and then folded outwards. The endocardial scar (gray area) is located in the septal and anterolateral region with extension into the posterior area. Numbers indicate recording sites. The characters A to G point to sites where electrograms with the same character were recorded. Short arrows in electrograms point to local activation times. Long arrows show the sequence of activation where applicable.

In figure 4.4 tracings are shown during sinus rhythm. Electrograms are fractionated, indicating that the recording sites are located in scar tissue. In figure 4.5 seven electrograms obtained during VT are shown. The sequence of activation

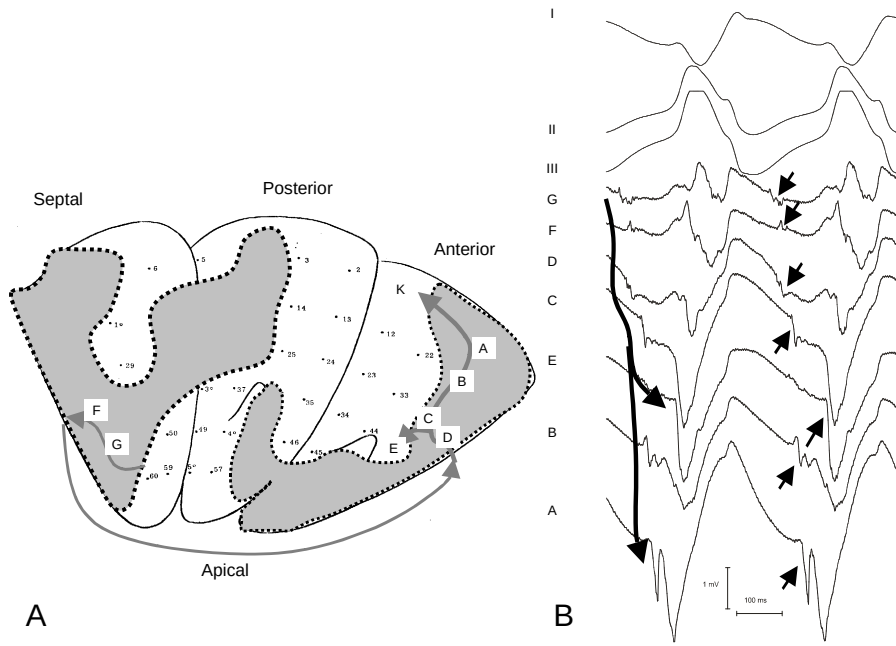

Figure 4.5: *Activation during ventricular tachycardia.* ***Panel A*** *as in figure 4.4.The arrow indicates the putative pathway of the reentrant circuit of the VT within the infarcted zone.* ***Panel B*** *shows electrographic tracings obtained during ventricular tachycardia. Small black arrows indicate local activation times. Diastolic pathways (long arrows) are demonstrated which run from the apicoseptal area through the anterior wall to a mid-anterolateral (E) and an anterolateral-basal breakthrough (K) as visualized by the arrow in* ***panel A****. I, II, III = standard extremity ECG leads.*

delineates a diastolic pathway (arrows in figure 4.5A), leading through the scar to 2 breakthrough sites in the mid-anterolateral (site E) and anterolateral-basal (site K) region respectively.

Pacing at electrode 42 (site J in figure 4.6), located adjacent to the diastolic pathway resulted in LADPs at sites where diastolic potentials were recorded during VT. Figure 4.7 shows the electrograms of figure 4.6 after subtraction of the exponential decay of the stimulus artifact and application of the Laplacian technique. Conduction delays between the sites D and A in the tract were similar during VT and stimulation (45 ms respectively 42 ms).

Conduction to the mid anterolateral VT breakthrough site (site E) occurred via an alternative tract, evidenced by the fact that site E was activated prior to site C. Activation proceeded towards the site where activation entered the diastolic pathway during VT (site G) via the same pathway, but in retrograde direction. Activation along this section of the pathway blocked near the entrance site (site G). Conduction delay between sites J and G was 62 ms during VT and 56 ms during

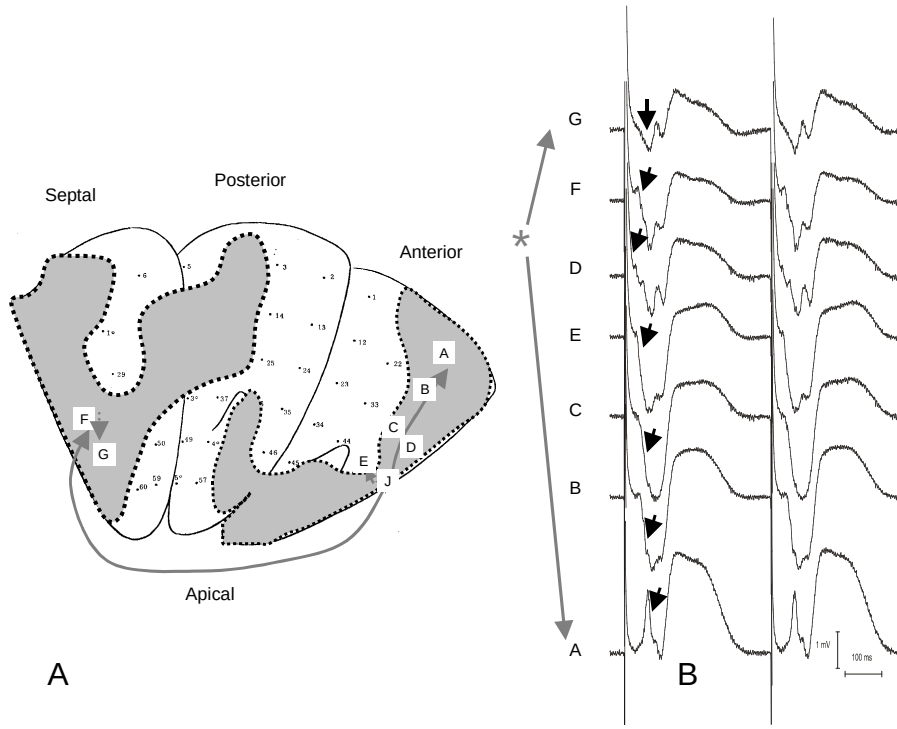

Figure 4.6: *Activation during stimulation at site J.* ***Panel A*** *as in figure 4.4. The arrow indicates the putative pathway of the reentrant circuit of the VT within the infarcted zone.* ***Panel B*** *depicts local endocardial electrograms obtained during unipolar pacing at electrode terminal J in sinus rhythm at pacing cycle length 500 ms. Note that the breakthrough into the viable myocardium at site E is the same as during VT (4.5,* ***Panel A****). Black arrows mark low amplitude discrete potentials (LADPs). Propagation from D to A and towards F is via the same route as during VT (long arrows in* ***Panel A****). Activation is conducted from J to E via an alternative tract (short arrow in* ***Panel A****). Retrograde conduction to F appears to block between F and G (no breakthrough at G).*

stimulation.

In the same heart, pacing from site A (the exit site of the VT in the anterolateral-basal area) resulted in a distant exit (site E in figure 4.8). Activation proceeded via the same diastolic pathway as during VT and stimulation at site J, but in opposite direction. Arrows in panel B point to activation times. Their sequence indicate spread of activation from B to E. Activation delay between site B and E was 68 ms, which is similar to the activation delay between these 2 sites during VT (72 ms). To justify the selected activation times, the same signal processing procedures as indicated in the methods were applied. Panel C shows the electrograms after subtraction of the exponential decay.

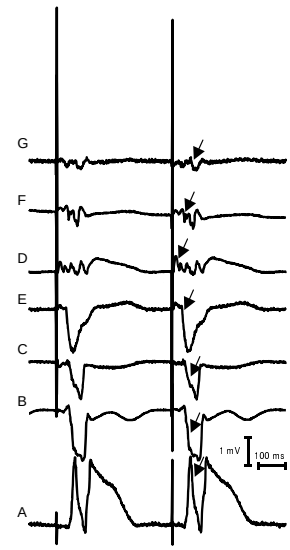

Figure 4.7: *Signal processing of electrograms shown in figure 4.6. Electrograms are displayed after subtraction of the exponential pacing decay and application of the Laplacian procedure. Arrows mark the moment of local activation in the signals. Note that in tracing D the local deflection was masked in the raw signal by the stimulus artifact*

4.5 Discussion

4.5.1 Main results

In our study, pacing with adequate capture was possible in 59 % of "scarred" electrode terminals although large stimulation amplitudes (9.9 V) were required in a number of pacing sequences. In approximately one third of electrodes displaying features of scarring the pacing breakthrough was found in the adjacent electrode. In these cases propagation of electrical activity was considered to be the result of capture of nearby non-infarcted myocardium. In 10 % of paced electrode terminals breakthrough site electrograms were found with variable delay in non-adjacent electrodes. In these cases conduction along a strand of surviving myocardial tissue, anatomically separated by fibrous tissue from surrounding myocardium, was postulated to take place. Therefore, these pacing sites were considered to be potentially located in the reentrant circuit. The exit site of 37 % of the VTs was identical with a distant breakthrough site during pacing.

The extent to which LADPs can be recorded during sinus rhythm appears to be limited. In our series less than 1 LADP on average was found per 64 electrode terminals. This number increases to 2.4 LADPs, which is the same number of LADPs found during VT, when pacing at a cycle length shorter than the sinus rhythm cycle length is applied. Signal processing techniques as described are necessary for reliable determination of LADPs in unipolar electrograms during pacing.

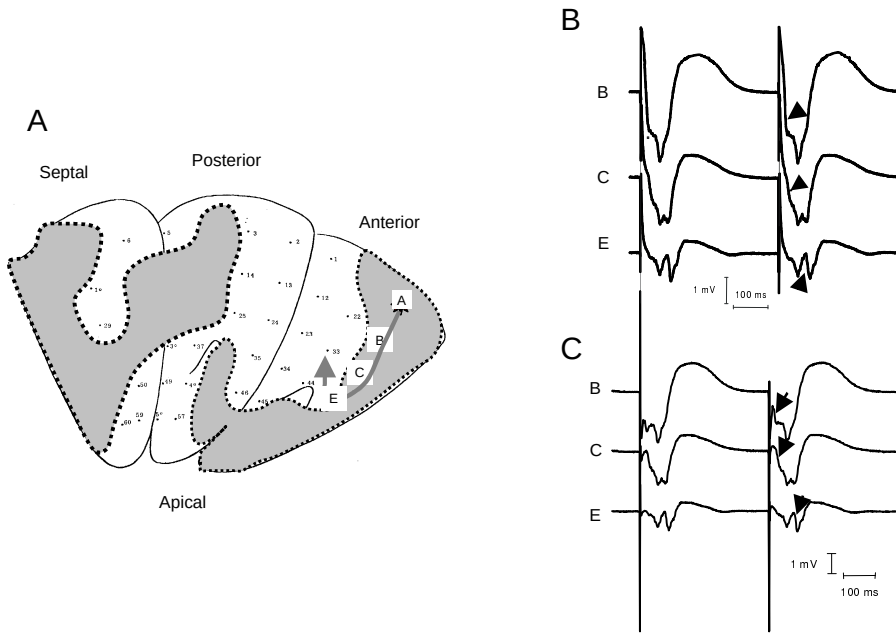

Figure 4.8: ***Panel A*** *as in figure 4.5. The arrow indicates the putative pathway of the reentrant circuit of the VT within the infarcted zone.* ***Panel B*** *depicts local endocardial electrograms at sites obtained during unipolar pacing at electrode terminal A in sinus rhythm at pacing cycle length 500 ms. The wave front propagates towards E via part of the diastolic pathway during VT (Figure 4.5).* ***Panel C*** *shows electrograms after subtraction of the exponential decay. Arrows mark the moment of local activation*

4.5.2 Signal processing

Unipolar electrograms were chosen in this study, because information on the timing of local activation is more precise [15]. Furthermore, the detection of a passing wave front is not dependent on the direction of this wave front. In our study interelectrode distance ranged from 1 to 1.5 cm. This spatial resolution may have implications for the number of LADPs found. It is conceivable that more LADPs can be found when mapping is performed with a mapping electrode with smaller interelectrode distance. Major disadvantage of the use of unipolar electrogram is that the LADPs are relative small compared to the remote deflections of the cavity potential. Using the Laplacian technique circumvents this disadvantage.

To increase the visibility of LADPs at recording sites near the stimulus exponential curve subtraction had to be used. Laplacian spatial filtering and exponential subtraction were the two signal processing techniques that highly improved detection of LADPs. The value of bi-directional Blackman filtering was less significant.

4.5.3 Pacing threshold

Stimulation was performed with just above pacing threshold. However, in a substantial number of cases fairly large stimulation currents were needed. This might be due to abnormal current flow in infarcted myocardium and the large distance from the site of stimulation to excitable non-infarcted myocardium. It cannot be ruled out that these stimulation currents may have caused capture of remote excitable tissue erroneously resulting in distant breakthroughs. It should be noted that distant breakthroughs were by definition at least two interelectrode distances (> 2 cm) from the pacing site and therefore it is unlikely that pseudo-distant breakthroughs by remote capture occurred in a large number of cases.

Secondly, pacing scarred tissue with sufficient stimulation strength to achieve capture often resulted in disfiguration of the initial unipolar electrogram following the pacing spike. To permit analysis of LADPs in the initial 30 ms following the pacing spike subtraction of an exponentially fitted curve from this segment of the electrogram was in fact obligatory. Since this malformation of the electrogram by pacing causes merely an RC exponential decay curve by the capacitive and resistance properties of the electrode-tissue interface, we believe that this signal processing did not introduce new artifacts or obscure true deflections in the original electrogram.

4.5.4 Related studies

Bogun et al. demonstrated that arcs of block that are anatomically determined and present during sinus rhythm bound the area of slow conduction [8]. The authors stated that sites displaying isolated diastolic potentials in VT that cannot be dissociated during concealed entrainment appear to represent effective sites for radiofrequency ablation. In addition, they showed that these LADPs also could be identified during pacing in sinus rhythm at these sites. However, in their study the presence of LADPs during sinus rhythm was investigated in patients, who exhibited isolated diastolic potentials during VT. This study was performed in incessant and hemodynamically stable VTs and only sites of interest that were already identified during VT were explored for the presence of LADPs during sinus rhythm. Therefore it cannot be concluded from the study of Bogun that in non-selected patients these sites can be identified without prior knowledge of their appearance during VT.

In our study, fractionated electrograms were identified in 23.5 of 64 electrodes (36.7 %). This is highly comparable to the spatial amount of electrocardiographical scarring in postinfarction sinus rhythm mapping that has been reported in other studies [16, 17]. Kienzle et al. reported that in 4 of 13 patients 5 % of mapped sites displayed isolated potentials during sinus rhythm [16]. This appears to correlate with the number of LADPs found during sinus rhythm in our study

4.5.5 Clinical significance of VT exit sites and LADPs

Ablation of infarct related VT can be carried out at the VT exit site as well as in the central common pathway. The latter is usually preferable because it affects the most vulnerable site with the smallest dimensions of the circuit. The exit site may be wide requiring more extensive ablation. The advantage of VT exit ablation is however the fact that this site can always be determined whereas signals generated by the common pathway are often too small to be detected.

We showed that VT exit sites can be determined by our pacing technique in 37 % of VTs. Several factors can be hold responsible for this rather poor yield. In the first place, the direction of conduction over the diastolic pathway may differ during VT and pacing. Therefore VT scar-entry sites may have been presented as endocardial breakthroughs during endocardial pacing. Since endocardial breakthrough was defined as the endocardial site which displays earliest radial endocardial spread of activation, the site where the diastolic pathway connects to the non-infarcted myocardium that is anatomically closest to the pacing site, will be presented as breakthrough, regardless whether it is the entry or exit site of the VT circuit. Secondly, it should be noted, that a pacing cycle length of 500 ms was used, which often is considerably longer than the VT cycle length. This difference in cycle length might affect the presence of unidirectional functional block within the circuit thereby again presenting VT entry sites as endocardial pacing breakthroughs. Thirdly, a 64-electrode balloon was used. It is conceivable, that the ability of pace mapping to detect pathways of slow conduction is dependent on the electrode resolution of the balloon and the size of the slow conduction pathway. Narrow tracts of fibers leading to VT exit sites may have been missed due to too low spatial electrode resolution. Better results may be achieved with a 256-electrode balloon. Fourthly, the yield of intraoperative VT induction is comparatively low. In order to position the endocardial balloon, the left ventricular postinfarction aneurysm was incised. Therefore, the postinfarction VT reentrant circuit may have been interrupted before measurements were made. Only 52 % of preoperative VT morphologies were re-induced during surgery. This may explain why more endocardial breakthrough sites were found during pacing than intraoperative VT exit sites. The latter may be an advantage over traditional activation sequence mapping since information on the arrhythmogenic substrate that otherwise might have been unobtainable can now be retrieved.

Stevenson et al. reported on the use of pacing interventions during VT for determining the functional significance of the various constituting parts of the reentry circuit [6]. Analysis of the post pacing interval following concealed entrainment can identify sites suitable for radiofrequency catheter ablation of a limited but crucial part of the arrhythmogenic substrate. However, localization of the common slow conducting pathway with concealed entrainment can only be performed if VT is inducible. Furthermore, it appears that not all sites fulfilling post pacing interval criteria that are compatible with a location in the central common pathway are in fact located along a crucial pathway [18, 19].

Finding the central common pathway of postinfarction VT in sinus rhythm

would substantially improve clinical applicability of radiofrequency ablation of postinfarction VT. Sinus rhythm mapping has, however, a number of drawbacks. We showed that, the number of LADPs recorded during sinus rhythm is smaller than during pacing. Furthermore, during sinus rhythm the direction of the wave front causing the LADP is not known since the onset of this wave front is not known. This precludes reconstruction of the path of propagation. In contrast, when ventricular pacing is performed the relation of the LADP with the direction of propagation of the activation front is known since the onset — i.e. the pacing electrode — and the destination — i.e. the endocardial breakthrough — of the wave front are known. This allows for reconstruction of a path between the pacing site and the endocardial breakthrough.

This study shows that pathways of conduction in the infarction scar can be found by using endocardial pacing. Whether the currently presented mapping technique is helpful in ablating the central common pathway of postinfarction VT can as yet not be concluded from these data. Firstly, it is not certain that all sites that display LADPs and that are located between pacing electrode and endocardial breakthrough are along the same path. It is possible that these sites are situated on interconnecting and branching paths. Secondly, the role these reconstructed connections fulfill in perpetuation of VT remains unclear. As outlined before, our pacemapping method only anatomically localizes surviving strands of myocardium in the endocardial scar. Whether these tracts are crucial parts of the reentrant circuit or merely play a role as bystander pathways cannot be derived from these data.

Currently, most of the data analysis was performed offline. The functional role of surviving strands in perpetuating VT could therefore not be proven by selective interruption of these strands and its effect on inducibility of VT. Online data analysis and selective interruption of these tracts, which results in non-inducibility of VT, will be necessary to identify the exact functional nature of the surviving strand. Online analysis of the data is feasible since all the algorithms required for signal processing have been developed. Also, newly developed mapping devices such as electromagnetic mapping and non-contact mapping may be very helpful in extending this mapping technique to the electrophysiology laboratory [20, 21].

4.6 Conclusion

Pacemapping and multi-electrode recording increases information on the course of conduction through the postinfarction scar. The extent to which LADPs are found is significantly greater than during sinus rhythm and comparable to VT. This localization method is less dependent on inducibility of VT or paucity of coexisting VT morphologies. At present, this mapping technique cannot be considered a replacement for activation sequence mapping for ablation of VT but it does provide information on arrhythmogenic regions in the postinfarction heart. To judge whether interruption of the pathways found results in curative termination of VT a prospective trial comparing this technique with entrainment mapping

is required.

Acknowledgements

This study was supported by grant 94.147 of the Dutch Heart Foundation.

References

1] H. J. Wellens, D. Durrer, and K. I. Lie. Observations on mechanisms of ventricular tachycardia in man. *Circulation*, 54:237–244, 1976.

2] M. E. Josephson, L. N. Horowitz, A. Farshidi, and J. A. Kastor. Recurrent sustained ventricular tachycardia. I. mechanisms. *Circulation*, 57:431–440, 1978.

3] W. G. Stevenson, N. W. James, I. Wiener, and K. Nademanee. Slow conduction in the infarct scar: relevance to the occurrence, detection and ablation of ventricular reentry circuits resulting from myocardial infarction. *American Heart Journal*, 117:452–467, 1989.

4] J. M. de Bakker, F. J. van Capelle, M. J. Janse, N. M. van Hemel, R. N. Hauer, J. J. Defauw, F. E. Vermeulen, and P. F. Bakker-de Wekker. Macroreentry in the infarcted human heart: the mechanism of ventricular tachycardias with a "focal" activation pattern. *Journal of the American College of Cardiology*, 18:1005–1014, 1991.

5] J. M. de Bakker, F. J. van Capelle, M. J. Janse, A. A. Wilde, R. Coronel, A. E. Becker, K. P. Dingemans, N. M. van Hemel, and R. N. Hauer. Reentry as a cause of ventricular tachycardia in patients with chronic ischemic heart disease: electrophysiologic and anatomic correlation. *Circulation*, 77:589–606, 1988.

6] W. G. Stevenson, H. Khan, P. Sager, L. A. Saxon, H. R. Middlekauff, P. D. Natterson, and I. Wiener. Identification of reentry circuit sites during catheter mapping and radiofrequency ablation of ventricular tachycardia late after myocardial infarction. *Circulation*, 88:1647–1670, 1993.

7] W. G. Stevenson, J. N. Weiss, I. Wiener, S. M. Rivitz, K. Nademanee, T. Klitzner, L. Yeatman, M. Josephson, and D. Wohlgelernter. Fractionated endocardial electrograms are associated with slow conduction in humans: evidence from pace-mapping. *Journal of the American College of Cardiology*, 13:369–376, 1989.

8] F. Bogun, M. Bahu, B. P. Knight, R. Weiss, R. Goyal, E. Daoud, K. C. Man, S. A. Strickberger, and F. Morady. Response to pacing at sites of isolated diastolic potentials during ventricular tachycardia in patients with previous myocardial infarction. *Journal of the American College of Cardiology*, 30:505–513, 1997.

9] N. M. van Hemel, J. H. Kingma, J. J. Defauw, F. E. Vermeulen, E. G. Mast, J. M. P. G. Ernst, and C. A. Ascoop. Left ventricular segmental wall motion score as a criterion for selecting patients for direct surgery in the treatment of postinfarction ventricular tachycardia. *European Heart Journal*, 10:304–315, 1989.

10] J. M. de Bakker, M. J. Janse, F. J. van Capelle, and D. Durrer. An interactive computersystem for guiding the treatment of life threatening ventricular tachycardias. *IEEE Transactions on Biomedical Engineering*, 31:362–368, 1984.

11] M. E. Josephson, L. N. Horowitz, A. Farshidi, J. F. Spear, J. A. Kastor, and E. N. Moore. Recurrent sustained ventricular tachycardia. 2. Endocardial mapping. *Circulation*, 57:440–447, 1978.

12] M. E. Josephson, A. H. Harken, and L. N. Horowitz. Endocardial excision: a new surgical technique for the treatment of recurrent ventricular tachycardia. *Circulation*, 60:1430–1439, 1979.

13] G. Huiskamp. Difference formulas for the surface laplacian on a triangulated surface. *Journal of Computational Physics*, 95:477–496, 1991.

14] N. Maglaveras, J. M. de Bakker, F. J. van Capelle, C. Pappas, and M. J. Janse. Activation delay in healed myocardial infarction: a comparison between model and experiment. *American Journal of Physiology*, 269:H1441–9, 1995.

15] G. Ndrepepa, E. B. Caref, H. Yin, N. El-Sherif, and M. Restivo. Activation time determination by high-resolution unipolar and bipolar extracellular electrograms in the canine heart. *Journal of Cardiovascular Electrophysiology*, 6:174–188, 1995.

16] M. G. Kienzle, J. Miller, R. A. Falcone, A. Harken, and M. E. Josephson. Intraoperative endocardial mapping during sinus rhythm: relationship to site of origin of ventricular tachycardia. *Circulation*, 70:957–965, 1984.

17] W. Kaltenbrunner, R. Cardinal, M. Dubuc, M. Shenasa, R. Nadeau, Tremblay, G, M. Vermeulen, P. Savard, and P. L. Page. Epicardial and endocardial mapping of ventricular tachycardia in patients with myocardial infarction. Is the origin of the tachycardia always subendocardially localized? *Circulation*, 84:1058–1071, 1991.

18] F. Bogun, B. Knight, R. Goyal, S. A. Strickberger, S. H. Hohnloser, and F. Morady. Clinical value of the postpacing interval for mapping of ventricular tachycardia in patients with prior myocardial infarction. *Journal of Cardiovascular Electrophysiology*, 10:43–51, 1999.

19] F. Bogun, M. Bahu, B. P. Knight, R. Weiss, W. Paladino, M. Harvey, R. Goyal, E. Daoud, K. C. Man, S. A. Strickberger, and F. Morady. Comparison of effective and ineffective target sites that demonstrate concealed entrainment in

patients with coronary artery disease undergoing radiofrequency ablation of ventricular tachycardia. *Circulation*, 95:183–190, 1997.

20] R. J. Schilling, N. S. Peters, and D. W. Davies. Mapping and ablation of ventricular tachycardia with the aid of a non-contact mapping system. *Heart*, 81:570–575, 1999.

21] L. Gepstein and S. J. Evans. Electroanatomical mapping of the heart: basic concepts and implications for the treatment of cardiac arrhythmias. *Pacing & Clinical Electrophysiology*, 21:1268–1278, 1998.

5 Correlation between endocardial late potentials during sinus rhythm and late potentials determined with signal averaged body surface mapping

P.F.H.M. van Dessel[1], A.C. Linnenbank[2,3],N.M. van Hemel[1], J.M.T. de Bakker[2,3], E.R. Jessurun[1], M. Potse[4], E.F.D. Wever [1]

From the Heart Lung Center Utrecht, Department of Cardiology[1], St Antonius Hospital, Nieuwegein, and Department of Cardiology[2], University Medical Center, Utrecht, Experimental and Molecular Cardiology Group of the Cardiovascular Research Institute[3], and Department of Medical Physics[4], Academic Medical Center, Amsterdam, The Netherlands

Submitted to Cardiovascular Research

5.1 Abstract

Objective: Signal averaged electrocardiography (SAECG) is used as a non-invasive tool to predict arrhythmic events in various subsets of patients. At present, information on the location of arrhythmogenic regions in the heart cannot be obtained from standard SAECG using 3 orthogonal leads. Objectives were (1) to investigate the sensitivity and specificity of signal averaged body surface mapping (SABSM) in detecting late potentials as compared to SAECG and (2) to localize non-invasively the arrhythmogenic regions in postinfarction ventricular tachycardia (VT) by SABSM.

Methods: Simultaneous 3-minute recordings with a 62-electrode body surface mapping (BSM) device to obtain SABSM and SAECG and a 64-electrode endocardial basket catheter were obtained during sinus rhythm as well as during VT in 16 patients (12 male) with remote (8.7 ± 5.1 years) myocardial (10 anterior, 6 inferior) infarction. In 12 patients without structural heart disease SABSM and SAECG were performed without endocardial mapping. QRS complexes obtained with BSM were signal averaged and a 25 Hz high-pass bi-directional filter was applied. Body surface integral maps of the 50 ms following the J-point (LPMAP) were constructed. Basket recordings were reviewed for late potentials. Electrodes displaying late potentials were marked on the 3D reconstruction of the basket catheter.

Results: None of the patients without structural heart disease showed activity in the LPMAP or had a positive SAECG. All postinfarction VT patients did show activity in the LPMAP, whereas in 13 of 16 patients the 3-lead SAECG was negative. In total 6.2 ± 5.7 (range 1–18) endocardial late potentials during sinus rhythm were found in the VT patients. Visual inspection showed anatomic correlation of 0.6 ± 0.12 between the basket site of diastolic potentials and activity in the LPMAP electrode.

Conclusion: SABSM has an increased sensitivity and specificity in detecting late potentials as compared to SAECG. Furthermore, SABSM is capable of delineation of these areas that are indispensable for the genesis of postinfarction VT. Whether SABSM may be useful in non-invasively confining areas that serve as target for VT ablation procedures remains to be established in a prospective study.

5.2 Introduction

High resolution signal averaged electrocardiograms (SAECG) have shown low-level, high-frequency potentials immediately after the QRS complex in patients suffering from coronary artery disease related ventricular tachycardia (VT) during sinus rhythm [1]. At present, SAECG is used to identify subjects prone to sustained VT, but detection of late potentials (LPs) has been of limited use [2–4]. Only 17% to 29% of postinfarction patients with LPs on the SAECG will experience sustained VT or ventricular fibrillation within 1 year [5]. Several authors reported that extending the number of surface electrodes and performing frequency domain analysis, may enhance the diagnostic value of signal averaging [6,7].

The mechanism underlying postinfarction VT can be attributed to reentry and the arrhythmogenic substrate is often situated in the subendocardium [8–10]. Surviving myocardial fibers, encased in a fibrous sheath, provide tracts of slow conduction that are essential for the emergence and perpetuation of postinfarction VT [11]. It has been suggested that late ventricular potentials on the SAECG arise from activation in these tracts of slow conduction [12, 13]. Therefore, late potentials are believed to reflect the presence of areas of delayed conduction, which are part of the reentrant circuit [14, 15]. Direct detection of these tracts of slow conduction of postinfarction VT by catheter mapping is often time consuming due to the extent of scarred endocardium. Non-invasive delineation or narrowing down of the regions where tracts of slow conduction can be found during sinus rhythm may greatly facilitate radiofrequency ablation of postinfarction VT.

At present, no spatial information on the anatomical sites of origin of LPs can be derived from the SAECG. A spatially high resolution body surface mapping electrode system, in addition to the low noise level obtained by signal averaging, may enhance non-invasive detection of the endocardial areas that generate LPs during sinus rhythm and may provide information on their anatomical location [13, 16, 17].

Therefore, we postulated that 1) the sensitivity for detection of LPs increases by signal averaged body surface mapping (SABSM) as compared to SAECG without loss of specificity and 2) SABSM is capable of anatomic delineation of endocardial areas with delayed conduction. To validate this hypothesis, 62-channel SABSM and 3-lead SAECG was performed in addition to simultaneous multisite endocardial mapping by means of a 64-electrode basket catheter in patients with postinfarction VT, whereas for comparison SABSMs and 3-lead SAECGs were obtained in 12 healthy controls.

5.3 Methods

5.3.1 Patient selection

The research protocol, which was approved by the Ethical Committee of our institution, was performed on two groups of patients who had given prior written informed consent. The control group consisted of 12 healthy controls (7 females, 5 males), mean age 42.1 $\pm$ 16.6 years (range 16 – 63 years), who had normal electrocardiograms, normal echocardiograms, no history of cardiovascular disease and who were not receiving medication. The patient group comprised 16 patients referred to our hospital between November 1997 and February 1999 for antiarrhythmic surgery or radiofrequency catheter ablation of infarct related VT. Specific eligibility criteria included both: (1) documented recurrent ventricular arrhythmias with or without aborted sudden cardiac death; (2) inducible sustained monomorphic VT during programmed electrical stimulation. The investigation conforms with the principles outlined in the Declaration of Helsinki. Characteristics of the patient group are presented in Table 5.1. In both groups SAECG and SABSM was performed, but only in the patient group a basket catheter was percutaneously

Age (years)	67.5 ± 9.3
Sex	
Male	12
Female	4
No. of VT morphologies per patient*	1.3 (1 – 4)
VT cycle length (ms)	318 ± 65
Scintigraphic LVEF (%)	26.0 ± 9.3
Echocardiographic dimensions	
LV end diastolic length (mm)	91.8 ± 9.7
LV end diastolic width (mm)	56.4 ± 7.9
Extent of CAD (> 70 % stenosis)	
1 vessel	6
2 vessel	5
3 vessel	5
Time since infarction (years)	8.7 ± 5.1
Site of myocardial infarction	
Anterior	10
Inferior	6

Table 5.1: *Patient characteristics (N=16). (CAD = coronary artery disease; LV = left ventricle; LVEF = left ventricular ejection fraction; VT = ventricular tachycardia. * = median (range))*

inserted in the left ventricle. Transthoracic echocardiography was applied before the procedure to assess the dimensions of the left ventricle and to exclude the presence of a mural left ventricular thrombus or significant aortic valve disease since these conditions interfere with safe deployment of the basket catheter. All antiarrhythmic drugs were discontinued in the patient group for at least 5 drug elimination halve times before the study. Two postinfarction patients were previously treated with amiodarone but in these patients amiodarone was discontinued 5 and 6 weeks before the study, respectively.

5.3.2 Electrophysiologic study

Induction of VT was carried out using a routine stimulation protocol including delivery of up to 3 extrastimuli following a drive train of 8 stimuli (2 ms pulse width at twice the diastolic threshold current) with three different cycle lengths (600, 500 and 430 ms). A 6 Fr quadripolar catheter was positioned in the right ventricular apex or right ventricular outflow tract for this purpose. If VT proved to be inducible, a 64-electrode unipolar basket catheter (Constellation Catheter™, Boston Scientific, Inc.) was percutaneously inserted after termination of VT. Then renewed induction of VT was attempted.

5.3.3 Data acquisition and mapping

Data from the endocardial basket catheter and BSM electrodes were recorded simultaneously using a 128-channel digital acquisition device (Biosemi Inc.) [18,19]. Analogue to digital conversion occurred at a sampling frequency of 2 kHz, 16-bits resolution and a bitstep of 2 μV/bit. Wilson's central terminal was used as reference for the BSM electrograms. The amplifier system had a bandpass characteristic using a frequency range of 0.16 – 400 Hz (3 dB frequencies). Data were transmitted using a fiberoptic transmission unit and stored in a Pentium based PC. Continuous 3-minute 128-channel recordings of sinus rhythm were obtained.

5.3.4 Signal averaged body surface mapping

Recording and signal averaging

Body surface ECGs were recorded using a radiotransparent carbon unipolar electrode grid that does not interfere with fluoroscopic imaging during catheterization. The 62 electrodes were positioned in 14 flexible vertical straps that were applied on the anterior and posterior thoracic surface as described elsewhere [20]. A mean of 2.0 ± 1.8 leads per map were rejected because of unsatisfactory signal quality and were replaced by a value computed from neighboring electrodes.

To calculate signal-averaged electrograms, a template QRS complex was selected. The beginning and end of the template QRS complex were set at the time at which one of the extreme amplitudes reached > 0.2 mV and at the J point, respectively. Then, an interval for signal averaging was selected comprising the template QRS complex and its subsequent T-wave. The QRS template was used to scan the entire lead recording for QRS complexes that fitted the QRS template with a correlation coefficient of more than 0.80. The selected intervals were time aligned and baseline correction was performed for all QRS complexes. Mean and standard deviation for the entire selected interval were computed for every time instant of the time aligned interval. To allow exclusion of non-sinus rhythm beats and intervals that contained artifacts, even if the artifacts were outside the QRS template, only selected intervals in which no sample exceeded the mean of the time aligned interval plus three times its standard deviation were used for signal averaging. The noise level in each interval was estimated in the filtered signal in a 100 ms interval near the end of the T-wave. This noise estimate was used to compute an averaged signal that was weighted for noise instead of a coherently averaged signal. This insured the reconstruction of a signal averaged QRS complex that contained minimal noise.

Three orthogonal X, Y, and Z leads were reconstructed from a selection of 3 electrode pairs from the 62 body surface electrodes that matched the positions of the XYZ leads best. The SAECG was obtained from these X, Y, and Z leads. Detection of LPs in the SAECG and the 62 body surface electrodes was performed as described earlier [5]. In short, a bi-directional Butterworth 25 Hz high pass filter was applied from beyond the end of the QRS complex and before the onset of the QRS complex towards the middle of the QRS complex. Finally, the root mean

squared filtered signal was computed. Parameters indicative for the presence or absence of LPs were defined according to the Simson criteria [1]. To summarize these criteria: end of the total filtered QRS complex was considered the time where - when searching in reverse direction from T-wave towards the filtered QRS complex - the signal amplitude became larger than the mean noise level and three times its standard deviation for more than 5 ms. Total QRS duration (QRSD) is the duration from onset to end of the filtered QRS complex [1]. The LAS40 was defined as the number of milliseconds preceding the end of the filtered QRS complex where the signal amplitude was smaller than 40 μV. The RMS40 was defined as the root mean square value of the voltage in the last 40 ms before the QRS offset of the filtered QRS complex.

Calculation of late potential maps

Body surface integral maps of LPs (LPMAP) were obtained by calculating the integral of the root mean squared filtered complex in the 50 ms segment following the end of the QRS complex (J-point) as determined in the unfiltered QRS complex for each of the 62 body surface electrodes. To correct for the influence of the distance of the body surface electrode to the heart, each integral value in the LPMAP was divided by the normalized integral value of the root mean squared filtered total QRS complex in that lead. The LPMAP was considered positive for LPs if its value exceeded the 50 ms integral of noise for that channel three times.

5.3.5 Multielectrode endocardial mapping

Catheter placement

The basket catheter consists of 8 self-expanding nitinol splines mounted on a 110 cm long 8 Fr catheter shaft. Each spline has 8 symmetrically arranged electrodes. Selection of catheter size was based on the dimensions of the left ventricle as determined by 2D transthoracic echocardiography. In our series a basket catheter with a diameter of either 75 mm or 94 mm was chosen implying a vertical interelectrode spacing of 7 mm or 9 mm, respectively. Horizontal electrode distance varied with the positioning and deployment of the catheter. An 11 Fr introducer was used to insert a long 10 Fr guiding sheath in the left ventricle across the aortic valve. The collapsed basket catheter was advanced through the guiding sheath and deployed in the left ventricle after pulling back the guiding sheath. The activated clotting time was kept longer than 300 seconds by full heparinization to avoid thromboembolic complications. A 6 Fr quadripolar catheter was inserted percutaneously through the right femoral vein and positioned in the intra-abdominal part of the inferior caval vein to serve as a far field recording and pacing reference electrode for the unipolar basket catheter electrodes.

Fluoroscopic localization of the basket catheter

Since basket catheter positioning varied from patient to patient, the exact position of the individual basket electrodes was determined using biplane right (RAO) and left anterior oblique (LAO) digital cine fluoroscopy (Philips Medical Systems Integris). After selecting the same end-diastolic frames from both fluoroscopic projections, two recognizable splines, which carry one and two additional radiopaque markers, respectively, were identified. After labeling the electrodes of these two splines, other splines could be identified by comparing their relative position with the known position of the first two splines. Each individual electrode and the central apical spline connector were then marked and given 2D coordinates in the RAO and LAO projection. Finally, by combining the data from the RAO and LAO projections, 3D coordinates for each electrode were calculated, thereby allowing a realistic anatomical rendering of the position and shape of the basket catheter in the left ventricle for each individual patient (figure 3.3).

Endocardial data processing

A software package was developed for on-line data processing based on Matlab 5.1 (The MathWorks, Inc. [21]. A surface Laplacian was used to detect small electrographic deflections in infarcted regions which may be masked by large remote components in the unipolar electrogram [22–24]. The Laplacian is the second spatial derivative of the unipolar electrogram and a measure for the transmembrane current at the recording site. It suppresses remote deflections, but still has the characteristics of the unipolar electrogram. In contrast to bipolar electrograms, the Laplacian is direction independent. In our study, the Laplacian was determined by subtracting the mean of the signals of the 8 surrounding electrodes, weighed for interelectrode distance, from the unipolar signal recorded at the central recording electrode.

5.3.6 Spatial correlation between endocardial recordings and SABSM

To correlate endocardial findings spatially with areas displaying late potentials on the body surface a transfer matrix was calculated. The physical principles are explained in Appendix A. In summary, for each patient the position of the basket catheter electrodes relative to the thoracic surface was derived computationally by placing the basket electrode virtually in the left ventricle of cross-sectional images of a human thorax as can be found on the internet[1]. Subsequently, a virtual line was drawn from each electrode in the body surface electrode array to the center of the basket catheter and for each basket electrode the distance perpendicular to this line was calculated. This resulted in a distance matrix containing the weighted contribution of each basket electrode to the electrical events recorded at each body surface site. Multiplying the endocardial map containing information

[1] *http://www.nlm.nih.gov/research/visible/visible_human.html* [25]

	Patient group (N=16)	Control group (N=12)	P-value
Number of complexes	231.7 ± 122.0	112.5 ± 49.9	P=0.0020
QRSD (ms)	131.8 ± 22.1	81.5 ± 14.0	P<0.0001
RMS40 (μV)	28.2 ± 21.7	143.0 ± 72.4	P<0.0001
LAS40 (ms)	34.2 ± 19.2	10.4 ± 5.6	P=0.0003
Noise (μV)	1.9 ± 1.4	4.0 ± 1.9	P=0.0021
Positive Simson criteria	1.3 ± 1.2	0 ± 0	P=0.0002

Table 5.2: *Standard 3-lead signal averaged ECG parameters.*

on the presence of diastolic potentials by the distance matrix then generated theoretical LPMAPs. The correlation coefficient between these theoretical LPMAPs and the actually recorded LPMAPs was calculated and used as a measure of spatial fit between LPMAPs and endocardial diastolic potentials.

5.3.7 Definitions of parameters and related terminology

Electrogram activity, either on the body surface or endocardium, exceeding the surface QRS offset of the unfiltered QRS complex during sinus rhythm was called a late potential. Endocardial diastolic potentials representing intracardiac post-QRS activity during VT were defined as endocardial electrogram deflections extending beyond the surface QRS offset of the unfiltered QRS complex. Body surface LPs were defined in the LPMAP as sites where the root mean square value of the filtered QRS complex exceeded the noise level and twice its standard deviation in the 50 ms interval following the J-point as determined in the unfiltered averaged QRS complex.

5.3.8 Statistical analysis

All data were stored in a computerized patient record database. Data analysis was performed on a personal computer using the "The SAS System for Windows v8" statistical software package (SAS Institute, Inc). Data are presented as mean values $\pm$ SD unless stated otherwise. Subgroup comparisons were made using Chi-square, Student T-test or Fisher's exact test, whenever appropriate. Statistical significance was defined as a P value < 0.05.

5.4 Results

5.4.1 Standard 3-lead SAECG

The standard parameters QRSD, LAS40, and RMS40 obtained with 3-lead SAECG are shown for patient and control group in 5.2. In the patient group, QRSD was significantly longer (131.8 ± 22.1 ms vs. 81.5 ± 14.0 ms, p<0.0001) as well as LAS40

	Patient group (N=16)	Control group (N=12)
0 criteria	5	12
1 criterion	3	0
2 criteria	5	0
3 criteria	3	0

Table 5.3: *Number of patients with positive Simson SAECG criteria.*

	Patient group (N=16)	Control group (N=12)	P-value
Number of complexes	220.7 ± 118.9	113.0 ± 50.8	P = 0.0049
QRSD (ms)	132.9 ± 31.4	90.7 ± 23.0	P = 0.1947
RMS40 (μV)	14.3 ± 12.3	88.0 ± 81.9	P < 0.0001
LAS40 (ms)	58.8 ± 25.9	25.0 ± 15.0	P = 0.0002
Noise (μV)	0.8 ± 0.7	1.4 ± 1.2	P = 0.3171
No. of leads with 3 LP criteria	20.1 ± 22.4	0.75 ± 1.7	P < 0.0001

Table 5.4: *Signal averaged body surface mapping. (LP = Late potential according to Simson [1])*

(34.2 ± 19.2 ms vs. 10.4 ± 5.6 ms, p=0.0003). RMS40 was significantly smaller as compared to the control group (28.2 ± 21.7 μV vs. 143 ± 72.4 μV, p<0.0001). Table 5.3 shows that in the patient group, 3 of 16 (18.8 %) patients had body surface LPs as defined by fulfillment of all 3 SAECG criteria [1]. None of the healthy control subjects had positive SAECG criteria. This implies that in this group the sensitivity of SAECG was 0.19 whereas the specificity was 1.00.

5.4.2 Signal averaged body surface mapping

In table 5.4 standard parameters QRSD, LAS40, and RMS40 derived from SABSM are shown. If Simson criteria were applied to define the presence of late potentials in a given SABSM surface lead, the following results were obtained: In 4 of 16 postinfarction patients (25 %) none of the 62 body surface leads were positive for all 3 Simson criteria, in 4 of 16 patients (25 %) less than 4 SABSM leads contained LPs. Eight patients were found to have 3 positive criteria for LPs in more than 4 SABSM leads (range 14 to 55 of 62 leads). In the control group, 8 of 12 subjects (66.6 %) had no SABSM leads positive for LPs, 3 of 12 (25 %) control subjects had 1 positive SABSM lead and 1 of 12 subject (8.3 %) had 6 SABSM leads positive for LP. This means that, defining SABSM as indicative of late potentials by the presence of at least 1 lead satisfying all 3 Simson criteria, will result in a sensitivity of 0.75, whereas the specificity of SABSM will be 0.66. Therefore, the likelihood ratio of a

	Patient group (N=16)	Control group (N=12)	P-value
Uncorrected LPMAP (μVms)	115.6 ± 120.2	67.8 ± 66.0	P < 0.0001
Corrected LPMAP(μVms)	577 ± 1077.1	248.8 ± 263.1	P < 0.0001
Total QRS integral value (μVms)	388.3 ± 239.8	383.0 ± 231.1	P = 0.2855
Number of subjects with positive LPMAP	14 (87.5 %)	1 (8.3 %)	

Table 5.5: *LPMAP data*

positive test equals 2.27, whereas the likelihood ratio of a negative test equals 0.38

In Table 5.5, the LPMAP calculation results are shown. In the patient group the integral values of the 50 ms post J-point segment contained significantly more energy. In the patient group, 14 of 16 patients (87.5 %) were positive on the LPMAP, whereas 1 of 12 controls (8.3 %) was positive in the LPMAP. Therefore, this method results in a sensitivity of 0.88 and a specificity of 0.92. The likelihood ratio of a positive test equals 11.0, whereas the likelihood ratio of a negative test equals 0.13.

5.4.3 Endocardial mapping

Late endocardial activity during sinus rhythm was found in 13 of 16 (81 %) subjects in the patient group during sinus rhythm. In these patients, a median of 6.3 of 64 leads (range 2 to 18) contained late potentials. During VT, 7 of 16 patients (43.8 %) were found to have diastolic potentials. These diastolic potentials were located on a median number of 11.0 of 64 leads (range 4 to 14 leads).

		Diastolic potentials (ventricular tachycardia)		
		Absent	Present	
Late potentials (Sinus rhythm)	Absent	-	52 (32.9 %)	52
	Present	81 (51.3%)	25 (15.8%)	106
		81	77	158 (100 %)

Table 5.6: *Endocardial basket catheter leads containing diastolic potentials.*

Table 5.6 displays the distribution of late and diastolic potentials during sinus rhythm and VT. In total, diastolic and late potentials during either VT or sinus rhythm or both were found on 158 basket catheter leads in 16 patients. Late potentials during sinus rhythm and diastolic potentials during VT were found at the same endocardial site in 25 of 158 leads (15.8 %). Diastolic potentials only present during VT or late potentials only discernable during sinus rhythm were found in 81 of 158 leads (51.3 %) and 52 of 158 leads (32.9 %), respectively.

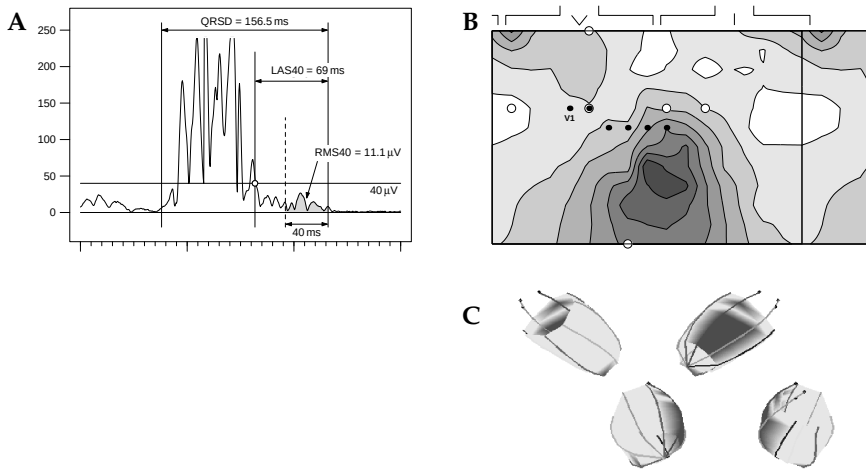

Figure 5.1: *In **Panel A** the 3-lead signal averaged ECG of a patient with previous infero-posterior myocardial infarction is shown. All three parameters (QRSD, RMS40, LAS40) indicate the presence of late potentials. **Panel B** displays the late potential map (LPMAP), i.e. the integral value of the 50 ms segment, following the unfiltered J-point, of the filtered QRS complex. Dark areas mark the presence of delayed activity following the J-point. The 3D reconstruction of the basket catheter are shown in **Panel C**. Dark areas signify areas where diastolic potentials are present. The 4 images of the basket catheter are displayed beneath the LPMAP such that the basket catheter is oriented towards the aspect of the thorax that is facing that particular side of the basket.*

5.4.4 Correlation between SABSM and sites of endocardial diastolic potentials

For the patient group, 3D anatomical activation maps of the left ventricle during sinus rhythm were reconstructed. This enabled comparison of the sites containing diastolic potentials and LPMAPs. In 13 of 16 patients (81 %), visual comparison of the LPMAPs and the endocardial maps suggested a correlation between the endocardial sites containing late potentials and evidence for LPs in the LPMAP. An example is shown in figure 5.1.

In 2 patients no clear late potentials were found during sinus rhythm and therefore no valid comparison could be made. In one patient with a previous apical myocardial infarction, diastolic potentials were clearly found in the apical region of the endocardium, whereas activity in the LPMAP was located high posterior on the thorax.

In order to quantify the similarity between endocardial findings and body surface LPs, LPMAPS were reconstructed from the endocardial maps utilizing the surface electrode/basket electrode distance matrix. An example is shown in figure 5.2.

A correlation coefficient of 0.6 ± 0.12 between actually recorded and virtually

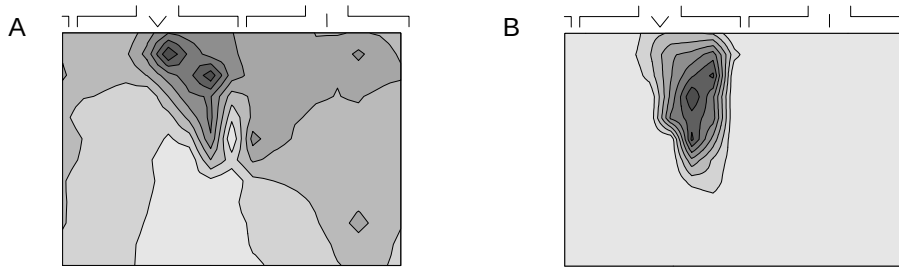

Figure 5.2: ***Panel A*** *displays the folded open anterior and posterior aspect of the recorded late potential map (LPMAP) of a patient with previous anterolateral myocardial infarction. Dark regions represent the presence of late potentials. A clear area of late potentials in this patient can be noted on the left upper and upper midsternal aspect of the thorax.* ***Panel B*** *shows the results of the theoretically reconstructed SABSM by multiplying the endocardial map with a transfer matrix. Late potentials can be noted in the same area as* ***Panel A*** *(r=0.75)*

reconstructed maps was found.

5.5 Discussion

SAECG is a non-invasive tool for detection of patients at risk for sudden cardiac death. Until now, the clinical predictive value for the individual patient is low. Although specificity of SAECG appears to be sufficient, sensitivity is disappointing. Furthermore, only a small proportion of patients with positive SAECGs will develop life threatening ventricular arrhythmias in the subsequent years [5]. This study shows that SABSM with multiple thoracic leads increases the spatial electrographic resolution for detection of LPs. Sensitivity is well improved (75 %) at the expense of a slight lowering of the specificity (66 %). Sensitivity and specificity of SABSM can be further improved by looking at the energy content corrected for distance in the 50 ms interval following the J-point. Sensitivity is then 88 %, whereas specificity is 92 %. SABSM also allows identification of endocardial areas where late potentials can be found during sinus rhythm in 81 % of patients. In this study, it was also shown that, in a substantial number of VTs, endocardial sites that show diastolic potentials during VT do not display endocardial late potentials during sinus rhythm at these sites.

5.5.1 Limitations of SAECG

In this study, 0 of 12 (0%) healthy control subjects had evidence of LPs on the SAECG. In 13 of 16 (18.8 %) postinfarction patients, who all had documented spontaneous and inducible sustained monomorphic VT, no LPs were present. Several factors may explain this lack of sensitivity of SAECG. Firstly, the presence of LPs

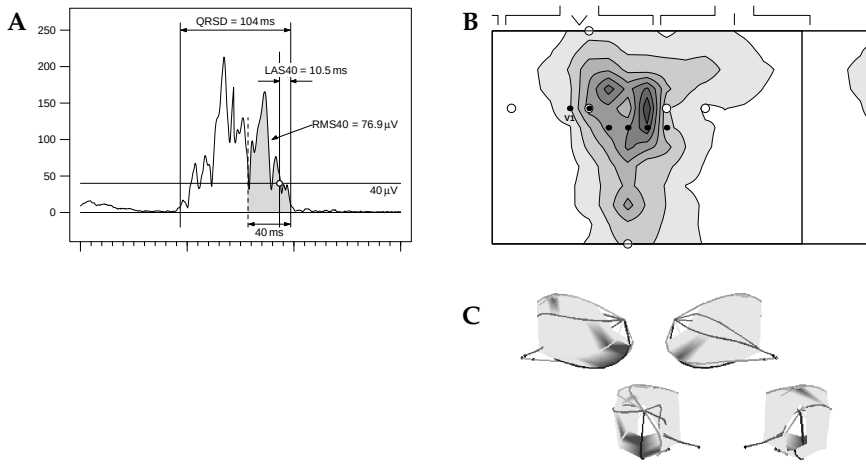

Figure 5.3: *Example of a false negative SAECG in a patient with previous anterior/apical myocardial infarction. In **Panel A**, the standard SAECG reconstructed from the orthogonal XYZ leads is shown. None of the 3 SAECG parameters (QRSD, LAS40 and RMS40) can be considered positive for late potentials. The late potential map (LPMAP) is depicted in **Panel B**. Dark areas indicate more activity in the segment — following the unfiltered J-point — of the filtered QRS complex. Most activity is located in the vicinity of the apex (left precordial) and the high-midanterior thorax. White dots mark the positions of the XYZ lead electrodes. All XYZ-electrodes are located in areas with little post-QRS activity thereby explaining the absence of late potential criteria in the SAECG. 3D reconstructions of the basket catheter are shown in **Panel C**. Dark areas signify areas where diastolic potentials are present. The 4 images of the basket catheter are displayed beneath the LPMAP such that the basket catheter is oriented towards the aspect of the thorax that is facing that particular side of the basket.*

on the body surface is inhomogeneously distributed as has been clearly demonstrated in this study. Therefore the detection of LPs by SAECG is dependent of the location of the electrodes of the 3-lead XYZ in thoracic areas with LPs. An example of a false negative SAECG is shown in figure 5.3.

Secondly, SAECG is only capable of detecting post QRS activity during sinus rhythm. This implies, that parts of the VT reentry circuit that display diastolic potentials during VT may be hidden in the QRS complex during sinus rhythm due to the different activation sequence of the left ventricle in different rhythms. In this study, it has been shown that 52 of 77 diastolic potentials (67 %) that can be recorded during VT are not present during sinus rhythm. Thirdly, false negativity of the SAECG may be due to the 'bi-directional' Butterworth filtering technique that is currently used. This filtering technique tends to give a time shift of high energy content of the filtered signal towards the middle of the QRS complex, thereby making LPs disappear within the main filtered QRS deflection.

5.5.2 Related studies

Faugère et al. showed increased sensitivity of SABSM using a 63-electrode array in 21 patients with postinfarction VT [17]. In this study isopotential mapping instead of isointegral mapping was performed. However, filtering of the QRS complex may result in time shifts and polarity reversal thereby distorting the instantaneous isopotential map [13]. Such a distortion does not occur when using isointegral maps.

Nakai et al. performed SABSM in 8 patients with previous myocardial infarction using a unipolar 45-electrode array [26]. They concluded that the distribution of delayed activity on the isointegral SABSM correlated well with the site of previous myocardial infarction. Freedman et al. investigated in an animal left lateral and right ventricular infarction model the correlation between SABSM and prolonged epicardial ventricular electrograms [16]. In this study most LPs were found on the SABSM leads that were located anterior, supporting our hypothesis that electrode-heart distance correction is necessary to improve accuracy of localization of endocardial areas of delayed potentials. Sasaki et al. performed SABSM in 50 postinfarction patients using a unipolar 16-electrode array that was repositioned three times to obtain a 48-lead SABSM [27]. Afterwards patients underwent left ventricular single catheter activation sequence mapping during sinus rhythm. They found that constructing isointegral maps that displayed activity of less than 28 μV in the last 20 ms of the QRS complex yielded a sensitivity of 91% and a specificity of 69% in predicting vulnerability to ventricular arrhythmias. These data are well comparable with our results.

Lacroix et al. investigated the use of 63-lead SAECG and subsequent epicardial and endocardial mapping in 16 patients. They found post-QRS activity in 83 % of patients without intraventricular conduction delay in 5 % of endocardial recording sites [13]. They also observed that 55 Hz-filtered isopotential maps of the thoracic and intracardiac signals showed a close spatial correlation between location, amplitude and orientation of the extremes. These data are very well in line with our results.

Finally, several authors have claimed that sensitivity and specificity of SABSM can be improved by frequency domain analysis. This technique has the advantage that identification of areas with high frequency content is not restricted by the limitation of conventional time domain SABSM analysis, namely that only post-QRS activity can be detected. Hosoya et al. performed this technique with an 87-lead unipolar electrode array in 50 patients with prior anterior myocardial infarction and suggested that activity in the 40-80 Hz frequency range predicted ventricular arrhythmias [28]. Kavesh et al. performed SABSM with a 192-lead electrode array in 43 postinfarction patients and found that patients displaying activity in the 1-7 Hz isoharmonic map were vulnerable to ventricular arrhythmias. Interestingly, again most isoharmonic 1-7 Hz activity was found in the electrodes nearest to the heart [7]. This suggests that some form of electrode-heart distance correction as performed in this study is also mandatory in frequency domain analysis of SABSM.

5.5.3 Parameterization and feature extraction from SABSM

When using the standard SAECG parameters LAS40, RMS40 and QRSD for interpretation of SABSM great care should be taken. All three parameters are heavily dependent on determination of the QRS offset, which in turn is determined by the signal-to-noise ratio. When using SABSM — in contrast to using an orthogonal bipolar XYZ lead system — the signal amplitude in the unipolar electrode is determined by the square of the distance of the electrode to the heart while the noise is mainly determined by local electrode conditions. Signal-to-noise ratio will tend to be lower in more remote electrodes and the QRS offset will be located more towards the middle of the filtered QRS complex. This will cause the QRSD and LAS40 to be shorter and the RMS40 to be larger.

Sasaki et al. decided in their study not to consider QRSD or LAS40, but merely to evaluate the averaged RMS of the last 20 ms before the offset of the filtered QRS complex [29]. This diminishes the influence of signal-to-noise ratio and electrode-heart distance, but does not eliminate it. Therefore, in the currently presented study a different parameter was selected, namely the integral of the root mean squared value of the 50 ms segment following the J-point of the unfiltered QRS complex. This may have lead to an underestimation of the energy content of this specific integral due to shift of high energy content towards the QRS complex caused by 'bi-directional' filtering, thereby masking true LPs within the QRS complex. However, any SAECG parameter derived after 'bi-directional' filtering will be hampered by this phenomenon. Second modification was a computation to correct for the distance of the electrode to the heart. This technique allows for better comparison between leads that are closely adjacent to the heart — such as the precordial leads — and leads more distant to the heart. This may have lead to an overestimation of the energy content contributed by noise in the more distant leads such as the leads on the posterior thoracic surface. However, since the noise level was low in this study, it is unlikely that this has major influence on the results.

5.5.4 Correlation between LPMAPs and SABSM

In order to compare endocardial maps quantitatively with body surface electrocardiographic data a transfer matrix was calculated. This resulted in a correlation of 0.6 ± 0.12 between recorded LPMAPs and computationally derived LPMAPs. Several assumptions were made when constructing the model. The currently described model does not account for individual differences in thorax geometry or torso volume conductor inhomogeneities. However, since these torso inhomogeneities appear to have minimal effect on the 12-lead ECG in the forward reconstruction of the surface ECG from epicardial potentials, this appears to be justified [30,31]. Furthermore, it should be noted that the reconstructed maps represent the binary presence of endocardial LPs. LPMAPs represent the body surface measurement of the amplitude magnitude of endocardial LPs and therefore display a more gradual representation of the endocardial presence of LPs. This may lower

the correlation coefficient between reconstructed maps and LPMAPs as well.

5.5.5 Clinical significance

SABSM allows the delineation of areas with delayed endocardial activation with higher sensitivity than standard SAECG while the specificity is comparable. Furthermore, non-invasive anatomical information can be obtained, identifying areas where endocardial diastolic potentials can be found in 80 % of cases. This may be helpful in limiting the endocardial area to be mapped for diastolic potentials and sites of entrainment during radiofrequency catheter ablation or surgical ablation of VT. However, one should realize that a difference exists between endocardial sites displaying late potentials during sinus rhythm and sites that are involved in the reentry circuit during VT [32]. On the other hand, since in a number of cases radiofrequency ablation of postinfarction VT can be exceedingly difficult due to non-inducibility or hemodynamical intolerance, new techniques to ablate the VT substrate during sinus rhythm are under investigation [33, 34]. In analogy of ablation of 'channels' of conduction — as is currently done with intra-atrial reentry tachycardia [35] — areas of delayed conduction within the infarction scar may be identified with SABSM, thereby facilitating the detection of channels of conduction.

5.5.6 Limitations of the study

When detecting delayed activity following the QRS complex in an electrode system other than the classic XYZ 3-lead orthogonal system, the distance of the particular surface electrode to the heart will affect the magnitude of the LPs. This will lead to overestimation of the energy content of late potential integral maps in the precordial leads as opposed to more remote electrodes. Since the magnitude of the entire electrogram will be dependent on electrode distance to the heart, integral values of the LPMAP were expressed relative to the value of the QRS integral. Of course, QRS complex and deflections in the LPMAP can result from wave fronts travelling in different directions, i.e. normal activation from endocardium to epicardium yielding a QRS complex and delayed activity in slow conduction pathways within the myocardial infarction scar, respectively. Since only unipolar electrodes were used, the magnitude of QRS integral and LPMAP were considered independent of the direction of the underlying wave front propagation.

To define which body surface electrode corresponded with a specific endocardial region a theoretical SABSM was computed with the aid of a projection of the basket catheter relative the thoracic surface. To be able to do this detailed anatomical information of the patient's build is mandatory, which requires magnetic resonance imaging (MRI) data. It is possible that better results would have been obtained if a magnetic resonance image of the thorax of each patient had been available. Since however changes in built of the thorax appear to have limited effect on the body surface electrograms a standardized cross-sectional thorax image was used [30, 31]. Better results might have been achieved when correla-

tions were made between endocardial sites and body surface leads by means of a mathematical inverse solution model.

Another limitation is that no basket catheter data are available for the healthy control subjects. None of the normal subjects, however, displayed positive SAECG or SABSM criteria and therefore it is not presumable that basket mapping would have provided new insights.

5.6 Conclusion

SABSM is a non-invasive tool to detect delayed endocardial activity on the body surface. SABSM has greater sensitivity than SAECG and comparable specificity. Furthermore SABSM is able to indicate the anatomical sites where endocardial late potentials originate during sinus rhythm in 81 % of cases.

5.7 Appendix

To estimate the weighted contribution of each basket electrode to the presence of late potentials on the SABSM a transfer matrix was calculated. This technique was based on the physical principle that each body surface electrogram is determined by the electrical dipole traveling through the heart and the space angle under which this dipole is observed. To estimate which basket electrodes (i.e. which part of the endocardial surface) are within the space angle of a specific body surface electrode, for each patient and for each of the 62 body surface electrodes a virtual line connecting both body surface electrode and center of the basket (i.e. center of the left ventricle) was computed (Figure 5.4). Then for each of the 64 basket electrodes the inverse of the distance perpendicular to this line was computed. This resulted in a 62 times 64 (BSM electrodes times basket electrodes) distance matrix containing weighing factors of the contribution of each basket electrode to each body surface electrode. Multiplying the 64 times 1 vector representing the endocardial activity by the distance matrix yields a 62 times 1 vector representing the SABSM.

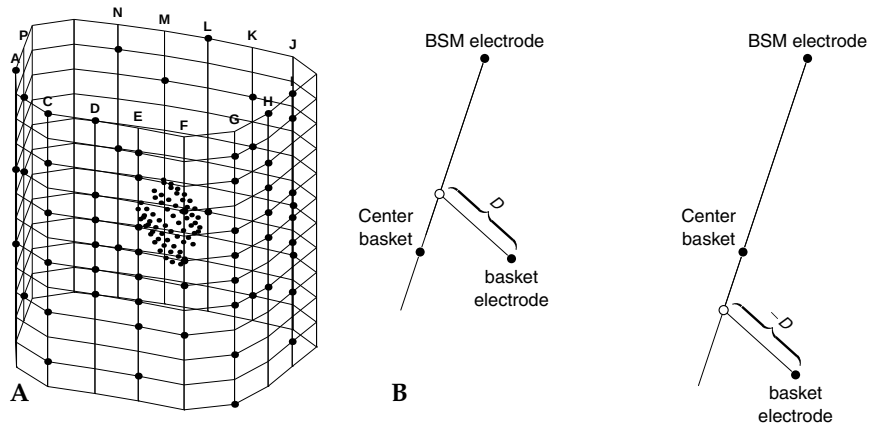

Figure 5.4: ***Panel A****. Reconstruction of the anatomical relation of the body surface electrodes and endocardial basket electrodes. The raster represents the thoracic cage. Solid black dots represent electrodes in the body surface electrode array. Smaller solid black dots in the center of the figure represent the basket electrodes.* ***Panel B*** *demonstrates how the distance between the basket electrodes and the intersecting line are calculated. Distances carry a positive value if basket electrodes are located on the same side of the basket center as the surface electrode, whereas distances are negative if the basket electrodes are locate on the opposite site of the basket center as the surface electrode.*

References

1] M. B. Simson. Use of signals in the terminal QRS complex to identify patients with ventricular tachycardia after myocardial infarction. *Circulation*, 64:235–242, 1981.

2] G. Breithardt, J. Schwarzmaier, M. Borggrefe, K. Haerten, and L. Seipel. Prognostic significance of late ventricular potentials after acute myocardial infarction. *European Heart Journal*, 4:487–495, 1983.

3] J. A. Gomes, S. L. Winters, D. Stewart, S. Horowitz, M. Milner, and P. Barreca. A new noninvasive index to predict sustained ventricular tachycardia and sudden death in the first year after myocardial infarction: based on signal-averaged electrocardiogram, radionuclide ejection fraction and holter monitoring. *Journal of the American College of Cardiology*, 10:349–357, 1987.

4] D. L. Kuchar, C. W. Thorburn, and N. L. Sammel. Prediction of serious arrhythmic events after myocardial infarction: signal-averaged electrocardiogram, holter monitoring and radionuclide ventriculography. *Journal of the American College of Cardiology*, 9:531–538, 1987.

5] G. Breithardt, M. E. Cain, N. El-Sherif, N. C. Flowers, V. Hombach, M. Janse, M. B. Simson, and G. Steinbeck. Standards for analysis of ventricular late potentials using high-resolution or signal-averaged electrocardiography. A statement by a task force committee of the european society of cardiology, the american heart association, and the american college of cardiology. *Circulation*, 83:1481–1488, 1991.

6] D. S. Ho, R. A. Denniss, J. B. Uther, D. L. Ross, and D. A. Richards. Signal-averaged electrocardiogram. improved identification of patients with ventricular tachycardia using a 28-lead optimal array. *Circulation*, 87:857–865, 1993.

7] N. G. Kavesh, S. E. Sarang, and M. R. Gold. Signal-averaged isoharmonic body surface maps of patients with ischemic cardiomyopathy. *Journal of Cardiovascular Electrophysiology*, 11:160–167, 2000.

8] H. J. Wellens, D. Durrer, and K. I. Lie. Observations on mechanisms of ventricular tachycardia in man. *Circulation*, 54:237–244, 1976.

9] M. E. Josephson, L. N. Horowitz, A. Farshidi, and J. A. Kastor. Recurrent sustained ventricular tachycardia. I. mechanisms. *Circulation*, 57:431–440, 1978.

10] W. G. Stevenson, N. W. James, I. Wiener, and K. Nademanee. Slow conduction in the infarct scar: relevance to the occurrence, detection and ablation of ventricular reentry circuits resulting from myocardial infarction. *American Heart Journal*, 117:452–467, 1989.

11] J. M. de Bakker, F. J. van Capelle, M. J. Janse, N. M. van Hemel, R. N. Hauer, J. J. Defauw, F. E. Vermeulen, and P. F. Bakker-de Wekker. Macroreentry in the infarcted human heart: the mechanism of ventricular tachycardias with a "focal" activation pattern. *Journal of the American College of Cardiology*, 18:1005–1014, 1991.

12] P. I. Gardner, P. C. Ursell, J. J. Fenoglio, and et al. Electrophysiologic and anatomic basis for fragmented electrograms recorded from healed myocardial infarcts. *Circulation*, 72:596–611, 1985.

13] D. Lacroix, P. Savard, M. Shenasa, W. Kaltenbrunner, R. Cardinal, P. Page, D. Joly, D. Derome, and R. Nadeau. Spatial domain analysis of late ventricular potentials. intraoperative and thoracic correlations. *Circulation Research*, 66:55–68, 1990.

14] J. P. Boineau and J. L. Cox. Slow ventricular activation in acute myocardial infarction. A source of re-entrant premature ventricular contractions. *Circulation*, 48:702–713, 1973.

15] N. El-Sherif, B. J. Scherlag, R. Lazarra, and R. R. Hope. Re-entrant ventricular arrhythmias in the late myocardial infarction period. 1. conduction characteristics in the infarction zone. *Circulation*, 55:686–702, 1977.

16] R. A. Freedman, M. S. Fuller, G. M. Greenberg, P. R. Ershler, R. L. Lux, McLaughlin, TB, R. Menlove, L. S. Green, D. Moddrelle, and R. Krall. Detection and localization of prolonged epicardial electrograms with 64-lead body surface signal-averaged electrocardiography. *Circulation*, 84:871–883, 1991.

17] G. Faugere, P. Savard, R. A. Nadeau, D. Derome, M. Shenasa, P. L. Page, Guardo, and R. Characterization of the spatial distribution of late ventricular potentials by body surface mapping in patients with ventricular tachycardia. *Circulation*, 74:1323–1333, 1986.

18] C. A. Grimbergen, A. C. Metting van Rijn, A. P. Kuiper, A. C. Linnenbank, and A. Peper. Instrumentation for the recording and digital processing of multichannel ECG data. *Proceedings of the IEEE Medical Biological Society*, 40:726–727, 1992.

19] A. C. Metting van Rijn, A. P. Kuiper, A. C. Linnenbank, and C. A. Grimbergen. Patient isolation in multichannel bioelectric recordings by digital transmission through a single optical fiber. *IEEE Transactions on Biomedical Engineering*, 40:302–308, 1993.

20] A. SippensGroenewegen, H. Spekhorst, R. N. Hauer, N. M. van Hemel, P. Broekhuijsen, and A. J. Dunning. A radiotransparent carbon electrode array for body surface mapping during cardiac catherization. *Proceedings of the IEEE Medical Biological Society*, pages 178–181, 1987.

21] M. Potse, A. C. Linnenbank, and C. A. Grimbergen. Software design for analysis of multichannel intracardiac and body surface electrocardiograms. *Computer Methods and Programs in Biomedicine*, In press, 2001.

22] G. Huiskamp. Difference formulas for the surface laplacian on a triangulated surface. *Journal of Computational Physics*, 95:477–496, 1991.

23] N. Maglaveras, J. M. de Bakker, F. J. van Capelle, C. Pappas, and M. J. Janse. Activation delay in healed myocardial infarction: a comparison between model and experiment. *American Journal of Physiology*, 269:H1441–9, 1995.

24] R. Coronel, F. J. Wilms-Schopman, J. R. de Groot, M. J. Janse, F. J. van Capelle, and J. M. de Bakker. Laplacian electrograms and the interpretation of complex ventricular activation patterns during ventricular fibrillation. *Journal of Cardiovascular Electrophysiology*, 11:1119–1128, 2000.

25] M. J. Ackerman. The visible human project. *Journal of Biocommunication*, 18:14, 1991.

26] K. Nakai, C. Itoh, N. Moriai, N. Chiba, T. Suzuki, K. Hiramori, S. Onishi, H. Kasanuki, and S. Hosoda. Spatial distribution of late potentials assessed by signal-averaged body surface mapping. *Japanese Circulation Journal*, 55:384–392, 1991.

27] Y. Sasaki, A. Furihata, and K. Suyama. Endocardial fragmented electrogram and prediction of ventricular tachycardia by body surface signal-averaged electrocardiographic mapping. *Pacing & Clinical Electrophysiology*, 18:1479–1486, 1995.

28] Y. Hosoya, I. Kubota, T. Shibata, M. Yamaki, K. Ikeda, and H. Tomoike. Spectral analysis of 87-lead body surface signal-averaged ECGs in patients with previous anterior myocardial infarction as a marker of ventricular tachycardia. *Circulation*, 85:2060–2064, 1992.

29] Y. Sasaki, A. Furihata, and K. Suyama. Correlation of the endocardial fragmented electrogram with body surface signal-averaged electrocardiographic mapping. *Pacing & Clinical Electrophysiology*, 17:1477–1486, 1994.

30] C. Ramanathan and Y. Rudy. Electrocardiographic imaging: I. effect of torso inhomogeneities on body surface electrocardiographic potentials. *Journal of Cardiovascular Electrophysiology*, 12:229–240, 2001.

31] C. Ramanathan and Y. Rudy. Electrocardiographic imaging: II. effect of torso inhomogeneities on noninvasive reconstruction of epicardial potentials, electrograms, and isochrones. *Journal of Cardiovascular Electrophysiology*, 12:241–252, 2001.

32] T. Harada, W. G. Stevenson, D. Z. Kocovic, and P. L. Friedman. Catheter ablation of ventricular tachycardia after myocardial infarction: relation of endocardial sinus rhythm late potentials to the reentry circuit. *Journal of the American College of Cardiology*, 30:1015–1023, 1997.

33] P. F. van Dessel, J. M. de Bakker, N. M. van Hemel, A. C. Linnenbank, E. R. Jessurun, and J. J. Defauw. Pace mapping of postinfarction scar to detect ventricular tachycardia exit sites and zones of slow conduction. *Journal of Cardiovascular Electrophysiology*, 12:662–670, 2001.

34] F. E. Marchlinski, D. J. Callans, C. D. Gottlieb, and E. Zado. Linear ablation lesions for control of unmappable ventricular tachycardia in patients with ischemic and nonischemic cardiomyopathy. *Circulation*, 101:1288–1296, 2000.

35] H. Nakagawa, N. Shah, K. Matsudaira, E. Overholt, K. Chandrasekaran, K. J. Beckman, P. Spector, J. D. Calame, A. Rao, C. Hasdemir, K. Otomo, Z. Wang, R. Lazzara, and W. M. Jackman. Characterization of reentrant circuit in macroreentrant right atrial tachycardia after surgical repair of congenital heart disease: isolated channels between scars allow "focal" ablation. *Circulation*, 103:699–709, 2001.

6 Comparison of repolarization properties using the 12-lead ECG, body surface mapping and multielectrode endocardial mapping in postinfarction patients

P.F.H.M. van Dessel[1], N.M. van Hemel[1], J.M.T. de Bakker[2,3], A.C. Linnenbank[2,3], E.R. Jessurun[1], E.F.D. Wever[1]

From the Heart Lung Center Utrecht, Department of Cardiology, St Antonius Hospital, Nieuwegein[1] and Department of Cardiology, University Medical Center, Utrecht[2], Experimental and Molecular Cardiology Group of the Cardiovascular Research Institute, University of Amsterdam, Amsterdam[3], The Netherlands

6.1 Abstract

Objectives: Despite the fact that data on direct comparison of QT dispersion (QTd) with invasively obtained repolarization characteristics in the human ventricle are scarce, QTd has been widely adopted as a measure of dispersion in repolarization. Objective of this study was to compare non-invasive and invasive measures of repolarization.

Methods: Simultaneous recordings with a 62-electrode body surface mapping (BSM) device and a 64-electrode endocardial basket catheter were obtained during sinus rhythm in 13 patients with remote myocardial infarction and documented spontaneous sustained ventricular tachycardia (VT). In 23 patients with remote myocardial infarction without VT and 19 healthy controls BSMs were obtained. Activation recovery intervals (ARIs) were calculated from the endocardial recordings. QTd, mean QT interval, T-wave peak to T-wave end (TE) were calculated for the 12-lead ECG. These same ECG indices as well as QRST integral maps were calculated for the BSM array. Activation recovery time gradients (ARTGs) were computed as a measure of local dispersion in repolarization for both BSM and basket catheter.

Results: Although 12-lead QTd correlated with endocardial ARTG standard deviation (r=0.39), BSM QTd correlated better (r=0.52). TE in V5 correlated strongly (r=0.87) with endocardial ARTG range and non-dipolar content on QRST integral maps were inversely related with the mean ARI (r=0.64). Finally, the range of body surface ARTGs correlated well with the range of endocardial ARTGs (r=0.63).

Conclusion: Although information on intracardiac repolarization properties can be derived from the 12-lead ECG QTd to some extent, its use appears limited. Extending the surface ECG lead set to cover the entire thorax offers better detection of endocardial repolarization properties. Non-dipolar content of BSM QRST integral maps and TE in V5, as well as surface ARTG range correlated strongly with variance in ARIs and endocardial ARTGs, indicating their predictive potential for detection of dispersion in repolarization.

6.2 Introduction

Evidence of T-wave end inequality among surface ECG leads traces back to the earliest days of electrocardiography [1]. Later, "disparity in repolarization times across the ventricles of the heart" was identified as an index of arrhythmia susceptibility [2]. Several investigational techniques were developed to quantify repolarization dispersion. Among these techniques are body surface mapping (BSM) and direct endocardial or epicardial recordings [3–8]. More recently, authors have tried to infer dispersion in repolarization from the 12-lead ECG [9–12]. Some controversies remain, especially concerning the value of QT dispersion (QTd) in identifying postinfarction patients at risk for sudden death. Zabel et al. failed to prove the predictive value of QTd for mortality in a large follow-up study [13]. Similar observations were made by the Diamond-CHF investigators, who failed to demonstrate any predictive value of QT dispersion in patients with severe heart failure [14].

At present, the only study that was done to compare electrocardiographic estimates with repolarization parameters obtained in the intact human ventricle was reported by Zabel et al [15]. In their study, monophasic action potential data obtained at a limited number of endocardial and epicardial sites were subsequently compared with 12-lead ECG variables to asses disparity in ventricular repolarization. They showed that dispersion in repolarization can be detected by the 12-lead ECG.

In the currently presented study, we were able to collect endocardial electrograms at 64 sites simultaneously with 62-channel body surface mapping (BSM) recording on a beat-to-beat basis in the intact normothermic human ventricle. For this purpose, several 12-lead ECG repolarization estimates, such as QTd and BSM QRST integral non-dipolar content were compared to endocardial activation-recovery-interval (ARI) related parameters. Finally, we developed the activation recovery time gradient (ARTG) as a new, electrode array independent, parameter to express local differences in repolarization duration between recording electrodes.

Aim of this study was 1) to investigate the relation between QTd and endocardial repolarization parameters; 2) to investigate the value of body surface QRST integral maps and T-wave peak to T-wave end intervals derived from precordial leads in quantifying nonuniform electrical recovery from excitation and 3) to evaluate activation recovery time gradients as a new parameter that may better express spatial dispersion in repolarization.

6.3 Methods

6.3.1 Patient selection

The research protocol, which was approved by the Ethical Committee of our institution, was performed on two groups of patients that had given prior written informed consent. The patient group (VT Group) comprised 13 patients referred to our hospital between November 1997 and February 1999 for antiarrhythmic surgery or radiofrequency catheter ablation of infarct related VT. Specific eligibility criteria included: (1) documented recurrent ventricular arrhythmias with or without aborted sudden cardiac death and (2) inducible sustained monomorphic VT during programmed electrical stimulation. The second group (non-VT Group) consisted of 23 patients with remote myocardial infarction in whom never any documentation of sustained or non-sustained ventricular arrhythmias was obtained, who did not have symptoms of unexplained syncope and for whom no suspicion of sustained ventricular arrhythmias existed at that point in time. These patients were not receiving antiarrhythmic medication. The control group (Control Group) consisted of 19 healthy controls, who had normal electrocardiograms, no history of cardiovascular disease and who were not receiving medication. Characteristics of all three groups are presented in Table 6.1. In all three groups BSM was performed, but only in the VT Group a basket catheter was percutaneously inserted in the left ventricle. In those patients, transthoracic echocar-

	VT Group (N=13)	non-VT Group (N=25)	Control Group (N=19)
Age (years)	67.7 ± 9.7	57.4 ± 8.9	40.7 ± 14.8
Gender			
Male	9	21	5
Female	4	4	14
LVEF	23.7 ± 9.0	41 ± 23.6	N/A
Extent of CAD			
(no. of vessels $>$ 70% stenosis)	1.9 ± 0.9	1.9 ± 1.0	N/A
Site of infarction			
Anterior	10	11	N/A
Inferior	3	14	N/A
Time since infarction (years)	7.4 ± 5.2	2.6 ± 3.3	N/A
VT cycle length (ms)	318 ± 70	N/A	N/A
No. of VT morphologies per patient	1.8 ± 0.9	N/A	N/A

Table 6.1: *Baseline characteristics. (CAD = coronary artery disease; LVEF = left ventricular ejection fraction; VT = ventricular tachycardia; N/A = Not available)*

diography was applied before the procedure to assess the dimensions of the left ventricle and to exclude the presence of a mural left ventricular thrombus or significant aortic valve disease since these conditions can interfere with safe deployment of the basket catheter. All antiarrhythmic drugs were discontinued in the patient group for at least 5 drug elimination halve times before the study. Two patients in the VT Group were previously treated with amiodarone but in these patients amiodarone was discontinued 5 and 6 weeks before the study, respectively.

6.3.2 Data acquisition and mapping

Data from the endocardial basket catheter and BSM electrodes were recorded simultaneously with a 128-channel digital acquisition device (Biosemi Inc.). Analogue to digital conversion occurred at a sampling frequency of 2 kHz, 16-bits resolution and a bitstep of 2 μV/bit. Wilson's central terminal was used as reference for the BSM electrograms. The amplifier system had a bandpass characteristic using a frequency range of 0.16 – 400 Hz (3 dB frequencies). Data were transmitted using a fiberoptic transmission unit and stored in a Pentium based PC.

6.3.3 Surface electrocardiographic estimation of repolarization dispersion

Body surface ECGs were recorded using a radiotransparent carbon unipolar electrode grid that does not interfere with fluoroscopic imaging during catheterization. The 62 electrodes were positioned in 14 flexible vertical straps that were applied on the anterior and posterior thoracic surface as described elsewhere [16]. Continuous 24-second recordings of sinus rhythm were obtained. A mean of 2.0 ± 1.8 leads per recording were rejected because of unsatisfactory signal quality and were replaced by a value computed from neighboring electrodes. Offset differences, linear baseline drifting, or both were corrected with a computer algorithm.

Selection of QRS complexes for analysis

Before analysis of the signals a 150 Hz low pass 4^{th} order Butterworth filter was applied to remove noise and facilitate detection of the onset and offset of the QT interval. Then, a template QRS complex was selected in precordial lead V2. The onset and offset of the template QRS complex were set at the time when the absolute value of the instantaneous voltage exceeded 0.02 mV and at the J point, respectively. Subsequently, an interval was selected comprising the template QRS complex and its subsequent T-wave. The QRS template was used to scan the entire lead recording for QRS complexes that fitted the QRS template with a correlation coefficient of more than 0.80. The selected complexes were time aligned and baseline correction was performed. Mean and standard deviation for the entire selected interval were computed for every instant of the time-aligned interval. Only intervals in which no sample exceeded the mean of the time aligned interval plus three times its standard deviation, were ultimately selected for analysis. This permitted exclusion of non-sinus rhythm beats and intervals that contained artifacts, even if the artifacts were outside the QRS template.

QT interval and T-Peak to T-End measurement

QT intervals were determined for each complex in each lead individually. Therefore, for each selected QRST interval in each of the 62 individual surface electrodes, the onset of the QRST complex was defined as the instant when the absolute value of the voltage exceeded 0.02 mV. Since the amplitude of the QRST complex is dependent on the distance of the recording electrode to the heart, an electrode specific criterion for determination of the offset of the T-wave was introduced. First, the top of the T-wave was determined by selecting the largest absolute voltage value between the manually indicated J-point and a marker set in the isoelectric baseline well after the offset of the T-wave. If the instantaneous value of the T-wave peak exceeded 0.1 mV, then the threshold for determination of the T-wave offset was set at 0.02 mV, else the T-wave offset threshold was set at 0.2 times the absolute value of the T-wave peak. The T-wave offset was considered the instant in time following the T-wave peak when the absolute value of the

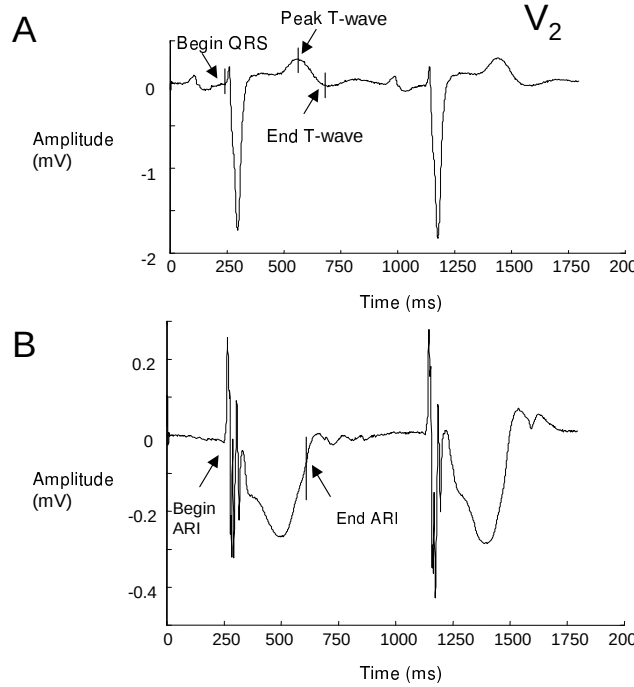

Figure 6.1: ***Panel A*** *displays calculation of QT interval and peak T-wave to end T-wave interval in surface electrogram lead V2. In* ***Panel B*** *the activation recovery interval (ARI) is indicated.*

voltage dropped below the T-wave offset threshold. All computationally assigned markers were checked by visual inspection and corrected if necessary. The QT interval was defined as the time interval between individually determined QRS onset and T-wave offset for each electrode. TE interval was defined as the time interval between T-wave peak and T-wave offset (Figure 6.1).

Body surface mapping

Mean total QRST integral maps were calculated as described previously [17–19]. In short, isopotential maps were generated at a 0.5-millisecond interval during the QRST complex. It should be noted, that for computation of QRST integrals, onset and offset of the QRST interval were, in contrast to QT interval determination, set at the same instant for all surface electrodes. The onset of the QRS complex was defined as the instant in time when the earliest activation exceeded 0.02 mV in any of the surface leads; offset of the T wave was set at the point in time when the absolute value of the voltage dropped below 0.02 mV in all leads or reached its minimum for all electrodes. U waves were not included in the QRST interval. Subsequently, an integral map of the complete QRST interval was constructed and

a quantitative analysis was carried out to estimate the nondipolar content of the QRST integral map. A previously developed software package for on-line data processing based on Matlab 5.1 (The MathWorks, Inc.) was used for this purpose [20]. Eigenvectors previously calculated from a set of 26 healthy controls were utilized for calculation of non-dipolar content of QRST integral maps [19]. In short, the 62-lead BSM vectors of these controls were extrapolated to an evenly distributed 16 x 12 array. Then singular value decomposition was performed. The 192 eigenvectors were calculated from the derived 192 x 26 array. The first 12 eigenvectors (figure 6.2) of the entire set of 192 eigenvectors were subsequently derived, and the QRST integral map of each patient was expressed in terms of these 12 eigenvectors as described by Lux et al [21]. These authors demonstrated that by using the first 12 eigenvectors of the complete data set, each individual map could be reconstructed without a significant loss of information. In addition, they showed that the first 3 eigenvectors of the eigenvector set reveal dipolar patterns, whereas eigenvectors 4 through 12 show non-dipolar patterns. Therefore, the non-dipolar content of each map was defined as the contribution of eigenvectors 4 through 12 relative to the contribution of eigenvectors 1 through 12 [22].

6.3.4 Multielectrode endocardial mapping

Catheter placement

For the purpose of endocardial mapping, a 64-electrode unipolar basket catheter (Constellation Catheter™, Boston Scientific, Inc.) was percutaneously inserted. This basket catheter consists of 8 self-expanding nitinol splines mounted on a 110 cm long 8 Fr catheter shaft. Each spline has 8 symmetrically arranged electrodes. Selection of catheter size (75 mm or 94 mm in diameter) was based on the dimensions of the left ventricle as determined by 2D transthoracic echocardiography. This implied that interelectrode spacing along the spline was 7 mm or 9 mm, respectively. Distance between splines varied with the positioning and deployment of the catheter. An 11 Fr introducer was used to insert a long 10 Fr guiding sheath in the left ventricle across the aortic valve. The collapsed basket catheter was advanced through the guiding sheath and deployed in the left ventricle after pulling back of the guiding sheath. The activated clotting time was kept longer than 300 seconds by full heparinization to avoid thromboembolic complications. A 6 Fr quadripolar catheter was inserted percutaneously and positioned in the intra-abdominal part of the inferior caval vein to serve as a far field recording and pacing reference electrode for the unipolar basket catheter electrodes.

Fluoroscopic localization of the basket catheter

Since basket catheter positioning varied from patient to patient, the exact position of the individual basket electrodes was determined using biplane right (RAO) and left anterior oblique (LAO) digital cine fluoroscopy (Philips Medical Systems Integris). After selecting the same end-diastolic frames from both fluoroscopic projections, splines A and B, which carry one and two additional radiopaque mark-

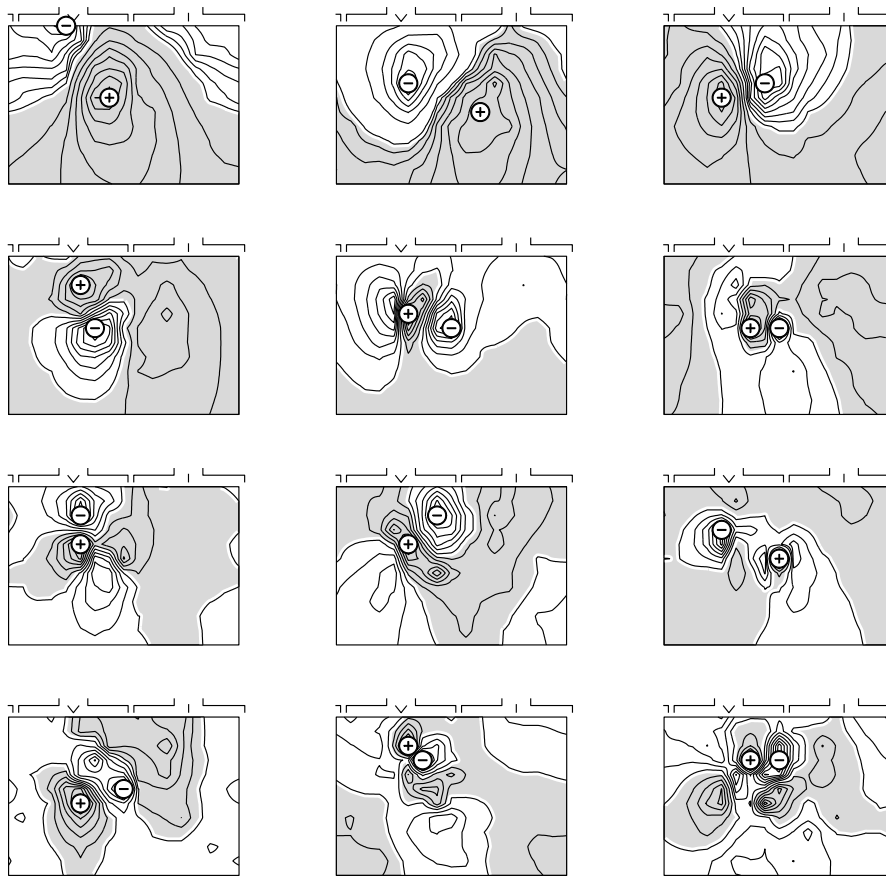

Figure 6.2: *Display of first 12 eigenvectors of the complete QRST integral data set. Each eigenvector is represented in the body surface map format. Eigenvectors are sorted by singular value in descending order. The top row contains the first three eigenvectors, which are considered to demonstrate dipolar patterns; row 2 through 4 displays eigenvectors 4 through 12, which show non-dipolar patterns.*

ers, respectively, were identified. After labeling electrodes of these two splines, the other splines could be identified by comparing their relative position with the known position of the first two splines. Each individual electrode and the central apical spline connector were then marked and given 2D coordinates in both RAO and LAO projection. Finally, by combining the data from the RAO and LAO projections 3D coordinates for each electrode were calculated thereby allowing a realistic anatomical rendering of the position and shape of the basket catheter in the left ventricle for each individual patient (figure 3.3).

Calculation of Activation-Recovery Intervals

A surface Laplacian was used to optimize the detection of local electrical events in the endocardial unipolar electrogram [23–25]. The Laplacian is the second spatial derivative of the unipolar electrogram and a measure for the transmembrane current at the recording site. It suppresses remote deflections, but still has the characteristics of the unipolar electrogram. In contrast to bipolar electrograms, the Laplacian is direction independent. In our study the Laplacian was determined by subtracting the mean of the signals of the 8 surrounding electrodes, weighed for interelectrode distance, from the unipolar signal recorded at the central recording electrode. ARIs were calculated as described by Gepstein et al [26]. In short, the ARI was defined as the interval between the instant showing the steepest descent in the unipolar electrogram during depolarization (dV/dt_{min}) and the steepest ascent in the Laplacian following the J-point on the surface ECG (Figure 6.1).

6.3.5 Estimates of spatial differences in repolarization duration.

Since electrodes in the BSM array and basket catheter electrodes are unevenly distributed, a new measure for interelectrode differences in QT interval or ARIs had to be developed. These estimates of spatial differences in repolarization were calculated as follows. For each patient the position of the basket catheter electrodes relative to the thoracic surface was derived computationally. For this purpose, cross-sectional images of a human thorax, as can be found on the internet[1] were utilized [27]. First, the 3D reconstructed basket catheter was virtually placed in the left ventricle, making the center of the left ventricle and the center of the basket catheter coincide. The BSM electrodes were then virtually positioned on the 3D human torso model. Subsequently, virtual lines were drawn from each electrode in the BSM electrode array and from each basket electrode to the center of the basket catheter (i.e. the center of the heart). Then for each electrode pair, the angle between the lines through these electrodes and the center of the heart was calculated. This resulted in a 62 x 62 angle matrix for the BSM array and a 64 x 64 angle matrix for the basket catheter, respectively. Dividing the QT difference, or the difference in ARI, between each electrode pair by the angle between these electrodes yielded spatial activation recovery time gradients (ARTGs, dimension ms/degree) for all surface electrodes as well as all basket electrodes (figure 6.3). Since main interest in this study was focused on increased dispersion in repolarization, for each electrode the largest ARTG with some other electrode was chosen. This ARTG is expected to be indicative of local repolarization duration differences independent of the used electrode system.

6.3.6 Definition of repolarization parameters.

All repolarization parameters were averaged per lead for a mean 21.1 ± 11.1 complexes before interelectrode comparisons were made. QT dispersion (QTd) was

[1] *http://www.nlm.nih.gov/research/visible/visible_human.html*

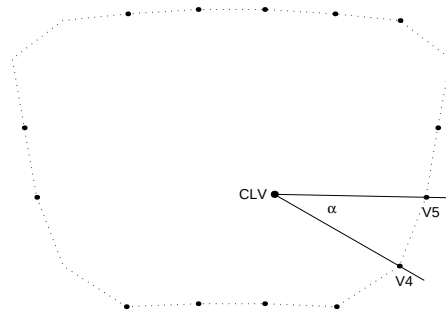

Figure 6.3: *Demonstration of our methods to calculate the angles between electrode pairs. In this case the specific transthoracic plain comprising precordial leads V4 and V5 is chosen as an example. Angle α denotes the angle between the lines through both electrodes and the center (C) of the left ventricle. The same procedure was repeated for every conceivable electrode pair in both the surface electrode set and basket catheter electrode set.*

defined as the difference between the longest (QT_{max}) and the shortest QT interval (QT_{min}) measured in all leads at the body surface. QT standard deviation (STDQT) was defined as the temporal variation in QT interval as measured per ECG lead. Mean QT was calculated as the averaged QT interval in all leads. TE V2 and TE V5 are the averaged TE interval in standard precordial lead V2 and V5 , respectively. Mean ARI was calculated as the averaged ARI in all basket catheter leads. STDARI was defined as the ARI standard deviation over all basket catheter electrodes, thereby being a measure for spatial variance in repolarization. ARI range was defined as the difference between the longest and the shortest ARI measured in all basket catheter leads. ARTG measures were calculated separately for body surface electrodes and basket catheter electrodes using QT interval and ARI, respectively. Mean ARTG was calculated as the averaged ARTG in all leads. STDARTG was defined as the ARTG standard deviation over all electrodes. ARTG range was calculated as the difference between the largest and the smallest ARTG. Maximal ARTG was considered the largest ARTG found in all electrodes.

6.3.7 Statistical analysis

All data were stored in a computerized patient record database. Data analysis was performed on a personal computer using the "The SAS System for Windows v8" statistical software package (SAS Institute, Inc). Data are presented as mean values $\pm$ SD unless stated otherwise. Group comparisons were made using Student T-test. Statistical significance was defined as a P value < 0.05. For continuous variables the Pearson's correlation coefficients were computed. Variables showing a correlation coefficient > 0.7 were selected for entry in a linear regression model for estimation of the independent predictive value of that variable.

	VT Group (N=13)	non-VT Group (N=25)	Control Group (N=19)	P-Values
QT duration (ms)	400 ± 82	407 ± 41	357 ± 29	[1] P=0.73 [2] P<0.0001 [3] P=0.04
QTd (ms)	61 ± 21	63 ± 22	52 ± 22	[1] P=0.74 [2] P=0.11 [3] P=0.27
STDQT (ms)	3.8 ± 2.3	5.1 ± 2.1	3.9 ± 2.13	[1] P=0.12 [2] P=0.09 [3] P=0.90
TE V2 (ms)	105.3 ± 34.7	98.2 ± 17.0	82.1 ± 25.3	[1] P=0.41 [2] P=0.02 [3] P=0.04
TE V5 (ms)	99.1 ± 31.6	89.6 ± 36.9	65.2 ± 18.0	[1] P=0.46 [2] P=0.01 [3] P=0.0009

Table 6.2: *12-lead ECG determinants of repolarization. (STDQT = QT Standard deviation; TE = T-Wave peak to T-Wave end. P-value [1] = VT Group vs. non-VT Group; P-value [2] = non-VT Group vs. Control Group; P-value; [3] = VT Group vs. Control Group)*

6.4 Results

6.4.1 12-lead ECG determinants of repolarization

Repolarization parameters derived from the standard 12-lead ECG are given for all three groups in table 6.2. Mean QT duration was longer in the VT Group and non-VT Group as compared to the Control Group (P=0.04 and P<0.0001, respectively), but not when the VT Group was compared to the non-VT Group (P=0.73). The QTd was not significantly different between groups. Temporal variation in QT duration per lead (QT standard deviation) was not significantly different between groups either. (P= 0.12 to P=0.90). T-wave peak to T-wave end in lead V2 and V5 were both in VT Group and non-VT Group significantly different from the Control Group, but no significant differences between infarction patients with VT (VT Group) and postinfarction patients without VT (non-VT Group) was noted.

6.4.2 BSM determinants of repolarization properties

Table 6.3 shows the results of repolarization parameter estimation utilizing the BSM electrode array. Mean QT duration was longer in the VT Group and non-VT Group as compared to the Control Group (P=0.05 and P<0.0001, respectively), but not when the VT Group was compared to the non-VT Group (P=0.71). The QTd

	VT Group (N=13)	non-VT Group (N=25)	Control Group (N=19)	P-Values
QT duration (ms)	398 ± 83	406 ± 39	355 ± 30	[1] P=0.71 [2] P<0.0001 [3] P=0.05
QTd (ms)	98 ± 31	101 ± 22	79 ± 22	[1] P=0.77 [2] P=0.003 [3] P=0.04
STDQT (ms)	4.7 ± 3.3	3.1 ± 1.6	2.3 ± 1.3	[1] P=0.06 [2] P=0.08 [3] P=0.008
QRSTi Non-dipolar content (%)	26.9 ± 14.1	17.9 ± 16.4	9.2 ± 3.7	[1] P=0.09 [2] P=0.03 [3] P<0.0001
Mean ARTG (ms/degree)	2.0 ± 0.7	2.4 ± 0.7	1.7 ± 0.7	[1] P=0.12 [2] P=0.004 [3] P=0.25
ARTG SD (ms/degree)	0.35 ± 0.33	0.35 ± 0.14	0.26 ± 0.11	[1] P=0.95 [2] P=0.03 [3] P=0.31
Max. ARTG (ms/degree)	10.5 ± 5.3	11.2 ± 3.8	8.7 ± 3.1	[1] P=0.65 [2] P=0.03 [3] P=0.23
ARTG range (ms/degree)	7.7 ± 4.5	6.6 ± 2.2	5.0 ± 1.8	[1] P=0.35 [2] P=0.03 [3] P=0.01

Table 6.3: *BSM determinants of repolarization (ARTG = Activation Recovery Time Gradient; QRSTi = QRST integral; STDQT = QT Standard deviation; P-value [1] = VT Group vs. non-VT Group; P-value [2] = non-VT Group vs. Control Group; P-value; [3] = VT Group vs. Control Group)*

was not significantly different between VT Group and non-VT Group (P=0.77), but did differ significantly between VT Group vs Control Group (P=0.04), and non-VT Group vs Control Group (P=0.003). STDQT tended to reach significance between the VT Group vs non-VT Group (P=0.06), and the non-VT Group vs Control Group (P=0.08), but the difference was highly significant between the VT Group and Control Group (P=0.008). Non-dipolar content of the QRST integral was significantly different between VT Group and Control Group as well as between non-VT Group and Control Group (P<0.0001 and P= 0.03). Differences in mean ARTG, ARTG standard deviation and maximal ARTG were consequently significantly different between non-VT Group and Control Group, but not between VT Group and non-

	Mean ARI	STD ARI	Range ARTG	Mean ARTG	STD ARTG
Mean QT	0.96 †	0.90 †	0.38	0.78 †	0.30
	(P<0.0001)	(P<0.0001)	(P=0.22)	(P=0.0029)	(P=0.34)
STDQT	0.30	0.42	0.01	0.52	0.59 †
	(P=0.35)	(P=0.18)	(P=0.98)	(P=0.08)	(P=0.044)
QTd	0.35	0.50	0.03	0.59 †	0.58 †
	(P=0.27)	(P=0.10)	(P=0.92)	(P=0.046)	(P=0.047)
TE V2	0.56	0.83 †	0.18	0.72 †	0.19
	(P=0.058)	(P=0.0007)	(P=0.58)	(P=0.0082)	(P=0.55)
TE V5	0.33	0.52	0.79 †	0.72 †	0.78 †
	(P=0.31)	(P=0.096)	(P=0.0041)	(P=0.012)	(P=0.0041)

Table 6.4: *Pearson's correlation between endocardial and12-lead parameters in the VT Group. Columns represent endocardial repolarization parameters. Rows represent body surface measures of repolarization. In each cell, the R-square value and significance level are denoted.* † *= Statistically significant; (ARI = Activation Recovery Interval; TE = T-wave peak to T-wave end interval)*

VT Group or Control Group. Only the range between minimal ARTG and maximal ARTG was significantly different between non-VT Group and Control Group (P= 0.03) and VT Group and Control Group (P= 0.01).

6.4.3 Endocardial vs. 12-lead ECG determinants of repolarization characteristics.

In the VT Group, an analysis was made to identify endocardial parameters that cause dispersion in 12-lead ECG estimates of repolarization. First, for each 12-lead ECG variable the correlation with endocardial measurements was calculated. The results are shown in table 6.4. To determine the independent predictive value of between each pair of variables, which showed correlation with a P-value of less than 0.05, forward selection linear regression models were constructed. The P value for entry into the model was set at 0.10. The results are shown in table 6.5. A strong correlation between mean QT interval and mean ARI was found (r=0.85). Weaker associations were found between QTd and endocardial ARTG standard deviation (r=0.39) and temporal QT standard deviation and endocardial ARTG standard deviation (r=0.41).

6.4.4 Endocardial vs. BSM estimates of repolarization characteristics.

Pearson's correlation coefficients between parameters derived from the BSM electrode array and endocardial parameters are shown in table 6.6. Results of the

	Mean ARI	STD ARI	Range ARTG	Mean ARTG	STD ARTG
Mean QT	rc=1.17 r=0.85 (P<0.0001)	N/A	N/A	rc=6.86 r=0.080 (P=0.016)	N/A
STDQT	N/A	N/A	N/A	N/A	rc=4.48 r=0.41 (P=0.035)
QTd	N/A	N/A	N/A	N/A	rc=12.71 r=0.39 (P=0.040)
TE V2	N/A	N/A	N/A	N/A	N/A
TE V5	N/A	N/A	rc=0.62) r=0.62 (P=0.0039)	N/A	rc=16.50 r=0.25 (P=0.0043)

Table 6.5: *Linear regression parameter estimates of endocardial and 12-lead ECG parameters in the VT Group. Columns represent endocardial repolarization parameters. Rows represent 12-lead ECG measures of repolarization. In each cell, the linear regression parameter estimate (rc), partial R-square value (r) and significance level (P) are denoted. N/A indicates that the variable was not selected for entry in the model. (ARTG = Activation Recovery Time Gradient; ARI = Activation Recovery Interval; STDQT = QT standard deviation per lead; TE = T-wave peak to T-wave end interval)*

linear regression models are shown in Table 6.7. Non-dipolar content of QRST integral maps correlated inversely in the linear regression model (r=0.64) with mean ARI. Mean QT interval was also independently predicted by mean ARI, combined with the ARI standard deviation over all endocardial leads (r=0.88 and r=0.048, resp.). Temporal standard deviation of the QT interval per lead, QTd and mean surface ARTG were independently predicted by the endocardial ARTG standard deviation (r=0.67, r=0.52 and r=0.51, respectively). Finally, surface ARTG standard deviation, ARTG range and maximal ARTG were all predicted by the endocardial ARTG range (r=0.53, r=0.63 and r=0.62, respectively).

6.5 Discussion

This is the first study that provides spatially high-resolution data on repolarization properties, obtained simultaneously from endocardium and body surface in the intact, normothermic human ventricle on a beat-to-beat basis. Although using the 12-lead ECG can derive some information on intracardiac repolarization properties, its use appears limited. Extending the surface ECG lead set to cover the entire thorax by means of a BSM array offers better detection of endocardial

	Mean ARI	STD ARI	Range ARTG	Mean ARTG	STD ARTG
QRSTi NDC	-0.79 †	-0.52	-0.17	-0.33	-0.15
	-0.79	(P=0.084)	(P=0.60)	(P=0.30)	(P=0.63)
Mean QT	0.96 †	0.89 †	0.34	0.74 †	0.27
	(P<0.0001)	(P<0.0001)	(P=0.28)	(P=0.0054)	(P=0.39)
STDQT	0.26	0.30	0.12	0.43	0.81 †
	(P=0.41)	(P=0.35)	(P=0.72)	(P=0.16)	(P=0.0015)
QTd	0.41	0.51	0.27	0.56	0.70 †
	(P=0.19)	(P=0.090)	(P=0.39)	(P=0.054)	(P=0.012)
Mean ARTG	0.09	0.23	0.11	0.36	0.70 †
	(P=0.78)	(P=0.45)	(P=0.73)	(P=0.24)	(P=0.011)
STD ARTG	0.52	0.69 †	0.61 †	0.71 †	0.56
	(P=0.085)	(P=0.013)	(P=0.036)	(P=0.0093)	(P=0.058)
Range ARTG	0.45	0.58 †	0.75 †	0.63 †	0.70 †
	(P=0.13)	(P=0.0498)	(P=0.0047)	(P=0.028)	(P=0.12)
Max. ARTG	0.44	0.56	0.61 †	0.71 †	0.56
	(P=0.15)	(P=0.058)	(P=0.036)	(P=0.0093)	(P=0.058)

Table 6.6: *Pearson's correlation between endocardial and BSM parameters in the VT Group. Columns represent endocardial repolarization parameters. Rows represent body surface measures of repolarization. Each cell contains Pearson's correlation coefficient and the level of significance (P).* † *= Statistically significant; (ARI = Activation Recovery Interval; ARTG = Activation Recovery Time Gradient; NDC = Non-dipolar content; QRSTi = QRST integral)*

repolarization properties.

To compare repolarization parameters derived at the endocardium to body surface differences in QT interval, a new parameter (ARTG) was defined that is capable of identifying spatial gradients in repolarization duration. ARTG is independent of variation in interelectrode distances or electrode distance to the heart. ARTG appears therefore to be a useful parameter that provides information on local spatial dispersion in repolarization and allows comparison of these parameters between different, unevenly distributed, lead systems.

6.5.1 QT dispersion

Predicting vulnerability for ventricular arrhythmias by using QTd derived from the 12-lead ECG is hampered by several problems. First, as has been elegantly demonstrated by Willems et al, it appears that measurements of the QT interval using surface ECG leads (or BSM) is subjected to a large intra- and interobserver variability, despite the development of dedicated computer algorithms [28]. Interobserver differences of measurements mount up to 30 ms, which is approximately

	Mean ARI	STD ARI	Range ARTG	Mean ARTG	STD ARTG
QRSTi	rc=–0.27	N/A	N/A	N/A	N/A
Non-dipolar content	r=064 (P=0.0031)				
Mean QT	rc=1.12 r=0.88 (P<0.0001)	rc=1.21 r=0.048 (P=0.054)	N/A	N/A	N/A
STDQT	N/A	N/A	N/A	N/A	rc=5.45 r=0.67 (P=0.0021)
QTd	N/A	N/A	N/A	N/A	rc=22.49 r=0.52 (P=0.012)
Mean ARTG	N/A	N/A	N/A	N/A	rc=0.50 r=0.51 (P=0.013)
STD ARTG	N/A	N/A	rc=0.02 r=0.53 (P=0.011)	N/A	N/A
Range ARTG	N/A	N/A	rc=0.14 r = 0.63 (P=0.0038)	N/A	N/A
Max. ARTG	N/A	N/A	rc=0.14 r=0.62 (P=0.0042)	N/A	N/A

Table 6.7: *Linear regression parameter estimates of endocardial and BSM parameters in the VT Group. Columns represent endocardial repolarization parameters. Rows represent body surface measures of repolarization. In each cell, the linear regression parameter estimate (rc), partial R-square value (r) and significance level (P) are denoted. N/A indicates that that variable was not selected for entry in the model. (ARI = Activation Recovery Interval; ARTG = Activation Recovery Time Gradient; STDQT = QT standard deviation per lead)*

in the same range as the QTd one is trying to establish. This QT measurement problem is predominantly caused by the unclear determination of the T-wave end, especially in the presence of U-waves. Fuller et al. tried to solve the problem of estimating the offset of the T-wave, in an electrolyte torso-shaped tank model with a suspended canine heart in it, by means of a curvature analysis of the T-wave shape [29]. Although this method appears promising, it should be noted, that this method requires minimum noise as can only be obtained in a torso-shaped electrolytic tank model with ideal electrode-torso contact. We found that – in vivo – it appears to be impossible to reach the required signal-to-noise ratio needed for this approach. Therefore, in our study we selected a more conventional method for determination of the offset of the T-wave followed by visual inspection. Variation in the QT interval on a beat-to-beat basis (STDQT) was 2.3 to 4.7 ms in the entire 62-lead BSM array, suggesting a stable determination of the QT interval in this study.

The second problem that emerges when QTd is used for determination of repolarization dispersion is that the QT interval is not reflecting myocardial characteristics of repolarization only. The QT interval is the summation of the entire depolarization and repolarization process in the myocardium underlying a particular surface electrode. The QT interval is therefore not only determined by local repolarization, but also by local depolarization characteristics, such as speed of wave front conduction and direction. Therefore one cannot state that differences in QT interval at the body surface will always reflect increased heterogeneity of repolarization in the heart, since this may also be caused by altered local activation in the heart.

The third issue is that QTd is currently calculated as the longest minus the shortest QT interval that can be recorded in a given electrode array system. Although this does provide some information on the QT interval distribution over the thorax, it is probably not the best measure to detect non-uniform local recovery from excitation in the heart. It is conceivable that large differences in QT interval that are found between electrode pairs that are far apart on the thorax do not bear much clinical relevance since they do not necessarily indicate large regional differences in repolarization in the heart. Increased local differences in repolarization predispose for functional re-entry potentially resulting in malignant tachyarrhythmias.

Finally, it should be noted that QTd estimation from the standard 12-lead ECG is limited by the paucity of electrodes. In this study it was shown that only 15 % of the variance in QTd (partial r=0.39 in the linear regression model in Table 5, therefore r^2=0.15) could be independently explained by endocardial ARTG standard deviation. This illustrates that some of the information on local endocardial differences in repolarization duration is preserved when the QTd is derived using only the 12-lead ECG. This percentage increases slightly to 27% (partial r=0.52 in table 6.7) when the entire BSM array is utilized.

6.5.2 Non-dipolar content of BSM QRST integrals.

The concept of the QRST integral or ventricular gradient was first introduced by Wilson et al, who suggested that the "deflection area of the QRST complex was determined by differences in the duration of repolarization" [1]. Subsequent theoretical models confirmed this relation [30, 31]. Abildskov et al provided direct evidence for this concept in an experimental study in dogs [32]. In their study, they concluded that QRST integrals represent primary repolarization characteristics, which are independent of the site of ventricular activation, as opposed to secondary repolarization characteristics, which are dependent on the activation site as well as on a disturbed activation sequence due to bundle-branch block or prior infarction. Later, clinical evidence was found that linked non-dipolar content with left ventricular dilatation following myocardial infarction [17] and various forms of intrinsic electrical heart disease [19] and cardiomyopathy [18]. In the presented study, a significant difference in non-dipolar QRST integral map content was found between VT Group vs. Control Group and non-VT Group vs. Control Group, respectively. The difference found between VT Group and non-VT Group did not reach significance (P=0.09). The relatively small patient groups may have caused this. Furthermore, one should realize that, although patients in the non-VT Group had never suffered from sustained ventricular arrhythmias, they potentially have the same arrhythmogenic postinfarction substrate. For instance, although anecdotal, the patient in the non-VT Group with the largest non-dipolar QRST map content (0.87) died suddenly 2 months after the BSM.

When non-dipolar QRST content was compared with direct endocardial repolarization measurements, it was found that the mean ARI duration was an independent predictor, explaining 41% (r=–0.64 in the linear regression model) of the non-dipolar QRST map content variance. Pearson's correlation coefficient proves that non-dipolar content is inversely related (r=–0.79) with mean ARIs. This implies that patients with significant non-dipolar QRST content will have short endocardial refractory periods. Short endocardial electrical recovery intervals may give rise to shorter reentry circuits thereby exposing the patient to more malignant ventricular arrhythmias.

Major advantages of the QRST integral map are its relative independence of noise and the exact determination of the T-wave end. Since stationary noise has zero mean and unity variance, its contribution to the integral value can be neglected. If the markers comprising the QRST interval can be set at the instant near the offset of the T-wave where instantaneous voltages are low (in our study $<$0.02 mV), only a small contribution to the QRST integral value will be missed at most. Major disadvantage of the QRST integral map is its relative sensitivity to baseline drifting. Therefore, a good baseline correction algorithm should be used.

6.5.3 Transmural dispersion

More recently, the concept of transmural dispersion in repolarization was introduced by Antzelevitch et al [33, 34]. They postulated the presence of specialized

cells, so-called M-cells, in the deeper layer of the ventricular myocardium, possessing specific repolarization properties. From their experimental work it appears that the J-T-peak interval is determined by the repolarization duration of the epicardial cells, whereas as the T-peak to T-end is determined by the difference in repolarization between M-cells and the epicardial layer, thereby representing a transmural repolarization gradient [35–37]. Most of the work by Antzelevitch et al was done in an arterially perfused myocardial wedge model with an electrode configuration resembling standard precordial lead V5 [35].

In the currently presented study the relation between the T-wave peak to T-wave end interval in the precordial leads V2 and V5 and endocardial repolarization estimates was determined. In both infarction patient groups (VT Group and non-VT Group) the TE interval in V2 and V5 was significantly larger than in the healthy controls (Control Group), but between VT Group and non-VT Group no significant differences were found. When compared to the invasive estimates of repolarization, TE V5 correlated strongly with the ARTG range and the ARTG standard deviation. Both parameters combined explained 76 % (r=0.62 and r=0.25, respectively) of the TE V5 variance. Interestingly, none of the endocardial parameters sufficed the P=0.10 threshold for entry in the linear regression model for TE V2. These data suggest that TE V5 is indeed a powerful predictor of dispersion in repolarization.

6.5.4 Activation Recovery Time Gradients

Since it was presumed that merely looking at differences in QT interval over the entire thorax was probably not the best measure to express local differences in repolarization, a new parameter was introduced in this study. ARTGs can be calculated both for ARIs as for QT intervals, allowing direct quantitative correlation between the two. ARTGs give information on the rate of local change in repolarization duration, expressed as ms per degree between 2 electrodes. We postulated that larger ranges in ARTG either at the endocardium or at the body surface represents increased dispersion in refractoriness. Indeed, correlations between endocardial ARTGs and TE V5 and the 12-lead QTd (Table 5), were found as well as between endocardial ARTGs and the BSM QTd, and between endocardial and BSM ARTGs (Table 6.7).

6.5.5 The 'ideal' non-invasive parameter to estimate repolarization dispersion

The ideal parameter for detection of repolarization dispersion and therefore for identification of patients prone to malignant ventricular arrhythmias would be a parameter that 1) can be reliably and reproducibly detected at the body surface 2) gives information on local differences in repolarization independent of the depolarization characteristics and 3) is able to discriminate patients with potentially the same arrhythmogenic substrate, who are not subjected to increased risk for sudden death, from those who are. From all parameters used in this study, non-

dipolar content of the QRST integral map appears to fit this description the best. Only the difference between VT Group vs. non-VT Group did not reach significance although a trend towards significance was present. The best way to resolve this issue would be to conduct a prospective study comprising a larger number of patients. The TE V5 interval is a simple to obtain parameter in daily clinical practice and also appears to correlate well with endocardial dispersion in refractoriness. In this study, TE V5 had less discriminative power between infarction patients, but again larger prospective studies will be needed to establish this.

6.5.6 Limitations of the study

The repolarization process in the human ventricle is a complicated 3D (or maybe even 4D when temporal dispersion is considered) process with possibly very different behavior in different layers of the myocardium. To investigate the repolarization in the heart an endocardial basket catheter was used as well as a BSM array. This means that no direct information could be obtained from the intramural myocardial and epicardial layers. Assumptions on transmural dispersion will therefore have to be made with caution. Furthermore, since the basket is not guaranteed to cover the entire endocardium, repolarization aspects of parts of the endocardium – and especially the apex of the left ventricle – may have been underestimated.

Finally, it should be noted that patients in the VT Group and non-VT Group were incomparable with respect to left ventricular ejection fraction and time since infarction. This was caused by the fact that the goal of this study was to compare postinfarction patients without ventricular arrhythmias with those who suffered from VTs. The concept that VTs develop late after myocardial infarction when left ventricular dilatation has progressed, appears well in line with the correlation between left ventricular dilatation and non-dipolar QRST content found by Dambrink et al [17].

Since infarction patients in the VT Group and non-VT Group all potentially are at risk for developing postinfarction ventricular arrhythmias, whether those are already manifest or not, further prospective data are needed to evaluate the discriminative powers of the variables between infarction patients that are and infarction patients that are not at risk for sudden cardiac death.

6.6 Conclusion

QT dispersion can be detected at the body surface by means of the 12-lead ECG to some extent. T-peak to T-wave end in precordial lead V5 appears to be a more promising parameter. Extending the lead set to cover the entire chest area increases the yield of QTd estimation for detection of disparity in repolarization, but several problems intrinsic to the nature of QTd persist. Non-dipolar content of the BSM QRST integral can identify patients with short mean endocardial repolarization duration, which are at risk for tachyarrhythmias with shorter cycle length. Finally, ARTG can be used to detect differences in duration of repolarization in

confined chest areas, indicative of spatial disparity of repolarization, instead of global difference in repolarization duration estimated over the entire thorax like QTd. To further evaluate the clinical use of body surface ARTG, the TE V5 interval and non-dipolar content of the QRST integral map, prospective trials are needed.

References

1] F. N. Wilson, A. G. MacLeod, P. S. Barker, and F. D. Johnston. Determination of the significance of the areas of the ventricular deflections of the electrocardiogram. *American Heart Journal*, 10:46–61, 1934.

2] C. J. Wiggers. The mechanism and nature of ventricular fibrillation. *American Heart Journal*, 20:399, 1940.

3] D. M. Mirvis. Spatial variation of QT intervals in normal persons and patients with acute myocardial infarction. *Journal of the American College of Cardiology*, 5:625–631, 1985.

4] L. De Ambroggi, T. Bertoni, E. Locati, M. Stramba-Badiale, and P. J. Schwartz. Mapping of body surface potentials in patients with the idiopathic long QT syndrome. *Circulation*, 74:1334–1345, 1986.

5] M. R. Franz, K. Bargheer, W. Rafflenbeul, A. Haverich, and P. R. Lichtlen. Monophasic action potential mapping in human subjects with normal electrocardiograms: direct evidence for the genesis of the T wave. *Circulation*, 75:379–386, 1987.

6] J. C. Cowan, C. J. Hilton, C. J. Griffiths, S. Tansuphaswadikul, J. P. Bourke, A. Murray, and R. W. Campbell. Sequence of epicardial repolarisation and configuration of the T wave. *British Heart Journal*, 60:424–433, 1988.

7] A. Ramdat Misier, T. Opthof, N. M. van Hemel, J. T. Vermeulen, J. M. de Bakker, J. J. Defauw, F. J. van Capelle, and M. J. Janse. Dispersion of 'refractoriness' in noninfarcted myocardium of patients with ventricular tachycardia or ventricular fibrillation after myocardial infarction. *Circulation*, 91:2566–2572, 1995.

8] M. Zabel, S. Portnoy, and M. R. Franz. Electrocardiographic indexes of dispersion of ventricular repolarization: an isolated heart validation study. *Journal of the American College of Cardiology*, 25:746–752, 1995.

9] C. P. Day, J. M. McComb, and R. W. Campbell. QT dispersion: an indication of arrhythmia risk in patients with long QT intervals. *British Heart Journal*, 63:342–344, 1990.

10] J. T. Hii, D. G. Wyse, A. M. Gillis, H. J. Duff, M. A. Solylo, and L. B. Mitchell. Precordial QT interval dispersion as a marker of torsade de pointes. disparate effects of class ia antiarrhythmic drugs and amiodarone. *Circulation*, 86:1376–1382, 1992.

11] S. G. Priori, C. Napolitano, L. Diehl, and P. J. Schwartz. Dispersion of the QT interval. A marker of therapeutic efficacy in the idiopathic long QT syndrome. *Circulation*, 89:1681–1689, 1994.

12] C. S. Barr, A. Naas, M. Freeman, C. C. Lang, and A. D. Struthers. QT dispersion and sudden unexpected death in chronic heart failure. *Lancet*, 343:327–329, 1994.

13] M. Zabel, T. Klingenheben, M. R. Franz, and S. H. Hohnloser. Assessment of QT dispersion for prediction of mortality or arrhythmic events after myocardial infarction: results of a prospective, long-term follow-up study. *Circulation*, 97:2543–2550, 1998.

14] B. Brendorp, H. Elming, L. Jun, L. Kober, M. Malik, G. B. Jensen, and C. Torp-Pedersen. QT dispersion has no prognostic information for patients with advanced congestive heart failure and reduced left ventricular systolic function. *Circulation*, 103:831–835, 2001.

15] M. Zabel, P. R. Lichtlen, A. Haverich, and M. R. Franz. Comparison of ECG variables of dispersion of ventricular repolarization with direct myocardial repolarization measurements in the human heart. *Journal of Cardiovascular Electrophysiology*, 9:1279–1284, 1998.

16] A. SippensGroenewegen, H. Spekhorst, R. N. Hauer, N. M. van Hemel, P. Broekhuijsen, and A. J. Dunning. A radiotransparent carbon electrode array for body surface mapping during cardiac catherization. *Proceedings of the IEEE Medical Biological Society*, pages 178–181, 1987.

17] J. H. Dambrink, A. SippensGroenewegen, W. H. van Gilst, K. H. Peels, C. A. Grimbergen, and J. H. Kingma. Association of left ventricular remodeling and nonuniform electrical recovery expressed by nondipolar QRST integral map patterns in survivors of a first anterior myocardial infarction. captopril and thrombolysis study investigators. *Circulation*, 92:300–310, 1995.

18] H. A. Peeters, A. SippensGroenewegen, B. A. Schoonderwoerd, E. F. Wever, C. A. Grimbergen, R. N. Hauer, and E. O. Robles de Medina. Body-surface QRST integral mapping. Arrhythmogenic right ventricular dysplasia versus idiopathic right ventricular tachycardia. *Circulation*, 95:2668–2676, 1997.

19] H. A. Peeters, A. SippensGroenewegen, E. F. Wever, M. Potse, M. C. Daniels, C. A. Grimbergen, R. N. Hauer, and E. O. Robles de Medina. Electrocardiographic identification of abnormal ventricular depolarization and repolarization in patients with idiopathic ventricular fibrillation. *Journal of the American College of Cardiology*, 31:1406–1413, 1998.

20] M. Potse, A. C. Linnenbank, and C. A. Grimbergen. Software design for analysis of multichannel intracardiac and body surface electrocardiograms. *Computer Methods and Programs in Biomedicine*, In press, 2001.

21] A. K. Evans, R. L. Lux, M. J. Burgess, R. F. Wyatt, and J. A. Abildskov. Redundancy reduction for improved display and analysis of body surface potential maps. II. Temporal compression. *Circulation Research*, 49:197–203, 1981.

22] J. A. Abildskov, L. S. Green, and R. L. Lux. *Detection of disparate ventricular repolarization by means of the body surface electrogram*, pages 495–499. Grune & Stratton, 1985.

23] G. Huiskamp. Difference formulas for the surface laplacian on a triangulated surface. *Journal of Computational Physics*, 95:477–496, 1991.

24] N. Maglaveras, J. M. de Bakker, F. J. van Capelle, C. Pappas, and M. J. Janse. Activation delay in healed myocardial infarction: a comparison between model and experiment. *American Journal of Physiology*, 269:H1441–9, 1995.

25] R. Coronel, F. J. Wilms-Schopman, J. R. de Groot, M. J. Janse, F. J. van Capelle, and J. M. de Bakker. Laplacian electrograms and the interpretation of complex ventricular activation patterns during ventricular fibrillation. *Journal of Cardiovascular Electrophysiology*, 11:1119–1128, 2000.

26] L. Gepstein, G. Hayam, and S. A. Ben-Haim. Activation-repolarization coupling in the normal swine endocardium. *Circulation*, 96:4036–4043, 1997.

27] M. J. Ackerman. The visible human project. *Journal of Biocommunication*, 18:14, 1991.

28] J. L. Willems, C. Abreu-Lima, P. Arnaud, J. H. van Bemmel, C. Brohet, R. Degani, B. Denis, J. Gehring, I. Graham, and G. van Herpen. The diagnostic performance of computer programs for the interpretation of electrocardiograms. *New England Journal of Medicine*, 325:1767–1773, 1991.

29] M. S. Fuller, G. Sandor, B. Punske, B. Taccardi, R. S. MacLeod, P. R. Ershler, L. S. Green, and R. L. Lux. Estimates of repolarization and its dispersion from electrocardiographic measurements: direct epicardial assessment in the canine heart [in process citation]. *Journal of Electrocardiology*, 33:171–180, 2000.

30] H. C. Burger. A theoretical elucidation of the notion 'ventricular gradient'. *American Heart Journal*, 53:240–246, 1957.

31] R. Plonsey. A contemporary view of the ventricular gradient of wilson. *Journal of Electrocardiology*, 12:341, 1979.

32] J. A. Abildskov, A. K. Evans, R. L. Lux, and M. J. Burgess. Ventricular recovery properties and QRST deflection area in cardiac electrograms. *American Journal of Physiology*, 239:H227–H231, 1980.

33] C. Antzelevitch, W. Shimizu, G. X. Yan, and S. Sicouri. Cellular basis for QT dispersion. *Journal of Electrocardiology*, 30:168–175, 1998.

34] C. Antzelevitch, W. Shimizu, G. X. Yan, S. Sicouri, J. Weissenburger, V. V. Nesterenko, A. Burashnikov, J. Di Diego, J. Saffitz, and G. P. Thomas. The m cell: its contribution to the ECG and to normal and abnormal electrical function of the heart. *Journal of Cardiovascular Electrophysiology*, 10:1124–1152, 1999.

35] G. X. Yan and C. Antzelevitch. Cellular basis for the normal T wave and the electrocardiographic manifestations of the long-QT syndrome. *Circulation*, 98:1928–1936, 1998.

36] C. Antzelevitch. Tpeak-tend interval as an index of transmural dispersion of repolarization. *European Journal of Clinical Investigations*, 31:555–557, 2001.

37] C. Antzelevitch. Transmural dispersion of repolarization and the T wave. *Cardiovascular Research*, 50:426–431, 2001.

7

Physical considerations when correlating BSM indices of arrhythmia vulnerability with endocardial multi-lead recordings

P.F.H.M. van Dessel [1], A.C. Linnenbank [2,3], J.M.T. de Bakker [2,3], M. Potse [4], N.M. van Hemel [1]

From the Heart Lung Center Utrecht, Department of Cardiology[1], St Antonius Hospital, and Department of Cardiology[2], University Medical Center, Utrecht, Experimental and Molecular Cardiology Group of the Cardiovascular Research Institute[3], and Department of Medical Physics[4], University of Amsterdam, Amsterdam, The Netherlands.

Presented in part at the 3rd International Symposium on Noninvasive Functional Source Imaging, Innsbruck, 2001

7.1 Introduction

Ventricular tachycardia (VT) late after myocardial infarction requires a substrate of surviving myocardial fibers within the infarcted area. Areas of slow conduction, revealing itself as late potentials at the body surface [1], and non-uniform recovery from excitability, possibly expressed by increased QT dispersion [2], appear to be indices of vulnerability for ventricular arrhythmias. Surface ECG data can be obtained with a body surface mapping (BSM) electrode array, whereas recently multi-electrode systems that are capable of obtaining instantaneous multi-site endocardial maps – such as a 'basket' catheter – have become available to study arrhythmogenic mechanisms in the human heart in vivo.

A number of issues will have to be resolved when trying to geometrically link late potentials from endocardial areas of slow conduction to signals that can be recorded at the body surface. First, the signal-to-noise ratio (SNR) is not high enough for these signals to be detected directly on a beat to beat basis at the body surface. This problem can be solved by signal averaging. Second, the amplitude of ECGs depends on the location of the recording electrodes. Signals are largest in the precordial region and smaller in regions more distant from the heart. To estimate the relative contributions of all surface leads, a correction for this distance effect is necessary. Third, standard criteria used in the context of late potentials are sensitive to the SNR. General criteria must be developed that identify late potentials less dependent on SNR, since SNR changes with the electrode position at the body surface. Fourth, electrodes of a basket catheter will be in a different position for each patient. It is therefore not possible to use a general forward or inverse solution. A tailor-made matrix that maps potentials at electrodes in the heart to potentials at the body surface, has to be estimated for every patient. Finally, the BSM electrode array and the basket catheter electrode system are quite different unevenly distributed electrode systems. When comparing data (e.g. repolarization estimates) from both electrode systems, a measure will have to be developed that not only corrects for different interelectrode distances within a lead system, but also has the same dimension and similar magnitude in both lead systems, allowing comparison between them.

7.2 Signal averaging of late potentials

When the signal-to-noise ratio of a repetitive signal is not large enough to reliably detect this particular signal, one can use its repetition to increase the SNR. Repetition can be used if it is possible to evoke the signal as a response to an external stimulus, like e.g. in the case of evoked potentials in neurology or endocardial paced ventricular activation in cardiology. Signal averaging can also be applied if the signal of interest has a causal relation with a signal that has a SNR large enough to be detected. The latter is the case for 'late potentials'. These are small deflections with a SNR below 1, occurring at the end of the QRS complex. They have, however, a fixed relation in timing with the much larger QRS complex. By deriving the timing from the QRS complex and averaging the entire signal, the

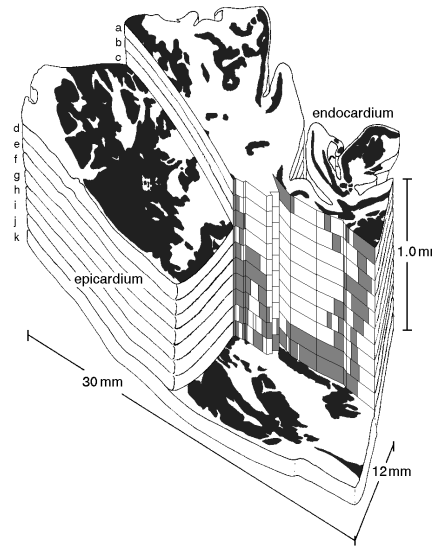

Figure 7.1: *Reconstructed histological slices from the infarcted area of a human heart. Grey and black areas depict surviving strands of myocardium. White areas denote fibrous tissue. Picture from De Bakker et al. [3].*

SNR of the late potentials can be increased.

7.2.1 Electrophysiological basis for signal averaging

Late potentials are generated by activation in myocardial bundles that survive in the infarcted area. As can be seen in figure 7.1 surviving 'bundles' are in fact a complex substrate consisting of tracts of preserved conduction within the infarction scar. These tracts tend to form a complex 3D structure with all sorts of twists and turns. Because activation in these bundles will not travel in a straight line, an ECG lead at the body surface will record the activation coming towards this lead at some instant – and hence show a positive signal – while the next moment the activation turns away and the signal diminishes and may even become negative. This will cause surface leads to record a quickly changing (high-frequency) signal from this substrate.

From the properties of these bundles we can derive the properties of signals at the body surface that may indicate such a substrate. First, because propagation is slower in surviving bundles these potentials will occur during sinus rhythm late in depolarization, hence the name 'late potentials'. Second, late potentials are of small amplitude because they are generated by small myocardial areas and third they are more prominent in the higher frequencies than the bulk of the ventricular activation.

These properties suggest the following method for detection: increase the SNR by signal averaging, use a high-pass filter to remove large, low-frequency signals and look at the end of the QRS complex. Of course, high frequency potentials generated by the arrhythmia substrate will also be present during the QRS complex but in this interval they will be masked by the much larger normal ventricular activation.

7.2.2 Coherent and weighted averaging

Coherent averaging

Usually, the standard procedure for signal averaging is to simply time-align all complexes. Beats with artifacts and excessive noise are rejected and the mean of the signal is used as an estimate of the signal. This is called coherent averaging. The fundamental assumption when using coherent averaging to average N signals is that the noise in the signal is stationary. The signal model, for stationary noise, of the kth complex is:

$$y_k(t) = x(t) + \sigma n(t), \quad (1 \leq k \leq N) \tag{7.1}$$

where $x(t)$ is the signal of interest, which is assumed to have an invariant morphology and to be uncorrelated with the noise $n(t)$ which has zero mean and unit variance. The standard deviation of the noise is σ for all beats. After averaging the resulting noise level will be $\sigma/\sqrt{N}$.

In biological signals the noise is generally not stationary. For non-stationary noise coherent averaging is not the optimal technique. Consider the case where two QRS complexes are averaged and one complex contains twice as much noise as the other complex. In this particular case coherent averaging will result in a new noise level of $\sqrt{(1^2 + 2^2)}/2 \approx 1.12$ times the lowest noise level. In this case, the resulting noise level is even more than that in the most optimal original measurement.

Weighted averaging

The signal model in the case of averaging of non-stationary noise is:

$$y_k(t) = x(t) + \sigma_k n(t) \tag{7.2}$$

where σ_k is the noise level in the kth signal.

If the signal had been stationary the variance of the coherent averaged signal would have been σ_k^2/N. If we now define the weighted averaged signal $\overline{y}_w(t)$ as:

$$\overline{y}_w(t) = \sum_{k=1}^{N} w_k y_k(t) \quad \text{with} \quad \sum_{k=1}^{N} w_k = 1 \tag{7.3}$$

then it can be shown that the minimum achievable variance is:

$$\overline{\sigma}^2 = \left(\sum_{k=1}^{N} \frac{1}{\sigma_k^2} \right)^{-1} \quad \text{for} \quad w_k = \frac{1}{\sigma_k^2} \cdot \left(\sum_{j=1}^{N} \frac{1}{\sigma_j^2} \right)^{-1} \tag{7.4}$$

For our example with one signal having twice the noise level of the other, after weighted averaging the total noise will be $\sqrt{1/(1/1+1/4)} \approx 0.9\sigma$, which is indeed lower than the noise in either signal.

7.2.3 Definition of parameters

Simson has proposed a method to detect late potentials in body surface signals and many variations on his scheme have since been proposed, all with basically the same ingredients. First all complexes in a long recording, often 300 complexes or more, are time-aligned. Then the X, Y, and Z leads are (coherently) averaged to increase the SNR. These X, Y, and Z are 'bidirectionally' filtered and combined in a vector magnitude. In this context 'bidirectionally' means that the first part of the signal is filtered forward to a point in the middle of the QRS complex and then the last part is filtered backwards up to this same point. The result is that the QRS duration is not overestimated as a result of leaking of energy out of the QRS complex into the adjacent isoelectric segments as a result of the filtering. From the vector magnitude the (filtered) QRS duration (QRSD, sometimes fQRSD) is determined by estimating the noise and subsequently setting the beginning of the QRS complex at the instant when the signal exceeds for 5 ms the noise plus 3 times its standard deviation. Then, the end of the QRS complex is determined by searching backwards from a point well beyond the J-point for the instant when the signal for the first time exceeds the noise plus 3 times its standard deviation for this same interval. After determining the end of the QRS complex, two more parameters can be computed viz. the RMS of the signal in the last 40 ms (the RMS40) and the time between the moment the signal drops below 40 μVand the end of the filtered QRS complex (LAS40).

All three parameters (QRSD, LAS40, and RMS40) are measures of late activation in the ventricles. For signals filtered with a low-pass of 25 Hz, clinical investigations show that QRSD>120 ms, RMS40<23 μV, and LAS40>38 ms are associated with patients prone to ventricular arrhythmias. When two out of the three parameters are different from the normal population the patient is said to have late potentials. For two patients, one with and one without late potentials data are shown in figure 7.2.

7.2.4 Limitations of standard method

The Simson method for signal averaging only determines whether late potentials are present. Since late potentials are detected on one single (compound) ECG trace, anatomical localization of late potentials is impossible. Moreover, because late potentials are defined as persistence of energy content of a specified amplitude during a specified period of time at the end of the QRS complex, instead of a specific deflection in the ECG representing *the* late potential, it is not possible to identify *the* corresponding deflection in invasively obtained intracardiac recordings.

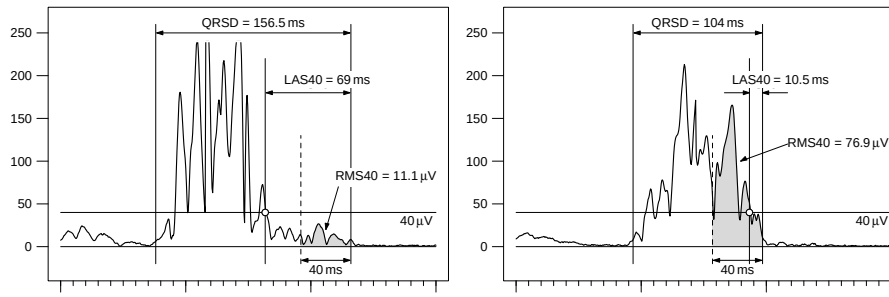

Figure 7.2: *Definition of parameters in the standard signal averaging procedure. QRSD is the total QRS duration of the filtered vector magnitude. RMS40 is the RMS energy in the last 40 ms of the QRS complex. LAS40 is the duration at the terminal part of the signal that is below 40 µV. The SAECG on the left is positive for late potentials (QRSD = 156.5 ms, RMS40 = 11.1 µV, LAS40 = 69 ms). The SAECG on the right contains no late potentials (QRSD = 104 ms, RMS40 = 76.9 µV, LAS40 = 10.5 ms).*

The requirement that the signal must cross the threshold for 5 ms is not consistent with the 250 Hz bandwidth. A 100 Hz signal will cross the zero line every 5 ms. So any substantial (interference) signal of 100 Hz or higher will not be above threshold for more than 5 ms in the vector magnitude. As is shown in figure 7.3 where a 150 Hz signal is artificially added to one of the leads, the QRS offset will be detected more or less at the same instant, whereas the 150 Hz signal is clearly present beyond that point. Therefore, the detection interval should be 2 ms and not 5 ms to accommodate the 250 Hz bandwidth or the bandwidth should be reduced to 100 Hz. The current method will not detect high-frequency late potentials in the 100–250 Hz range, but the frequencies between 100 and 250 Hz will still contribute to the noise.

7.3 Lead dependent late potential criteria

When a multi-lead electrode system with variable heart – electrode distances is used to detect late potentials instead of a 3-lead orthogonal lead system, a new criterium for the presence of late potentials will have to be defined. All parameters used in the standard procedure to detect late potentials depend on SNR. The end of the filtered QRSD is defined as the instant in the electrogram when the instantaneous voltage drops below the mean plus three times the standard deviation of the estimated noise. In effect, this implies that if the noise level decreases, the QRSD will increase and as a result the LAS40 will also increase, while the RMS40 will decrease. The SNR is larger in the precordial region than in the posterior regions of the chest. Using any of these parameters in the aforementioned multi-lead electrode system will underestimate the presence of late potentials originating from e.g. the posterior wall of the left ventricle.

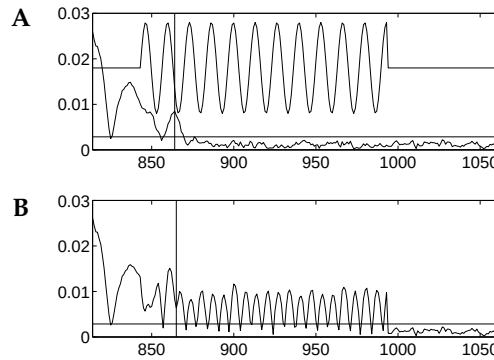

Figure 7.3: *High frequency interference in pass band. A train of 150 Hz sinuses is added to an averaged signal from a patient to the positive X-lead (**panel A**). Although this is in the pass band of the standard averaging procedure this signal will cross the zero-line every 3.3 ms. The vector amplitude (**panel B**) will therefore not be above the threshold (horizontal line) for more than 5 ms and the 'end of QRS complex' (vertical line) will be detected at the approximate same time as in the **panel A**.*

Another reason for not using LAS40 or RMS40 is that their determination also depends on the signal amplitude. Signal amplitude varies with the distance of the electrode to the heart, i.e. the position of the electrode on the thorax, whereas noise will be mainly determined by local skin-electrode conditions. This will cause the SNR to be less favorable in the areas of the thorax more distant from the heart. Since the QRSD has an unknown distribution over the thorax, it is not possible to use this parameter by itself to quantify late potentials in the heart at the body surface.

Because criteria that depend on the signal can not be used, the only parameters left are those that use a fixed time interval. This interval should not depend on the presence or absence of late potentials, in fact ruling out the use of the filtered ECG's for defining this interval.

Therefore, we propose to use the interval from the J-point — as determined in the unfiltered QRS complexes from the precordial leads V1 to V6 — to 50 ms after the J-point to include all late potentials. The J-point was defined as the time when a tracing changes slope abruptly at the end of the S-wave [4].

7.4 Distance Effect

The amplitude of late potentials in averaged signals in any lead will not only be influenced by the size and orientation of the underlying electrical wave front but also by the distance of the source to the electrode. The amplitude of a signal generated by a dipole will diminish rapidly with the distance between source and recording electrode. This means that irrespective of the location of the substrate

in the heart the maximum amplitude of late potentials will usually be recorded in the precordial region. To avoid underestimation of the significance of late potentials in other chest areas, a correction for the effect of electrode-source distance is needed. Actually, the standard late potential analysis uses *un*corrected X, Y, and Z leads. This analysis therefore also overestimates late potentials from the anterior wall and underestimates those from other sites of the heart.

The potential (V_t) measured at point x on the surface is a result of the potential distribution (V_h) at all points p in the heart and a transfer matrix (**A**).

$$V_t(\vec{x}, t) = \int_{\text{myocard}} \mathbf{A}(\vec{x}, \vec{p}) V_h(\vec{p}, t)\, d\vec{p} \tag{7.5}$$

A implicitly includes the distance effect and torso inhomogeneities. This can be simplified by assuming that all cells have the same contribution. Then we only have to estimate

$$D(\vec{x}) = \int_{\text{myocard}} \mathbf{A}(\vec{x}, \vec{p})\, d\vec{p} \tag{7.6}$$

For any lead set with leads at positions x_i we can now estimate the potential distribution corrected for the distance effect $\overline{V_i}$ from a measured potential distribution V_i.

$$\overline{V_i} = V_i \cdot D(\vec{x_i}) \tag{7.7}$$

The distance matrix can be computed from volume conductance theory and information derived from MR images. For practical purposes, however, a measure that can be derived from the data itself is preferable.

7.4.1 Methods for distance correction

We recorded 65 leads at the body surface (62 leads according to the Amsterdam lead system plus three extremity leads) simultaneously with 64 endocardial leads from a Constellation™ basket catheter (Boston Scientific Inc.) in 16 patients. Biplane X-ray images were acquired and digitized to obtain 3D positions of all endocardial electrodes.(See § 7.5)

Standard X, Y, and Z leads were reconstructed from the three best matching electrode pairs selected from the 65 body surface electrodes. The standard SAECG was obtained from these X, Y, and Z leads to compare SABSM with the signal averaging method that is currently applied clinically. In the literature various criteria for the detection of late potentials have been proposed, depending among other things on the cut-off frequency used in the high-pass filter [5, 6]. In this study, late potentials were defined as a QRSD>120 ms, RMS40<23 μV, and LAS40>38 ms in accordance with commercially available equipment used in our hospital for traditional SAECG.

As a time reference for all surface leads the J point in the unfiltered QRS was chosen as described above. The energy in the 50 ms following this point was integrated and plotted as a body surface map.

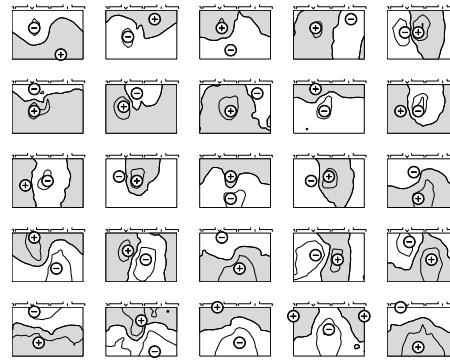

Figure 7.4: *Isopotential maps obtained at 5 ms intervals in the filtered signal averaged QRS complex of sinus rhythm in one patient.*

The following physical reasoning was adopted to derive the correction factors for heart – electrode distance. During left ventricular depolarization every cell generates a small current, the summation of which results in the QRS complex at the body surface. It would seem that for every point at the surface, the average energy during the QRS complex can be used as an estimate of the distance effect matrix $D(\vec{x})$ (see equation (7.6)), because it depends on the average distance of all points in the heart to the recording electrode. This assumption, however, should be treated with caution since most dipoles during cardiac activation point more or less in the same direction. So the energy content at positions at the body surface that are perpendicular to the heart axes, will then be underestimated. For a better estimate of the distance effect we need a collection of dipoles instead of a single dipole. Pacing at multiple sites in the ventricle could be employed, but this is rather time consuming and only possible during catheterization. Another option would be to remove the preferential direction of the heart axis by high-pass filtering. After filtering, the surface distribution consists of rapidly changing, nearly dipolar patterns (see figure 7.4). Based on these physical considerations it was expected that high-pass filtered activation during the QRS complex may serve as a good estimation of the distance effect.

$$D(\vec{x_i}) \approx \left(\int_{\text{QRS onset}}^{\text{J point}} V_i(t) \otimes \text{high-pass}_{25\,\text{Hz}} dt \right)^{-1} \tag{7.8}$$

The distance corrected late potentials are therefore computed as:

$$L_t(i) = \frac{\int_{\text{J point}}^{\text{J point}+50\,\text{ms}} V_i(t) \otimes \text{high-pass}_{25\,\text{Hz}} dt}{\int_{\text{QRS onset}}^{\text{J point}} V_i(t) \otimes \text{high-pass}_{25\,\text{Hz}} dt} \tag{7.9}$$

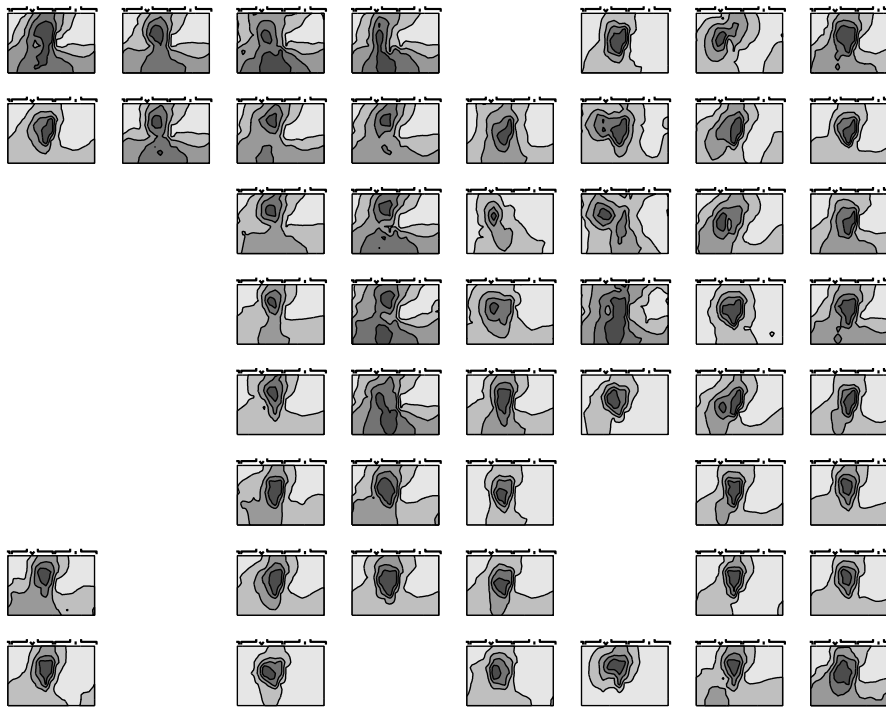

Figure 7.5: *For the same patient as in figure 7.4, filtered QRS integral maps obtained by ectopic stimulation at 50 endocardial sites using the basket catheter are shown. From left to right are the 8 splines of the basket catheter and from top to bottom the 8 electrodes on each spline.*

To illustrate that high-pass filtering of the QRS complex indeed removes the preferential direction, filtered QRS integral maps obtained by pacing 50 of the 64 basket electrodes where capture could be obtained in the same patient are shown in figure 7.5. Similar filtered QRS integral maps are obtained, regardless on the site of origin of endocardial activation. The correlation coefficient (r) between each individual paced map and the mean paced QRS integral map is 0.98. There is also excellent correlation between the mean paced filtered QRS integral map and the filtered QRS integral map of sinus rhythm in this patient (r=0.97)

Since detection of late potentials is done using high-pass filtered electrocardiographic data, using these same signals for the correction procedure seems very efficient. To be able to compare maps from different patients, the correction vector should have an amplitude that does not depend on the total energy in the QRS complex for that patient. This can be achieved by normalizing the correction factor.

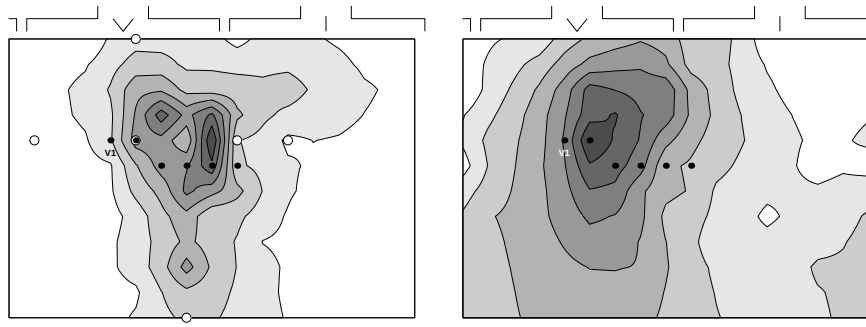

Figure 7.6: *Left panel: the uncorrected energy distribution in the 50 ms interval following the J-point for a patient without late potentials in the standard SAECG. The approximate positions of the X, Y, and Z electrodes are shown as open circles. The darkest area has 3.6 times as much energy as the lightest. Right panel: the mean energy distribution during the QRS complex in the same patient. The darkest area has 6.0 times as much energy as the lightest. In both panels the positions of precordial leads V1–V6 are indicated by dots.*

7.4.2 Results of distance correction

The patient in the right panel of figure 7.2 on page 146 has no late potentials on the standard SAECG although this patient had documented VT. In the left panel of figure 7.6 the uncorrected energy of the late potentials is shown for this patient. In this panel also the approximate positions of the standard X, Y, and Z electrodes are shown. The standard SAECG procedure did not show late potentials probably because the area is relatively small and the electrodes are just outside this area. The right panel shows the average energy during the QRS interval. It is obvious that, as expected, the amplitude is largest in the precordial region.

In the upper panel of figure 7.7, the corrected energy i.e. the energy in the 50 ms following the J-point (left panel in figure 7.6) divided by the normalized energy during the QRS complex (right panel in figure 7.6) is shown. Darker areas correspond to higher energies. For clarity, the left part of the map is repeated on the right. This map shows that the energy above the V2–V3 area in the left panel of figure 7.6 is not a result of late potentials in local heart tissue, but that the maximum around V5 does reflect late potentials. Note that there is now also an area high on the back of the patient that shows a high energy contribution. These two areas correspond to the two areas of the basket catheter (lower panel) that show late potentials (dark areas) during sinus rhythm. The basket is shown in four views, one from the front, one from the right, one from the back and one from the left. They are positioned under the map at positions that correspond to these views from that aspect of the thorax.

In figure 7.8, data from a patient in whom all three SAECG late potential criteria are positive are shown. The standard SAECG analysis for this patient is shown in the left panel of figure 7.2. Like in figure 7.7 the upper panel of figure 7.8 shows

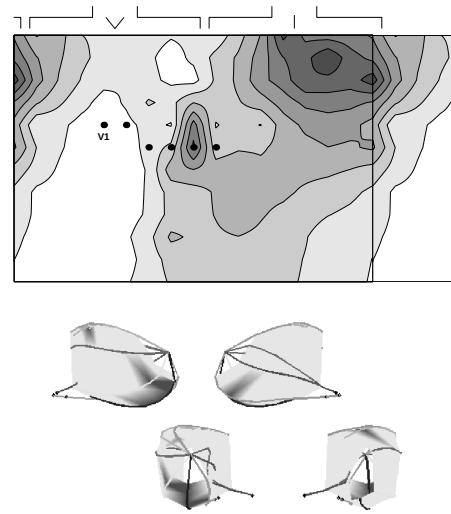

Figure 7.7: *Top panel: energy distribution in the same patient as in figure 7.6 after correction for the distance effect. Lower panel: the late potentials as recorded with the basket catheter. Dark colors indicate electrodes with late potentials. The darkest area has 4.0 times as much energy as the lightest. Note that the two areas with late potentials correspond to the dark areas in the top panel.*

the energy distribution over the body in the 50 ms after the J-point, corrected for the distance. The lower panel shows the late potentials as recorded by the basket catheter.

7.5 Spatial correlation of basket and surface leads

7.5.1 Reconstruction of 3D position of basket electrodes

During catheterization simultaneous biplane x-ray images were acquired using right (RAO) and left anterior oblique (LAO) digital cine fluoroscopy (Philips Medical Systems Integris). The same end-diastolic frames from both fluoroscopic projections were selected. Starting at the A and B spline, which are easily identified by one resp. two extra radiopaque markers at the proximal end, all electrodes were labelled in both views. Correct labelling was checked by a team of experienced cardiologists.

If the positions of individual electrodes in the two perpendicular views are known, it is possible to compute their 3D positions within the left ventricle. In both views a line can be drawn from the pixel of the image in the detector to the corresponding x-ray source. These two lines must intersect at the 3D position of the object under consideration. In practice because of measurement errors the two

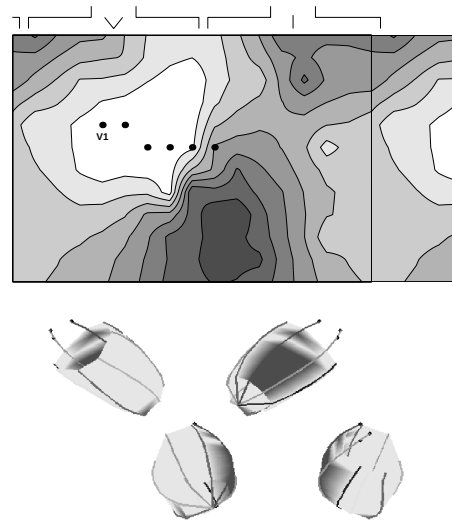

Figure 7.8: *Late potentials in a patient with positive SAECG. Layout is the same as in figure 7.7. Again, two endocardial as well as two body surface areas of late potentials are found.*

lines will not intersect but cross at a certain distance. For the 3D position of the electrodes of the basket the midpoint of the shortest line segment connecting the two crossing lines was taken. The length of this line segment is an indication of the accuracy of the reconstruction. For the basket electrodes the mean length of this segment was 3 mm.

7.5.2 3D positions of surface electrodes

For each patient the position of the surface electrodes relative to the heart was derived computationally. For this purpose, cross-sectional images of a human thorax, as can be found on the internet, were utilized [7]. The image at the level of the center of the left ventricle was used (figure 7.9). The approximate positions of the 14 BSM straps and the center of the left ventricle were determined on this selected slice. By repeatedly translating the surface positions over a vertical distance of 3 cm, a simple model of the torso was constructed.

This 3D information was used in combination with the computed 3D positions of the basket electrodes, placing the basket virtually in the same image while making the center of the basket and the center of the left ventricle coincide. This allowed investigation of the spatial relations of surface ECGs and endocardial signals.

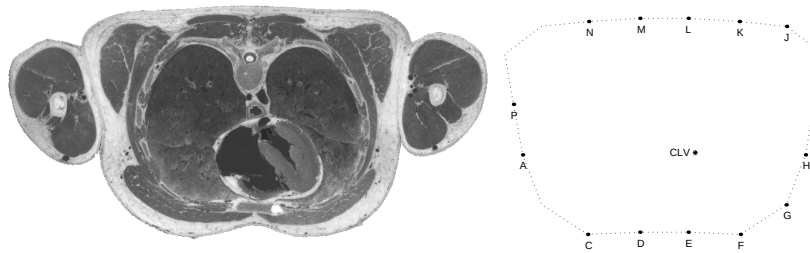

Figure 7.9: *Left Panel: Cross-sectional image of the human thorax at the level of the center of the left ventricle. Right panel: The approximate position of the 14 straps on the body surface as determined from the left panel. At the positions where the straps 'B' and 'O' would be the Amsterdam Lead set does not contain electrodes. The asterisk denotes the approximate position of the center of the left ventricle (CLV).*

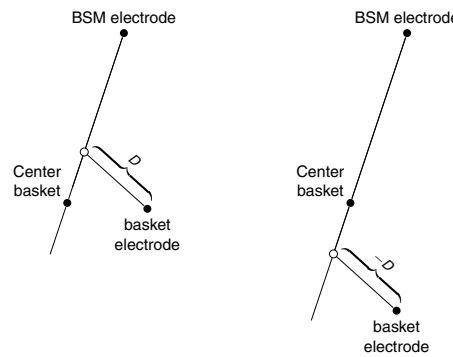

Figure 7.10: *Computation of distance (D) of the basket electrodes from the line connecting a surface electrode with the center of the basket catheter.*

7.5.3 Matching surface and endocardial electrodes

Electrodes at the body surface are most sensitive to regions in the heart that are nearest to them. When interested in the value of a parameter in a certain region of the heart one should select an electrode that observes this region and subsequently compare its value with those obtained at other sites. To determine which regions on the heart project to which regions on the body surface a forward computation can be employed if the exact geometry of the patient is known. No MRI or other 3D information were available in our study, however.

To be able to make the comparison between recorded endocardial late potentials and late potentials that were detected after signal averaging, a matrix should be constructed that indicates the weighted contribution of each basket electrode to all of the BSM electrodes in each individual patient.

For all 62 BSM and all 64 endocardial electrodes the 3D positions can be calculated utilizing the aforementioned techniques. We postulated that every electrode

at the surface is most sensitive to those parts of the heart that lie close to the line connecting this electrode to the center of the left ventricle. We therefore computed for each pair of surface electrode and basket electrode the distance of the basket electrode to the line that connects the surface electrode to the center of the basket (see figure 7.10). Since electrodes at the opposite side of the center of the basket may also be close to this line through the center of the basket, these distances were rendered negative to distinguish these electrodes from the electrodes close to the line on the same side of the basket as the surface electrode. Because basket electrodes closest to this line contribute most to that particular surface electrode, the inverse of these distances was used to establish a weighted contribution. The inverse distances were then normalized such that the maximal contribution of each endocardial electrode to the surface was 1 (arbitrary unit). Final result of these calculations is a 62×64 transfer matrix. The total distribution of late potentials at the surface that can be expected from recorded endocardial late potentials can now be computed by summation of all contributions of basket electrodes where late potentials were present.

$$L_t(i) = \sum_j L_h(j) \cdot W_{i,j} \tag{7.10}$$

where $L_t(i)$ is the predicted magnitude of the late potentials at surface lead i, $L_h(j)$ indicates the presence of late potentials at lead j of the basket and $W_{i,j}$ is the inverse of the distance of basket electrode j from the line that connects the surface lead i to the center of the basket.

In equation (7.10) there is still a choice to be made for the set of j's that is used in the forward computation. To optimize discriminating power of the computed maps, the optimal number of electrodes in the neighborhood of the connecting line that should be used was investigated. As can be seen in figure 7.11 the resolving power of the forward computed late potential map increases with decreasing number of contributing electrodes. Using all electrodes results in a smooth dipolar pattern without specific details. Restricting the electrodes to those that are on the same side of the center of the basket as the surface electrode results in a little more detail. When the six nearest electrodes are used, the pattern resolves to that of two areas of the heart that do contain late potentials. Reducing the number of electrodes further will result in a patchier pattern that is harder to interpret. It was concluded that about 4 to 8 closest electrodes yielded the best resolution without being too patchy. An example of the patterns for one electrode are shown in figure 7.12. Figure 7.11 is the result of the sum of such maps from the 15 basket electrode leads with late potentials in this patient.

Restricting the selected basket electrodes by a threshold on the maximal distance from the line instead of reducing the number of electrodes also resulted in either too smooth or too patchy patterns, depending on the threshold chosen. However, a maximum distance that gave satisfactory results for all patients could not be found.

It should be noted that in each patient the basket catheter is deployed differently. This causes the electrodes of the basket to be in a different position for every

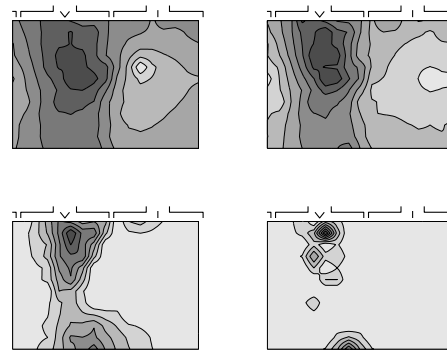

Figure 7.11: *Effect of number of contributing endocardial electrodes on localizing power. From left to right and from top to bottom, maps constructed by using all basket electrodes (with negative values for electrodes at the other side of the center of the basket), using only basket electrodes on the same side of the basket as the surface electrode, using the 6 closest basket electrodes, and using only the closest one are shown.*

patient. Therefore, the matrix $W_{i,j}$ in equation (7.10) was calculated for each patient. Figure 7.13 displays the results in four patients for an arbitrarily selected basket electrode.

In principle, also the inverse approach could have been used to estimate late potentials at the left ventricular endocardium from those at the surface. Superiorly and inferiorly positioned electrodes in the heart do not project well on the surface electrodes, however. This tends to give rise to systematic errors in the comparison. The basket electrodes cover more of the space angle than the body surface electrodes. Therefore, this problem of unequal coverage did not complicate the forward computation, but would have posed a problem in the inverse computation.

7.6 Spatial gradients in unevenly distributed electrode systems

When, for instance measures of spatial inhomogeneity in repolarization such as QT intervals or endocardial activation recovery intervals (ARIs) are computed, it may be useful to take the geometrical relation between measuring positions into account. Measuring a difference of 30 ms in QT interval between sides that are located at opposite sites of the chest will probably not be as indicative of arrhythmia vulnerability as the same difference in electrodes 2 mm apart. We therefore considered methods to compute in an identical way the repolarization difference corrected for interelectrode distance in quite different lead systems. If physical interelectrode distances would have been used such an index would have very different values at the body surface as compared to values obtained from endo-

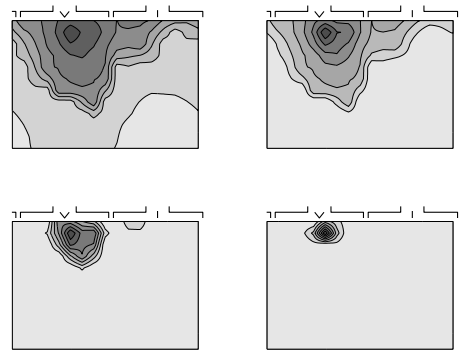

Figure 7.12: *Contribution of arbitrarily selected basket electrode B4 to the surface distributions for four numbers of contributing endocardial electrodes. From left to right and from top to bottom, maps constructed by using all basket electrodes (with negative values for electrodes at the other side of the center of the basket), using only basket electrodes on the same side of the basket as the surface electrode, using the 6 closest basket electrodes, and using only the closest one are shown.*

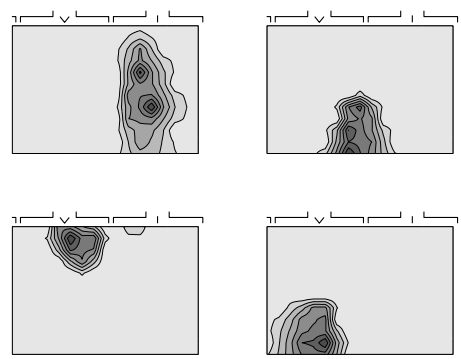

Figure 7.13: *Map showing the contribution of an arbitrarily selected basket electrode (B4) to the surface distribution of late potentials for four patients. Since the endocardial location of basket electrode B4 will be different in individual patients, due to the nature of the basket catheter used, different maps are obtained.*

cardium or epicardium. This would have complicated quantitative comparison. A measure, however, that is independent of physical interelectrode distances and can be defined both at the body surface and in the heart is the timing difference between 2 electrodes divided by the angle between them. For two points $\vec{x_i}$ and $\vec{x_j}$ at the surface, the angle between the lines connecting them to the center of the left ventricle is easily computed as the inverse cosine of the dot product of the vectors.

$$\alpha_{i,j} = \arccos\left(\vec{x_i} \cdot \vec{x_j}\right) \tag{7.11}$$

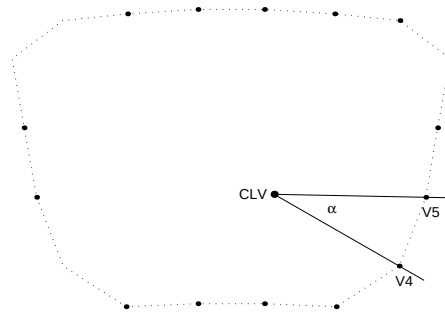

Figure 7.14: *Calculation of angle α between electrodes V4 and V5 in the torso model as described in § 7.6. CLV = Center of the left ventricle.*

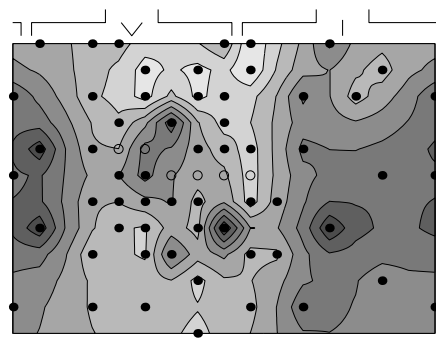

Figure 7.15: *Map of minimal angles between pairs of electrodes in the Amsterdam lead set. Dark areas indicate large angles (maximum about 29 degrees) light colors small angles between neighboring electrodes (minimum about 6.3 degrees).*

The principle is shown in figure 7.14. Again, the 3D torso model is derived from the 'Visible Human Project' internet site as described earlier (§ 7.5.2).

Plotting the minimum angle between each lead and any other lead (i.e how far the nearest electrode is) as a body surface map confirms that the Amsterdam lead set is reasonably homogenously distributed over the thorax (see figure 7.15).

When repolarization estimates at point $\vec{x_i}$ and $\vec{x_j}$ are t_i, respectively, t_j the repolarization index per degree is computed as

$$C_{i,j} = \frac{|t_i - t_j|}{\arccos(\vec{x_i} \cdot \vec{x_j})} \tag{7.12}$$

This will result in a N x N matrix containing the difference in repolarization, divided by the angle between electrodes for each possible electrode pair in the electrode array. The maximum of every row in the matrix, signifies the largest dispersion gradient for every electrode. This is the activation recovery time gradient

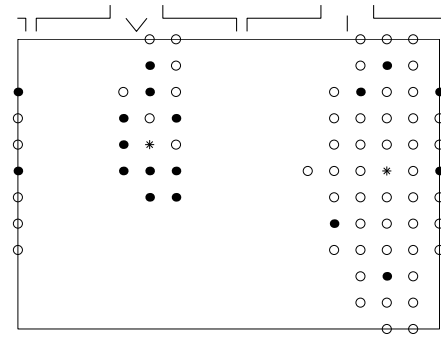

Figure 7.16: *Area within 45 degrees from electrode. For precordial lead V2 and for lead N6 located on the patient's back (indicated with asterisks), all electrode positions of the Amsterdam lead set (solid dots) that are within 45 degrees of these electrodes are indicated. For clarity also the electrodes in the 16 by 12 grid, from which the Amsterdam lead set is a subset, are shown with open circles.*

(ARTG).

It appears to be better to restrict the analysis per electrode to a more confined neighborhood of electrode pairs. Comparing electrodes that are far away does not result in physiological relevant data. On the other hand using a too small area may mean that only a few electrodes are compared and that not all directions will be covered. For the body surface mapping system used in this study, using a cut-off angle of 45 degrees means that there are at least 6 neighbors for each electrode. For two arbitrarily selected leads (precordial lead V2 and lead N6 located on the back of the patient) all electrodes that were within a 45 degree angle are depicted in figure 7.16. The areas appear elongated. This is because the aspect ratio of the map is not the same as on the actual body surface. Average distances between straps vary between patients and is about 5 to 7 cm whereas the vertical distance is fixed at 3 cm.

7.7 Conclusions

Comparing spatially high resolution electrocardiographic body surface data with simultaneously derived multi-lead endocardial data poses specific technical problems. Specific signal averaging methods, filter techniques, correction for inequality in electrode heart distances, 3D reconstruction of electrode arrays and translation schemes between different electrode systems as currently presented allow direct comparison between intracardiac and body surface data thereby increasing our insight in the arrhythmogenic substrate of postinfarction ventricular arrhythmias.

References

1] M. B. Simson. Use of signals in the terminal QRS complex to identify patients with ventricular tachycardia after myocardial infarction. *Circulation*, 64:235–242, 1981.

2] C. P. Day, J. M. McComb, and R. W. Campbell. QT dispersion: an indication of arrhythmia risk in patients with long QT intervals. *British Heart Journal*, 63:342–344, 1990.

3] J. M. de Bakker, R. Coronel, S. Tasseron, A. A. Wilde, T. Opthof, M. J. Janse, F. J. van Capelle, A. E. Becker, and G. Jambroes. Ventricular tachycardia in the infarcted, Langendorff-perfused human heart: role of the arrangement of surviving cardiac fibers. *Journal of the American College of Cardiology*, 15:1594–1607, 1990.

4] Roger C. Barr. Genesis of the electrocardiogram. In Peter W. MacFarlane and Veitch T.D. Lawrie, editors, *Comprehensive electrocardiology - Theory and Practice in Healt and Disease*, chapter 5. Pergamon Press 1st edition, 1989.

5] G. Breithardt, M. E. Cain, N. El-Sherif, N. Flowers, V. Hombach, M. Janse, M. B. Simson, and G. Steinbeck. Standards for analysis of ventricular late potentials using high resolution or signal-averaged electrocardiography. A statement by a task force committee between the european society of cardiology, the american heart association and the american college of cardiology. *European Heart Journal*, 12:473–480, 1991.

6] J. Brachmann, T. Hilbel, M. Schweizer, and W. Kübler. Cardiac late potentials for diagnosis in heart failure. *European Heart Journal*, 14:49–51, 1994.

7] M. J. Ackerman. The visible human project. *Journal of Biocommunication*, 18:14, 1991.

8 General discussion

This study was designed to explore new technologies for analysis of the substrate of postinfarction ventricular arrhythmias with respect to prevention and treatment of these arrhythmias. Until now, most of our knowledge of the human postinfarction arrhythmogenic substrate has been gathered by performing endocardial mapping during ventricular tachycardia (VT) [1–5]. In addition, endocardial mapping performed during ventricular antiarrhythmic surgical procedures has contributed invaluably to the current scientific concept of postinfarction VT [6]. Traditionally, endocardial mapping was focused on delineation of the exit site of VT. In the last decade, the potential of BSM to localize the site of origin of VT (representing the VT exit site) prior to antiarrhythmic surgery or radiofrequency ablation was explored [7, 8].

Until the advent of radiofrequency catheter ablation, ventricular antiarrhythmic surgery was the only curative approach for ventricular tachycardia. Most centers have abandoned antiarrhythmic surgery because of its invasive nature and disappointing results as compared to ICD therapy with regard to survival. Our evaluation in **chapter 2** demonstrates that antiarrhythmic surgery performed by a skilled surgeon in an experienced electrophysiologic center still results in clinical outcome that is at least comparable to the results of radiofrequency catheter ablation of postinfarction VT [9, 10]. Furthermore, little evidence is presented in the literature on the long-term follow-up and success rate of radiofrequency ablation of postinfarction VT. Therefore, antiarrhythmic surgery remains an additional optional therapy in a selected subset of postinfarction patients who are due for open-heart surgery, such as left ventricular aneurysm remodeling, coronary artery bypass grafting or valve surgery [11, 12].

Body surface mapping (BSM) is evaluated for its clinical value and accuracy for localization of sites of origin of the postinfarction VT in **chapter 2**. The major advantage of knowing the exit site of VT is that at least for one part of the reentrant circuit (that is obligatory connected to the critical isthmus of slow conduction), the approximate location is known. Our results show that, despite the fact that BSM offers many advantages (such as ease-of-use and capability of mapping of non-sustained and hemodynamical poorly tolerated arrhythmias) the clinical value of

BSM for antiarrhythmic surgery or radiofrequency catheter ablation of postinfarction VT is limited. This is caused primarily by the limitations of exit site guided VT ablation. Histology of the postinfarction scar taught that the arrhythmogenic substrate is in fact a too complicated structure for mere exit site ablation. It contains multiple potential tracts of slow conduction (only some of which are critical to the reentrant circuit), which can lead to multiple exit sites [13]. Therefore, exit site guided ablation results in abolishment of parts of the reentrant circuit that are critical to that specific VT morphology. It does not imply elimination of the critical part of the reentrant circuit. Therefore the occurrence of VTs with different morphology, utilizing in part the same critical pathways, may persist in this patient. Furthermore, exit site directed VT ablation will only be able to eliminate exit sites that are revealed by induction of the corresponding VT morphology which not necessarily needs to be a spontaneous clinical VT morphology.

Second reason why BSM is of limited use for ablation of postinfarction VT is that its localization performance is also influenced by histologic and electrocardiographic characteristics of the arrhythmogenic substrate in the individual patient. As has been demonstrated in **chapter 3**, differences in extent of conduction block, inhomogeneous distribution of endocardial electrogram amplitudes and the presence of sometimes multiple exit sites in the active VT circuit, all complicate the task of reference database oriented localization of VT sites of origin. Although Sippens Groenewegen et al. introduced BSM reference databases that are specific for anterior or inferior myocardial infarction, this can never account for differences among patients in infarction size, intramural extension of the infarct, shape of the left ventricle and involvement of the interventricular septum. This also explains the difference in accuracy reported between body surface mapping in patients with and patients without structural heart disease [14, 15].

All factors mentioned above urge us to develop methods for localization of confined, critical parts of the reentrant circuit such as the tracts of slow conduction. At present, concealed entrainment during VT is a clinically evaluated methodology that functionally differentiate critical tracts of slow conduction from bystander tracts and that has proven to yield satisfactory clinical outcome [16]. Still, in order to apply the principle of concealed entrainment, sustained VT should be inducible, and the patient should be able to tolerate prolonged periods of arrhythmia.

Ideally, the critical parts of the arrhythmogenic substrate should be detected during sinus rhythm. Tracts of delayed conduction displaying fractionated electrograms, continuous electrical activity or isolated diastolic potentials can be localized during sinus rhythm. Major impediment, however, is that their functional significance for the emergence and perpetuation of VT cannot be established by mere localization mapping [17]. Furthermore, in **chapter 5**, it was shown that only at 24 % of the sites that display late potentials during sinus rhythm also contain diastolic potentials during VT, whereas at 68 % of sites that show diastolic potentials during VT, no late potentials are found during sinus rhythm. Finally, the relation between sites containing late potentials (i.e. whether or not they are located along an interconnecting strand) is not known by performing activation mapping alone.

Therefore, in **chapter 4**, new ways were explored to analyze the substrate dur-

ing sinus rhythm. Functional properties of the arrhythmogenic substrate during sinus rhythm can possibly best be studied - in analogy to concealed entrainment during VT - by delivering a perturbation (for instance by means of ventricular pacing) and subsequent study of the response of the substrate. In the past, the significance of the relation of delay between pacing stimulus and onset of the body surface QRS complex during sinus rhythm was studied, but this did not provide discrimination between critical and non-critical sites [18]. In our study, we not only observed the delay between stimulus and body surface QRS complex, but also reconstructed the tract of conduction between stimulus site and border of the scar. This further clarifies the contribution of tracts of surviving fibers in the infarcted area to arrhythmogenesis, but does not discriminate between critical and bystander tracts.

Novel developments, however, that allow instantaneous multi-site mapping of the entire left ventricle are currently available. This means that the methodology and signal processing algorithms that were developed in **chapter 4**, can be used in the catherization laboratory [19,20]. Instantaneous multi-site pace mapping of the postinfarction substrate combined with beat-to-beat multi-site mapping will identify surviving bundles within the postinfarction scar. Since other authors have shown that it is feasible to perform radiofrequency ablation of VT by means of creation of linear lesions across these tracts of slow conduction, it appears to be possible to eliminate the arrhythmia substrate during sinus rhythm [21, 22]. This approach resembles the technique suggested by data reported by Ciaccio et al in an experimental study [23]. If the area for pace mapping (e.g. the postinfarction scar) during sinus rhythm could be confined, more detailed pace mappings could be obtained in less time. In **chapter 5** it was shown that signal averaged BSM gives regional information on endocardial localization of areas with late potentials. Theoretically, the same signal averaging and localization methodology can be applied for mapping of VT. If this same procedure could be ported to mapping of sustained, hemodynamical well-tolerated VT, information could already be obtained of the clinical VT at the bedside of the patient. Mathematical analysis in **chapter 7** suggests that weighted signal averaging lowers the noise with the approximate square root of the number of complexes even when the noise level changes during the recording. The difference between the noise that you can expect in a clinical ECG recording setting and the noise level required for analysis of a signal averaged ECG is only a factor of about 5. This would mean that weighted averaging of an interval of only 8 seconds could be enough to enable anatomical delineation of diastolic potentials during a non-sustained VT of cycle length 300 ms. This needs to be confirmed in a prospective study.

Not all survivors of myocardial infarction will develop life-threatening arrhythmias. Identification of patients at risk for potentially fatal cardiac arrhythmias becomes of utmost importance, both for primary and secondary prevention of postinfarction ventricular arrhythmias. From the arrhythmogenic mechanisms, it has been shown that both anisotropy in conduction and disparity in ventricular repolarization are an index of vulnerability to postinfarction ventricular arrhythmias. Signal averaged electrocardiography has proven to be an easy to perform

diagnostic tool that has a reliable specificity for identification of patients at risk for sudden death, especially when other clinical variables are incorporated in the decision making process [24]. It should be noted that for purposes of prevention, a diagnostic tool should especially be sensitive to a specific event. In **chapter 5** it was shown that sensitivity for late potentials can be well increased, while specificity is still excellent, by extending the number of surface leads used. Signal averaged BSM may play a role in the near future in identifying postinfarction patients needing further electrophysiological work-up, but this remains to be confirmed by a prospective study.

Much work has been devoted in recent years to techniques for identification of repolarization dispersion, but clinical studies evaluating their use are controversial [25–27]. Several factors, which can be held responsible for the poor predicting value of currently available non-invasive repolarization estimates, are discussed in **chapter 6**. Major impediment in clinical research directed at non-invasively identifying nonuniform recovery of excitation is the lack of a "golden standard". To overcome this problem, spatially dense body surface electrocardiograms and multi-lead endocardial data obtained in the intact human left ventricle were compared in **chapter 6**. It is for the first time that data derived from the entire chest area combined with left ventricular endocardial multi-site data are presented that were recorded simultaneous on a beat-to-beat basis in a human being. Since the main interest in dispersion in repolarization stems from the role it plays in the emergence of functional conduction block, local differences in refractory period in the heart appear to be more meaningful than differences in QT interval over the entire thorax. Therefore, a new parameter for non-invasive expression of local dispersion in refractoriness was introduced. This parameter - activation time recovery gradient - expresses local differences in repolarization in a similar way for endocardial end surface electrode systems. It emerged from these data that T-wave peak to T-wave end duration, non-dipolar content in BSM QRST integral maps and activation recovery time gradients all correlated well with intracardiac estimates of repolarization. It is conceivable that these findings have clinical relevance. T-wave peak to T-wave end in precordial lead V_5 as well as the range of surface activation recovery time gradients were found to be associated with increased dispersion in endocardial repolarization. This is a condition that favors the occurrence of functional arcs of block. Non-dipolar content of BSM QRST integral maps was shown to indicate short endocardial activation-recovery-intervals. Since the wavelength of functional reentry is determined by conduction speed and repolarization duration, ventricular arrhythmias in patients with high non-dipolar QRST content can expected to be exposed to more malignant ventricular arrhythmias. Therefore, these parameters should be analyzed in a prospective study.

Finally, it should be noted that many physical science issues arise when correlating endocardial data with body surface electrocardiography, all of which will have to be solved. Some of these problems are connected with the inverse solution problem of electrocardiography, which nearly is as old as electrocardiography itself [28]. In this thesis, solutions for 3D reconstructions of electrode arrays, surface Laplacian techniques for endocardial electrograms, extraction of meaningful

electrograms from pacing artifacts, correction for differences in heart-surface electrode distance, optimal signal averaging techniques, projections between surface and endocardial lead systems, and methods to compare spatial gradients within a lead system and between different unevenly distributed electrode systems, are presented. Our main goal was to search for solutions that could be derived from the data itself, since this would make application of these solutions in daily clinical practice possible. The methodology described in **chapter 7** increases our insight in the genesis of the electrocardiogram.

References

1] H. J. Wellens, K. I. Lie, and D. Durrer. Further observations on ventricular tachycardia as studied by electrical stimulation of the heart. chronic recurrent ventricular tachycardia and ventricular tachycardia during acute myocardial infarction. *Circulation*, 49:647–653, 1974.

2] H. J. Wellens, D. Durrer, and K. I. Lie. Observations on mechanisms of ventricular tachycardia in man. *Circulation*, 54:237–244, 1976.

3] M. E. Josephson, L. N. Horowitz, A. Farshidi, and J. A. Kastor. Recurrent sustained ventricular tachycardia. I. mechanisms. *Circulation*, 57:431–440, 1978.

4] M. E. Josephson, L. N. Horowitz, A. Farshidi, J. F. Spear, J. A. Kastor, and E. N. Moore. Recurrent sustained ventricular tachycardia. 2. Endocardial mapping. *Circulation*, 57:440–447, 1978.

5] M. E. Josephson, L. N. Horowitz, A. Farshidi, S. R. Spielman, E. L. Michelson, and A. M. Greenspan. Recurrent sustained ventricular tachycardia. 4. Pleomorphism. *Circulation*, 59:459–468, 1979.

6] J. M. de Bakker, F. J. van Capelle, M. J. Janse, A. A. Wilde, R. Coronel, A. E. Becker, K. P. Dingemans, N. M. van Hemel, and R. N. Hauer. Reentry as a cause of ventricular tachycardia in patients with chronic ischemic heart disease: electrophysiologic and anatomic correlation. *Circulation*, 77:589–606, 1988.

7] A. SippensGroenewegen, H. Spekhorst, N. M. van Hemel, J. H. Kingma, R. N. Hauer, J. M. de Bakker, M. J. Janse, and A. J. Dunning. The value of body surface mapping in localization of the site of origin of ventricular tachycardia: catheter pacemapping compared with intraoperative activation mapping. *Circulation*, 82:237, 1990.

8] A. SippensGroenewegen, H. Spekhorst, N. M. van Hemel, J. H. Kingma, R. N. Hauer, J. M. de Bakker, C. A. Grimbergen, M. J. Janse, and A. J. Dunning. Localization of the site of origin of postinfarction ventricular tachycardia by endocardial pace mapping. Body surface mapping compared with the 12-lead electrocardiogram. *Circulation*, 88:2290–2306, 1993.

9] W. G. Stevenson and E. Delacretaz. Strategies for catheter ablation of scar-related ventricular tachycardia. *Current Cardiology Reports*, 2:537–544, 2000.

10] W. G. Stevenson, P. L. Friedman, D. Kocovic, P. T. Sager, L. A. Saxon, and B. Pavri. Radiofrequency catheter ablation of ventricular tachycardia after myocardial infarction. *Circulation*, 98:308–314, 1998.

11] N. M. van Hemel, J. H. Kingma, J. J. Defauw, F. E. Vermeulen, E. G. Mast, J. M. P. G. Ernst, and C. A. Ascoop. Left ventricular segmental wall motion score as a criterion for selecting patients for direct surgery in the treatment of postinfarction ventricular tachycardia. *European Heart Journal*, 10:304–315, 1989.

12] N. M. van Hemel, J. H. Kingma, J. J. Defauw, E. Hoogteijling-van Dusseldorp, J. C. Kelder, W. P. Beukema, and F. E. Vermeulen. Continuation of antiarrhythmic drugs, or arrhythmia surgery after multiple drug failures. A randomized trial in the treatment of postinfarction ventricular tachycardia. *European Heart Journal*, 17:564–573, 1996.

13] J. M. de Bakker, F. J. van Capelle, M. J. Janse, S. Tasseron, J. T. Vermeulen, N. de Jonge, and J. R. Lahpor. Slow conduction in the infarcted human heart. 'Zigzag' course of activation. *Circulation*, 88:915–926, 1993.

14] A. SippensGroenewegen, H. Spekhorst, N. M. van Hemel, J. H. Kingma, R. N. Hauer, J. M. de Bakker, C. A. Grimbergen, M. J. Janse, and A. J. Dunning. Value of body surface mapping in localizing the site of origin of ventricular tachycardia in patients with previous myocardial infarction. *Journal of the American College of Cardiology*, 24:1708–1724, 1994.

15] H. A. Peeters, A. SippensGroenewegen, E. F. Wever, H. Ramanna, A. C. Linnenbank, M. Potse, C. A. Grimbergen, N. M. van Hemel, R. N. Hauer, and E. O. Robles de Medina. Clinical application of an integrated 3-phase mapping technique for localization of the site of origin of idiopathic ventricular tachycardia. *Circulation*, 99:1300–1311, 1999.

16] W. G. Stevenson, H. Khan, P. Sager, L. A. Saxon, H. R. Middlekauff, P. D. Natterson, and I. Wiener. Identification of reentry circuit sites during catheter mapping and radiofrequency ablation of ventricular tachycardia late after myocardial infarction. *Circulation*, 88:1647–1670, 1993.

17] T. Harada, W. G. Stevenson, D. Z. Kocovic, and P. L. Friedman. Catheter ablation of ventricular tachycardia after myocardial infarction: relation of endocardial sinus rhythm late potentials to the reentry circuit. *Journal of the American College of Cardiology*, 30:1015–1023, 1997.

18] W. G. Stevenson, P. T. Sager, P. D. Natterson, L. A. Saxon, H. R. Middlekauff, and I. Wiener. Relation of pace mapping QRS configuration and conduction delay to ventricular tachycardia reentry circuits in human infarct scars. *Journal of the American College of Cardiology*, 26:481–488, 1995.

19] R. J. Schilling, N. S. Peters, and D. W. Davies. Feasibility of a noncontact catheter for endocardial mapping of human ventricular tachycardia. *Circulation*, 99:2543–2552, 1999.

20] A. J. Greenspon, S. S. Hsu, and S. Datorre. Successful radiofrequency catheter ablation of sustained ventricular tachycardia postmyocardial infarction in man guided by a multielectrode "basket"catheter. *Journal of Cardiovascular Electrophysiology*, 8:565–570, 1997.

21] F. E. Marchlinski, D. J. Callans, C. D. Gottlieb, and E. Zado. Linear ablation lesions for control of unmappable ventricular tachycardia in patients with ischemic and nonischemic cardiomyopathy. *Circulation*, 101:1288–1296, 2000.

22] K. Soejima, M. Suzuki, W. H. Maisel, C. B. Brunckhorst, E. Delacretaz, L. Blier, S. Tung, H. Khan, and W. G. Stevenson. Catheter ablation in patients with multiple and unstable ventricular tachycardias after myocardial infarction: short ablation lines guided by reentry circuit isthmuses and sinus rhythm mapping. *Circulation*, 104:664–669, 2001.

23] E. J. Ciaccio, A. C. Tosti, and M. M. Scheinman. Relationship between sinus rhythm activation and the reentrant ventricular tachycardia isthmus. *Circulation*, 104:613–619, 2001.

24] J. A. Gomes, S. L. Winters, D. Stewart, S. Horowitz, M. Milner, and P. Barreca. A new noninvasive index to predict sustained ventricular tachycardia and sudden death in the first year after myocardial infarction: based on signal-averaged electrocardiogram, radionuclide ejection fraction and holter monitoring. *Journal of the American College of Cardiology*, 10:349–357, 1987.

25] C. P. Day, J. M. McComb, and R. W. Campbell. QT dispersion: an indication of arrhythmia risk in patients with long QT intervals. *British Heart Journal*, 63:342–344, 1990.

26] M. Zabel, T. Klingenheben, M. R. Franz, and S. H. Hohnloser. Assessment of QT dispersion for prediction of mortality or arrhythmic events after myocardial infarction: results of a prospective, long-term follow-up study. *Circulation*, 97:2543–2550, 1998.

27] B. Brendorp, H. Elming, L. Jun, L. Kober, M. Malik, G. B. Jensen, and C. Torp-Pedersen. QT dispersion has no prognostic information for patients with advanced congestive heart failure and reduced left ventricular systolic function. *Circulation*, 103:831–835, 2001.

28] W. M. Smith and R. C. Barr. The forward and inverse problems: what are they, why are they important, and where do we stand? *Journal of Cardiovascular Electrophysiology*, 12:253–255, 2001.

9 Samenvatting

Hart- en vaatziekten vormen nog steeds de voornaamste doodsoorzaak in de Westerse wereld. Een groot gedeelte hiervan komt voor rekening van onbehandelbare ritmestoornissen of pompfalen in de acute fase van het hartinfarct. Echter ook een gedeelte van de patiënten die de acute fase van een hartinfarct overleven blijft een verhoogde kans op overlijden houden in de jaren hierna. Het overgrote deel van dit late overlijden is te wijten aan het optreden van zo geheten late kamerritmestoornissen. De oorzaak voor deze kamerritmestoornissen is gelegen in het infarctlitteken. Het infarctlitteken is een complex substraat waarin spiervezels kunnen overleven, die een waar doolhof kunnen vormen in het littekenweefsel (zie figuur 7.1). Deze kleine, overlevende bundels van spiervezels die vaak een veranderde, trage geleiding hebben kunnen onder specifieke omstandigheden een aaneengesloten circuit vormen waarin de elektrische prikkelsblijven 'rondzingen' en zo tot ongewenste, zeer snelle kamerritmestoornissen aanleiding kunnen geven. Tevens zal door het infarctlitteken het niet geïnfarceerde deel van het hart functioneel zwaarder belast worden. Deze zwaardere belasting uit zich vaak in een geleidelijk verwijding van de linker hartkamer. Deze verwijding van de hartkamer leidt via een reeks van processen tot veranderde elektrische hersteleigenschappen (repolarisatie), welke op hun beurt de patiënt op den duur ook blootstellen aan het optreden van levensbedreigende kamerritmestoornissen.

Voor de behandeling en voorkoming van kamerritmestoornissen na het hartinfarct zijn de laatste jaren diverse therapieën ter beschikking gekomen. Deze therapieën kunnen in 3 categorieën onderverdeeld worden. Geprobeerd kan worden bij een verder ongemoeid gelaten substraat het optreden van kamerritmestoornissen te voorkomen door de elektrische eigenschappen van de hartspier te veranderen met behulp van medicijnen (antiaritmica). Daar deze antiaritmica in sommige gevallen juist echter het optreden van ritmestoornissen kunnen bevorderen kan het resultaat hiervan zeer teleurstellend zijn.

De tweede categorie van behandeling wordt gevormd door therapieën die de fatale afloop van het optreden van een ritmestoornis voorkomen. Met behulp van deze zogenaamde implanteerbare cardioverter/defibrillator (ICD) worden levensbedreigende ritmestoornissen automatisch herkend en middels een elektri-

sche schok beëindigd. Met deze therapie worden uitstekende resultaten bereikt voor wat betreft overleving. Implantatie van een ICD kan ook consequenties hebben voor de kwaliteit van leven van de patiënt, omdat hij immers blootgesteld blijft aan ritmestoornissen welke op een onvoorspelbaar moment aanleiding kunnen geven tot bewustzijnsverlies. Tevens bestaat de mogelijkheid, dat de patiënt onterechte ontladingen ervaart van de ICD voor snelle, maar niet levensbedreigende ritmestoornissen, welke niet uit de hartkamer komen of terechte ontladingen tijdens kamerritmestoornissen zonder dat hij het bewustzijn verloren heeft.

De laatste behandelingscategorie wordt gevormd door therapieën die het infarctlitteken zodanig modificeren dat late kamerritmestoornissen niet meer op kunnen treden. Derhalve behoren tot deze categorie behandelingen, die curatief zijn in opzet. Tot deze therapieën moeten ritmechirurgie en catheterablatie gerekend worden. Tijdens ritmechirurgie wordt een ablatie van de aritmogene zone uitgevoerd, terwijl bij catheterablatie op percutane wijze via cathetertechnieken getracht wordt de bron van ritmestoornissen uit te schakelen. Willen deze behandelingen succesvol zijn dan is kennis van de lokalisatie van het substraat bij de individuele patiënt noodzakelijk. De tot dusver beschikbare methoden om ritmestoornissen in kaart te brengen ('mapping') kunnen onderverdeeld worden in invasieve en niet-invasieve methoden. Met invasieve methoden (zoals cathetermapping en intraoperatieve mapping waarbij één meerkanaals ballonelectrode tijdens een operatie in de linker hartkamer geplaatst wordt, zie figuur 4.1) wordt kartering van ritmestoornissen bereikt door op meerdere plaatsen in het hart het moment van plaatselijke activatie te meten. Zodoende wordt niet alleen de oorsprongsplaats van de ritmestoornis, maar tevens ook het gehele circuit dat de ritmestoornis binnen de hartkamer aflegt, gevisualizeerd. Om reeds voor de catheter ablatie of de operatie geïnformeerd te zijn over de lokatie van het aritmogene substraat worden reeds voor de operatie ook mapping van de kamerritmestoornissen gedaan. Met niet-invasieve methoden (zoals 'body surface mapping'), wordt — door op vele plaatsen op het lichaamsoppervlak elektrocardiogrammen tijdens de ritmestoornis te meten — de oorsprongsplaats van kamerritmestoornissen gevonden door de metingen te vergelijken met bibliotheken van elektrocardiogrammen van kamerritmestoornissen met bekende oorsprongsplaats (figuur 3.1 en 3.2). Voordeel van niet-invasieve mapping methoden zijn, dat ze voor de patiënt minder belastend en in het ziekenhuis makkelijk toepasbaar zijn.

9.1 Bepaling van de oorsprongsplaats van kamerritmestoornissen

In het hier gepresenteerd promotieonderzoek zijn methoden ontwikkeld om het substraat van late kamerritmestoornissen na het infarct beter in kaart te brengen. In **hoofdstuk 2** werd de invloed op het success van een ritme-operatie van de tot dan toe gebruikelijke technieken om de oorsprongsplaats van ritmestoornissen voorafgaand aan en tijdens een operatie in kaart te brengen, geanalyseerd. Hiertoe werden bij de eerste groep van 54 patiënten achtereenvolgens alle beschik-

bare karteringsmethoden gebruikt (catheter-mapping, body surface mapping en ballon-mapping tijdens de operatie) en de mapping resultaten onderling vergeleken. Het bleek dat de overeenkomst tussen de lokalisatie van de oorsprongsplaats van 128 verschillende kamerritmestoornissen met mapping tijdens de operatie, die als gouden standaard gebruikt werd, en body surface mapping en catheter-mapping redelijk was. Het bleek verder, dat met body surface mapping veruit de meeste kamerritmestoornissen gekarteerd konden worden. Overeenkomst in oorsprongsplaats plaats tussen catheter-mapping en body surface mapping bedroeg 79 %, terwijl enerzijds de overeenkomst tussen ballon-mapping en body surface mapping en anderzijds die tussen ballon-mapping en catheter-mapping respectievelijk 58 % en 56 % bedroeg. Gekeken werd of de catheter-mapping voortaan weggelaten kon worden in de pre-operatieve voorbereiding voor ritmechirurgie. De overleving na 4 jaar (70 % vs 87 %, figuur 2.4) en vrijheid van ritmestoornissen na 4 jaar (74 % vs 90 %, figuur 2.5) verschilde niet in patiënten onderzocht met of zonder catheter-mapping. Geconcludeerd kon worden, dat patiënt belastende catheter-mapping veilig weggelaten kon worden voorafgaand aan een ritme-operatie. Opvallend was, dat de correlatie tussen body surface mapping en intraoperative ballon-mapping niet hoger was dan $\pm$ 60 % bij de onderzochte patiënten. Overwogen werd, dat veranderingen van elektrische geleiding over de hartspier, welke door het voorafgaande hartinfarct veroorzaakt waren en bij iedere individuele patiënt anders kunnen zijn, hiervoor verantwoordelijk waren. Om dit te onderzoeken werd in **hoofdstuk 3** bij 14 patiënten met kamerritmestoornissen na het hartinfarct gelijktijdig gedetailleerde metingen in de linker hartkamer tesamen met body surface maping gedaan. Met een speciale 64-polige catheter (basketcatheter, figuur 3.3) en voor dit onderzoek ontwikkelde computerprogrammatuur, konden op minimaal invasieve wijze van hartslag tot hartslag gedetailleerde kaarten van activatie van de linker hartkamer gemaakt worden tijdens de ritmestoornis en elektrische stimulatie van de linker hartkamer. Door het verloop van elektrische activatie over de hartspier te visualiseren, kon meer inzicht in het substraat van de kamerritmestoornissen verkregen worden. Daarmee werden de redenen waarom er soms discrepantie was tussen de door body surface mapping aangewezen oorsprongsplaats en de met de ingebrachte catheter gevonden oorsprongsplaats opgespoord. In totaal werd voor 17 kamerritmestoornissen en 322 geconstrueerde kaarten tijdens elektrische stimulatie op diverse plaatsen van het hart een overeenkomst van de oorspongsplaats van 59 % en 70 % gevonden. Er werden vier verklaringen voor verschil in lokalisaties gevonden: (1) gebieden van niet elektrisch activeerbaar hartspierweefsel, waardoor het elektrisch activatie front gedwongen werd een ander beloop te nemen; (2) regionale verschillen in grootte van de in het hart gevonden elektrogrammen; (3) het feit, dat één ritmestoornis tegelijkertijd meerdere oorsprongsplaatsen kon hebben; (4) sommige ritmestoornissen hadden mogelijk een oorsprongsplaats, die dieper in de spier gelegen is, waardoor de metingen met de catheter aan de binnenkant van het hart slechts de doorbreekplaats van de ritmestoornis aan de binnenkant van het hart registreerde. Uit dit onderzoek bleek dat het elektrocardiogram van kamerritmestoornissen gemeten aan het lichaamsoppervlak sterk beïvloed wordt door

structurele veranderingen in het hart, veroorzaakt door het eerdere hartinfarct.

9.2 Lokaliseren van het substraat van kamerritmestoornissen tijdens normaal sinusritme

Idealiter zou het substraat van kamerritmestoornissen gelokaliseerd moeten kunnen worden tijdens normaal hartritme (sinusritme). Dit zou immers de patiënt de belasting van het opwekken van ritmestoornissen kunnen besparen. Bovendien blijkt het in een aantal gevallen technisch niet mogelijk een kartering van de kamerritmestoornis uit te voeren, omdat de ritmestoornis niet opwekbaar blijkt of omdat de patiënt de ritmestoornis niet kan verdragen en het bewustzijn verliest. Daarom werd in **hoofdstuk 4** onderzoek gedaan naar de mogelijkheden om het substraat van ritmestoornissen in kaart te brengen zonder de ritmestoornis op te wekken. Hiertoe werd bij 13 patiënten, die ritmechirurgie ondergingen, stimulatie met een pacemaker op zoveel mogelijk plaatsen in het infarctlitteken uitgevoerd met behulp van een veelkanaals ballonelektrode. Door vervolgens activatiekaarten te registreren van de volgorde van activatie vanaf het stimulatiepunt kon het beloop van het activatie front vanaf de plaats van stimulatie naar de uitgang van het doolhof aan de rand van het infarctlitteken bestudeerd worden. Vervolgens werden de kamerritmestoornissen opgewekt en de oorsprongsplaatsen bepaald. Het bleek, dat 46 % van de oorsprongsplaatsen van kamerritmestoornissen middels de stimulatietechniek tijdens sinusritme gelokaliseerd konden worden. Tevens bleek, dat de geleiding in het infarctlitteken op dezelfde wijze in kaart gebracht kan worden als tijdens de kamerritmestoornis. Hiermee kan nu gedetailleerd het circuit van de ritmestoornissen bestudeerd worden. Tevens kunnen in dit circuit plaatsen worden aangewezen welke geschikt zijn voor het verrichten van de ablatie.

Omdat mapping van ritmestoornissen op niet-invasieve wijze minder belastend is voor een patiënt werden in **hoofdstuk 5** de mogelijkheden bestudeerd om met body surface mapping de paden van langzame geleiding in het infarctlitteken op te sporen. Het gaat bij deze paden van langzame geleiding vaak om vezelbundels van geringe omvang. Daarom kunnen deze elektrische signaaltjes (late potentialen), die door deze bundels gegenereerd worden niet direct aan het lichaamsoppervlak gemeten worden, omdat deze signaaltjes niet van ruis te onderscheiden zijn. Met behulp van een speciale signaalbewerkingstechniek (signal-averaging) kunnen deze signalen echter toch gedetecteerd worden. Daarom werd bij 16 patiënten met een eerder hartinfarct gelijktijdige metingen met een basketcatheter aan de binnenzijde van het hart en body surface mapping ('buitenzijde' van het lichaam) verricht. Aan de hand van de signalen gemeten met de basketcatheter werden gebieden met vertraagde geleiding gedetecteerd. Voor de body surface mapping registraties werd met signal-averaging technieken versterking van 'late potentialen' bewerkstelligd en werd hun aan- en afwezigheid op het lichaamsoppervlak vastgesteld. Middels projectietechnieken werd gekeken of er een relatie in anatomische zin bestond tussen oppervlakte gebieden met 'late potentialen' en

gebieden met vertraagde geleiding in het hart. Het bleek dat bij 12 van de 13 patiënten er visueel een goede correlatie was tussen binnenkant van het hart en lichaamsoppervlak. Kwantitatieve vergelijking van direct gemeten signal-averaged body surface mapping kaarten en kaarten, die middels projectietechnieken van in het hart gemeten signalen geconstrueerd waren, leverde een correlatie op van 0.6 $\pm$ 0.12. UIt de studie blijkt, dat met signal-averaged body surface mapping gebieden met vertraagde geleiding in het hart geïdentificeerd kunnen worden en dat op die manier het gebied dat tijdens catheterablatie onderzocht moet worden, verkleind kan worden.

9.3 Herkenning van patiënten met een verhoogde kans op ritmestoornissen na het hartinfarct

Naast behandeling van patiënten met late kamerritmestoornissen na het hartinfarct, is de identificatie van patiënten met een verhoogd risico op deze ritmestoornissen van wezenlijk belang. Traditioneel worden hier klinisch twee elektrocardiografische technieken voor gebruikt. Signal-averaged elektrocardiografie en meting van regionaal verschil in duur van repolarisatie van de hartspier middels meting van dispersie in het QT-interval op het elektrocardiogram.

Bij signal-averaged elektrocardiografie worden met behulp van drie standaard afleidingen en speciale signaalverwerkende technieken gebieden met vertraagde geleiding aangetoond in het hart. Dit betekent, dat bij patiënten na het hartinfarct aannemelijk gemaakt kan worden dat het substraat voor ritmestoornissen potentieel aanwezig is. Hoewel de specificiteit van signal-averaged elektrocardiografie goed is, lijkt de sensitiviteit teleur te stellen (**hoofdstuk 5**). Gedacht werd, dat dit te wijten was aan de beperkte elektrode resolutie van een 3 afleidingen systeem. Daarom werd in **hoofdstuk 5** gekeken naar invloed van het uitbreiden van het aantal elektroden op de sensitiviteit en specificiteit. Signal averaged body surface mapping werd vergeleken in twee groepen patiënten: een groep van 16 patiënten met een eerder hartinfarct en 12 controlepersonen zonder structurele hartafwijkingen. Het bleek, dat de sensitiviteit van signal-averaged body surface mapping toenam van 0.19 tot 0.88, terwijl de specificteit slechts daalde van 1.0 naar 0.92.

Thans is gebruikelijk om veranderingen in dispersie in repolarisatie te meten met behulp van het QT interval in het 12-kanaals elektrocardiogram. Tot dusver zijn er weinig gegevens voorhanden van metingen in het intacte menselijke hart, die kunnen bevestigen of dispersie in het QT interval daadwerkelijk dispersie in repolarisatie aangeven. Daarom werd in **hoofdstuk 6** in 3 patiëntengroepen metingen gedaan: een groep van 13 patiënten met een eerder hartinfarct en bewezen spontane kamerritmestoornissen; een groep van 23 patiënten met een eerder hartinfarct, die nog nooit kamerritmestoornissen hadden gehad; en een groep van 19 gezonde vrijwilligers. Bij de patiënten met bewezen hartritmestoornissen werd tevens een basketcatheter ingebracht.

Ten slotte dient opgemerkt te worden, dat een groot aantal methoden ontwikkeld moest worden om invasief verkregen data te kunnen vergelijken met me-

tingen gedaan aan het lichaamsoppervlak. Hiertoe behoren technieken zoals 3D reconstructie van de positie van de basketcatheter, signaalverwerkingstechnieken zoals berekening van de oppervlakte Laplaciaan en subtractie van stimulatieartefacten en correctie voor afstand van huidelektroden tot het hart. De fysische achtergrond van deze technieken wordt verantwoord in **hoofdstuk 7**.

9.4 Toekomstig onderzoek

Een groot aantal vragen blijft open staan bij het begrijpen van late kamerritmestoornissen na het infarct. Zo treden deze ritmestoornissen niet bij alle infarct patiënten op. En ook is het niet altijd mogelijk om een bij een patiënt — die spontane kamerritmestoornissen heeft — deze op te wekken. Een groot aantal factoren kunnen deze opwekbaarheid beïnvloeden. Een beter begrip van de omstandigheden die het ontstaan van ritmestoornissen mogelijk maken of uitlokken geeft meer houvast om voor de individuele patiënt de geschikte therapie te selecteren en te controleren of een ingestelde therapie zoals geneesmiddelen of catheterablatie effectief is. Met de in dit onderzoek ontwikkelde methoden om gelijktijdig anatomische informatie te krijgen over repolarisatie eigenschappen van het hart en zones van langzame geleiding is het wellicht mogelijk meer inzicht te krijgen in de opwekbaarheid van kamerritmestoornissen. Dit dient prospectief onderzocht te worden.

In **hoofdstuk 5** worden technieken gebruikt om zones van trage geleiding tijdens sinusritme anatomisch in kaart te brengen. Dezelfde techniek zou toegepast kunnen worden tijdens de kamerritmestoornis, zodat het pad van trage geleiding dat daadwerkelijk gebruikt wordt inzichtelijk gemaakt zou kunnen worden. Deze informatie zou gebruikt kunnen worden tijdens catheterablatie van kamerritmestoornissen.

Ten slotte is een methode ontwikkeld om tijdens sinusritme het doolhof van het infarctlitteken in kaart te brengen. Met elders ontwikkelde technieken, waarmee activatie van de linker hartkamer van slag op slag in beeld gebracht kunnen worden, zou het in **hoofdstuk 4** ontwikkelde protocol toegepast kunnen worden op de catheterisatiekamer.

Publicaties

1] Beukema WP, van Dessel PF, van Hemel NM, Kingma JH: Radiofrequency catheter ablation of accessory pathways associated with a coronary sinus diverticulum. *European Heart Journal* 1994; 15(10):1415-1418.

2] Buys EM, van Hemel NM, Jessurun ER, Kelder JC, van Dessel PF: Temporary pacing after His bundle ablation for drug-refractory atrial fibrillation: a risky enterprise? *Europace* 2000; 2(3):187-190.

3] Buys EM, van Hemel NM, Kelder JC, Ascoop CA, van Dessel PF, Bakema L, Kingma JH: Exercise capacity after His bundle ablation and rate response ventricular pacing for drug refractory chronic atrial fibrillation. *Heart* 1997; 77(3):238-241.

4] Buys EM, van Hemel NM, Kelder JC, van Dessel PF, Bakema L: Unsatisfying results in long-term atrial pacing with a bipolar active fixation atrial lead. *Pacing & Clinical Electrophysiology* 1994; 17(12 Pt 1):2292-2296.

5] Derksen R, van Hemel NM, van Dessel PF, Kelder JC, Kingma JH, Ernst JMPG: Coronary revascularization in management of survivors of out-of-hospital cardiac arrest: arguments for a prospective study. *Cardiologie* 1997; 4(4):115-121.

6] Kimman GP, van Hemel NM, Jessurun ER, van Dessel PF, Defauw JJ: Radiofrequency catheter ablation in patients with atrioventricular nodal reentry tachycardia is as effective as rhythm surgery, but less stressful. *Nederlands Tijdschrift voor Geneeskunde* 1998; 142(46):2525-2529.

7] Kimman GP, van Hemel NM, Jessurun ER, van Dessel PF, Kelder JC, Defauw JJ, Guiraudon GM: Comparison of late results of surgical or radiofrequency catheter modification of the atrioventricular node for atrioventricular nodal reentrant tachycardia. *European Heart Journal* 1999; 20(7):527-534.

8] Linnenbank AC, van Dessel PF, Potse M, de Bakker JM, van Hemel NM: Localization of late potentials using body surface mapping. *Biomedizinische Technik* 2001; 46:204-206.

9] Potse M, Linnenbank AC, van Dessel PF, SippensGroenewegen A, Grimbergen CA: Integration of body surface mapping and biplane fluoroscopy for guidance of catheter ablation of ventricular tachycardia. *Biomedizinische Technik* 2001; 46:210-212.

10] van Dessel PF, de Bakker JM, van Hemel NM, Linnenbank AC, Jessurun ER, Defauw JA: Pace mapping of postinfarction scar to detect ventricular tachycardia exit sites and zones of slow conduction. *Journal of Cardiovascular Electrophysiology* 2001; 12(6):662-670.

11] van Dessel PF, Hasman A, van der Linden CJ: ProtoVIEW: a workstation for the use of clinical algorithms. *Proceedings of MIE* 1991;233-237.

12] van Dessel PF, van Hemel NM, SippensGroenewegen A, de Bakker JM, Linnenbank AC, Defauw JJ: Mapping strategies for surgical ablation of postinfarction ventricular tachycardia. *Journal of Electrocardiology* 2001; To be published.

13] van Dessel PF, van Hemel NM, de Bakker JM, Linnenbank AC, Potse M, Jessurun ER, SippensGroenewegen A, Wever EF: Relation between body surface mapping and the endocardial spread of ventricular activation in the postinfarction heart. *Journal of Cardiovascular Electrophysiology* 2001; To be published November 2001.

14] van Dessel PF, van Hemel NM, Beukema WP, Kingma JH, Ascoop CA: Selective radiofrequency ablation for atrioventricular nodal reentrant tachycardia. *Cardiologie* 1994; 1(2):56-65.

15] van Dessel PF, van Hemel NM, van Swieten HA, de Bakker JM, Jessurun ER: Successful surgical ablation of sustained ventricular tachycardia associated with mitral valve prolapse guided by a multi-electrode basket catheter. *Pacing & Clinical Electrophysiology* 2001; 24:1029-1031.

Abstracts en presentaties

1] Buys EM, van Hemel NM, Kelder JC, van Dessel PF, Bakema L. High dislodgement rate of the bipolar sickle shaped active fixation lead in long-term atrial pacing. Pacing & Clinical Electrophysiology 18, 783. 1994.

2] Derksen R, van Dessel PF, van Hemel NM, Hoogteijling-van Dusseldorp E, Kelder JC, Kingma JH. Out of hospital cardiac arrest related to coronary artery disease: benefits of a therapeutical strategy. Cardiologie . 1995.

3] van Dessel PF, de Bakker JM, van Hemel NM, Jessurun ER. Pacemapping of the postinfarction arrhythmogenic substrate: Identification of the common pathway of the reentrant circuit. Pacing & Clinical Electrophysiology 20[4], 391-391. 1997.
Presented at the annual meeting of the NASPE, 1997, New Orleans

4] van Dessel PF, de Bakker JM, van Hemel NM, Jessurun ER. Pacemapping of the postinfarction arrhythmogenic substrate: identification of the common pathway of the reentrant circuit. Cardiologie 4, 189. 1997.
Presented at the annual meeting of the NVVC 1997, Amsterdam

5] van Dessel PF, van Hemel NM, Beukema WP, Kingma JH, Ascoop CA. Selective radiofrequency ablation for atrioventricular nodal reentrant tachycardia. Netherlands Journal of Cardiology 6, 393. 1993.
Presented at the annual meeting of the NVVC 1993, Garderen

6] van Dessel PF, van Hemel NM, de Bakker JM, SippensGroenewegen A, Kingma JH, Defauw JJ. Comparison of body surface mapping and catheter activation sequence mapping of postinfarction ventricular tachycardia. Cardiologie . 1994.
Poster annual meeting of the NVVC 1994, Garderen

7] van Dessel PF, van Hemel NM, de Bakker JM, SippensGroenewegen A, Kingma JH, Defauw JJ. Comparison of preoperative body surface mapping and catheter activation sequence mapping of postinfarction ventricular tachycardia. Circulation 90[I], 485. 1994.
Poster AHA, 1994, Dallas,

8] van Dessel PF, van Hemel NM, Kingma JH, Defauw JJ. Risk of recurrence of ventricular tachycardia is related to the localization ofthe site of origin. Pacing & Clinical Electrophysiology 18, 812. 1995.
Presented at the annual meeting of the NASPE 1995, Boston

9] van Dessel PF, van Hemel NM, de Bakker JM, SippensGroenewegen A, Kingma JH, Defauw JJ. Comparison of preoperative body surface mapping and catheter activation sequence mapping of postinfarction ventricular tachycardia. European Heart Journal 16, 721. 1995.
Presented at the ESC 1995, Amsterdam

Dankwoord

Het wezen van wetenschappelijk onderzoek doen naast een volledige baan in een perifeer ziekenhuis werd al getypeerd door A.A. Milne in 1926. Op de eerste pagina van "Winnie-The-Pooh" schreef hij immers: *"Op het eerste plaatje zie je Eduard Beer de trappen afkomen, boem, boem, boem, boem op zijn achterhoofd, achter Janneman Robinson aan. Hij weet niet beter, of dit is de enige manier om een trap af te gaan; maar hij krijgt tòch wel eens even een gevoel alsof hij er nog wel wat anders op zou kunnen vinden, als hij er maar één enkel ogenblikje rustig over na kon denken. Maar dan voelt hij toch ook weer, dat er geen andere manier is."* Promovendi behoren echter tot de categorie mensen, die de laatste zin van dit citaat zeker niet zomaar over hun kant laten gaan. Uiteraard dient opgemerkt te worden, dat daarbij de onmisbare steun van velen nodig is. Daarom wil ik in het algemeen iedereen bedanken die op wat voor manier dan ook behulpzaam is geweest bij het tot stand komen van dit proefschrift en een aantal mensen in het bijzonder :

Eerst en vooral mijn promotor en voormalig opleider, prof. dr. N.M. van Hemel. Beste Norbert, jou bedanken zou eigenlijk heel wat meer ruimte vragen dan kan binnen het kader van een proefschrift. Niet alleen was jij de eerste om de geheimen van de electrofysiologie voor me te ontsluieren, niet alleen ben je mijn opleider in de Cardiologie geweest: het is een cliché om te zeggen, dat deze thesis zonder jouw enthousiasme, gedrevenheid en warme belangstelling niet tot stand gekomen zou zijn. Met veel genoegen denk ik aan de regelmatige 'zondagsavondtelefoontjes' en de vele discussies die we hebben gevoerd over onderwerpen die de Electrofysiologie vaak ruim ontstegen. Hoewel er op een bepaald moment een schaduw van onzekerheid over onze samenwerking trok, ben ik om meerdere redenen heel dankbaar dat we deze klus samen hebben mogen afronden. Marijke van Hemel, bedankt dat ik zo vaak beslag mocht leggen op je man (of andersom?)!

Mijn tweede promotor, prof. dr. ir. J.M.T. de Bakker. Beste Jacques, ook jouw inbreng in dit proefschrift was van onschatbare waarde. Ook jij hebt je altijd allesbehalve een contrafessor getoond. Je grote bescheidenheid dwingt een promovendus om de literatuur goed bij te houden en zich zodoende jouw grote bijdrage aan de wetenschap op het gebied van ritmestoornissen te realiseren. Waar ik soms de neiging had om teveel hooi op mijn vork te nemen, was jij er altijd om me op het belang van het bedrijven van onderzoek op een meer pragmatiche manier te wij-

zen en zodoende mijn vizier scherp te houden. Ik ben zeer dankbaar, dat ik van je inspiratie, eruditie en visie op het gebied van de electrofysiologie heb mogen profiteren.

Mijn co-promotor en naaste mede-onderzoeker dr. A.C. Linnenbank. Beste André, wat nu nog te zeggen? De software die je voor me ontwikkelde, de illustraties die je voor me maakte en de stof voor vele inhoudelijke discussies worden in kwaliteit slechts geëvenaard door de vanzelfsprekendheid waarmee jij die leverde. Ik denk dat we een sterk team geweest zijn en dat de kracht van onze samenwerking vooral het plezier is geweest dat we er allebei aan beleefd hebben. De vele avonden samen doorgebracht achter de computer waarbij het programmeren en signaal analyse doorspekt waren met citaten uit Monty Python en de Hitchhiker's Guide maakten promoveren bijna tot een genoegen....

De leden van de beoordelingscommisie: prof. dr. ir. C.A. Grimbergen, prof. dr. R.N.W. Hauer, prof. dr. H. Jongsma, dr. W.G. Stevenson en prof. dr. H.J.J. Wellens, dank ik voor hun bereidwilligheid om naast hun drukke werkzaamheden tijd vrij te maken ten einde dit proefschrift kritisch te beoordelen.

I'd like to express my special thanks to dr W.G. Stevenson for the fact that he came all the way from Boston to honor our pre-dissertation symposium and my actual dissertation with his presence.

Mijn paranimfen dr. H.P.A. van Dongen en ir. V.L.J. Karthaus. Beste Eric en Vincent: het schrijvcn van een proefschrift is één, het orchestreren van alles wat daarna komt is twee. Ik dank jullie dan ook voor jullie morele ondersteuning tijdens het promotieproces en jullie hulp bij het afhandelen van alle organisatorische kwesties.

Mijn naaste collega's van de afdeling Klinische Electrofysiologie van het St. Antonius Ziekenhuis te Nieuwegein: dr. E.F.D. Wever en dr. E.R. Jessurun. Beste Eric en Emile, ik ben jullie dankbaar voor jullie bijdrage aan mijn opleiding tot Electrofysioloog, jullie hulp bij het plaatsen van de basket catheters voor mijn onderzoek en het geduld bij het doen van mijn metingen. Ook dit is onmisbaar geweest bij het schrijven van dit proefschrift. En, Emile, kamergenoot en vriend, hoewel het beeld van je rokende zwijgzaamheid, naast me, aan ons gemeenschappelijk bureau, onuitwisbaar op mijn netvlies gebrand staat, zal ik toch vooral de wijze lessen, die je altijd voor me had op de momenten dat je niet zwijgzaam was, blijven onthouden....

De leden van de maatschap Cardiologie van de locatie St. Antonius Ziekenhuis van het Heart Lung Center Utrecht: dr C.A.P.L. Ascoop, drs. E.T. Bal, drs. J.M. ten Berg, dr. J.M.P.G. Ernst, drs. E.G. Mast, dr. W. Jaarsma, dr. H.W.M. Plokker, dr. M.J. Suttorp, dr. E.F.D. Wever en de recentelijk tot de maatschap toegtreden dr. B.J.W.M. Rensing alsmede zijn voorganger prof. dr. J.H. Kingma, dank ik voor de

opleiding tot cardioloog en het feit dat ik van het patiëntenmateriaal van het St. Antonius Ziekenhuis gebruik kon maken voor mijn onderzoek.

De maatschap Thoraxchirurgie van het St Antonius Ziekenhuis te Nieuwegein, in het bijzonder drs. J.J.A.M.T. Defauw, voor hun expertise op het gebied van ritmechirurgie en – opnieuw – voor hun geduld tijdens de metingen die ik bij de door hen uitgevoerde operaties kwam doen.

drs. M. Potse van de afdeling Medische Fysica van het Academisch Medisch Centrum te Amsterdam. Beste Mark, je behulpzaamheid om software op maat te schrijven, je ontwikkeling samen met André Linnenbank van het prachtige software pakket MapLab en de vele illustraties die je altijd bereid was om voor me te maken, waardeer ik bijzonder. Dat jouw 's' over twee weken ook maar mag sneuvelen.

dr. A. Sippens Groenewegen wil ik bedanken voor de vele potloden die hij versleten heeft bij het zwart arceren van mijn artikelen. Beste Arne, ik heb veel geleerd van je enorme kennis van body surface mapping en de kritisch manier van lezen van mijn stukken.

Mevrouw G.J. van der Kuijl en mevrouw E. Hoogteijling-van Dusseldorp. Gerda, het feit, dat je menig vrije dag opofferde om ons van jouw kunde op het gebied van het maken van dia's, posters en het verzendklaar maken van artikelen te laten genieten is niet onopgemerkt gebleven. Bedankt hiervoor! Beste Elly, ik ben je dankbaar voor de gedrevenheid en precisie waarmee je altijd onze database onderhouden hebt en de follow-up gegevens van onze patiënten hebt verzameld.

De medewerkers van de afdeling Cardiomeettechniek van het St. Antonius Ziekenhuis te Nieuwegein: Erik Stel, Peter van Hartingsveld, Barbara Maat-Poot en Rob Thijssen. Jullie ondersteuning bij het maken van de body surface mappings en het verrichten van de electrofysiologische metingen op de catheterisatiekamer en operatiekamer waren cruciaal bij het schrijven van dit proefschrift.

Van mijn collega assistenten tijdens de Cardiologie opleiding, wil ik met name Rob van Tooren en Braim Rahel danken, die zo vriendelijk waren om mijn klinische afdeling waar te nemen als ik een paar uur uit de roulatie was om al mijn metingen op de elctrofysiologie kamer te kunnen doen. Hans Kelder en Monique Stofmeel : bedankt voor jullie epidemiologische terugkoppelingen en het kritisch uitvoeren van de laatste syntax check.

Één-na-laatst-maar-niet-lest wil ik mijn zus, broers, schoonzussen, neefjes, nichtjes, klimmaatjes, vrienden en vriendinnen bedanken voor het begrip en het geduld dat ze opbrachten als ik het weer eens te druk had om op regelmatige tijden contact te houden of op het laatste moment weer eens een vakantie af zegde omdat ik toch moest "typen".

Lieve Vader en Moeder, de zekerheid, dat ik altijd kan terugvallen op een warm nest, heeft de afgelopen jaren een project als het schrijven van dit proefschrift voor mij haalbaar gemaakt. Maar alles, wat ik opgestoken heb bij het werken aan deze dissertatie, verbleekt bij wat ik allemaal al van jullie heb mogen leren. Als ik de normen en waarden half zo goed mag uitdragen als jullie die me bijgebracht hebben, prijs ik mij een gelukkig mens. Ik dank jullie voor alles.

Curriculum Vitae

The author was born on April 29, 1963, in Bergen op Zoom, The Netherlands. He obtained his secondary school certificate at the R.K. Gymnasium Juvenaat H.H. in Bergen op Zoom. In August 1981, he entered Medical Scool at the State University of Utrecht, where he obtained his medical degree on October 28, 1988. Subsequently, he worked at the Department of Medical Informatics and Statistics of the State University of Maastricht (Chairman prof. dr. ir. A. Hasman). In May 1991, he started working at the Department of Cardiology of the Zuiderziekenhuis in Rotterdam (Chairman dr X.H. Kraus). In 1992, the author started working in the Department of Cardiology of the St. Antonius Hospital in Nieuwegein (Chairman dr. C.A.P.L. Ascoop). Initially, he followed his Electrophysiology training (prof. dr. N.M. van Hemel) from May 1992 until March 1995. Then he followed his Internal Medicine training (dr O. Meeuwessen and dr. H.C.M. Haanen) from March 1995 to March 1997. From March 1997 to March 2000, he completed his training as cardiologist (prof. dr. N.M. van Hemel and dr. W Jaarsma). Since March 2000, the author is working as cardiac electrophysiologist and chef de clinique Cardiology at the location St Antonius Ziekenhuis of the Heart Lung Center Utrecht.